Swansea University
Prifysgol Abertawe

Cronfa
Setting Research Free

Swansea University E-Theses

Nonequilibrium quantum field dynamics from the two-particle-irreducible effective action.

Laurie, Nathan S

How to cite:

Laurie, Nathan S (2008) *Nonequilibrium quantum field dynamics from the two-particle-irreducible effective action..* thesis, Swansea University.
http://cronfa.swan.ac.uk/Record/cronfa42254

Use policy:

This item is brought to you by Swansea University. Any person downloading material is agreeing to abide by the terms of the repository licence: copies of full text items may be used or reproduced in any format or medium, without prior permission for personal research or study, educational or non-commercial purposes only. The copyright for any work remains with the original author unless otherwise specified. The full-text must not be sold in any format or medium without the formal permission of the copyright holder. Permission for multiple reproductions should be obtained from the original author.

Authors are personally responsible for adhering to copyright and publisher restrictions when uploading content to the repository.

Please link to the metadata record in the Swansea University repository, Cronfa (link given in the citation reference above.)

http://www.swansea.ac.uk/library/researchsupport/ris-support/

Nonequilibrium Quantum Field Dynamics from the Two-Particle-Irreducible Effective Action

Nathan S. Laurie

Department of Physics, Swansea University
Singleton Park, Swansea, SA2 8PP, United Kingdom

Submitted to the University of Wales in fulfilment
of the requirements for the Degree of

Doctor of Philosophy

Swansea University

2008

ProQuest Number: 10797962

All rights reserved

INFORMATION TO ALL USERS
The quality of this reproduction is dependent upon the quality of the copy submitted.

In the unlikely event that the author did not send a complete manuscript
and there are missing pages, these will be noted. Also, if material had to be removed,
a note will indicate the deletion.

ProQuest 10797962

Published by ProQuest LLC (2018). Copyright of the Dissertation is held by the Author.

All rights reserved.
This work is protected against unauthorized copying under Title 17, United States Code
Microform Edition © ProQuest LLC.

ProQuest LLC.
789 East Eisenhower Parkway
P.O. Box 1346
Ann Arbor, MI 48106 – 1346

UNIVERSITY OF
LIBRARY
WALES SWANSEA

Abstract

The two-particle-irreducible effective action offers a powerful approach to the study of quantum field dynamics far from equilibrium. Recent and upcoming heavy ion collision experiments motivate the study of such nonequilibrium dynamics in an expanding space-time background. For the O(N) model I derive exact, causal evolution equations for the statistical and spectral functions in a longitudinally expanding system. It is followed by an investigation into how the expansion affects the prospect of the system reaching equilibrium. Results are obtained in $1+1$ dimensions at next-to-leading order in loop- and $1/N$-expansions of the 2PI effective action. I focus on the evolution of the statistical function from highly nonequilibrium initial conditions, presenting a detailed analysis of early, intermediate and late-time dynamics. It is found that dynamics at very early times is attracted by a nonthermal fixed point of the mean field equations, after which interactions attempt to drive the system to equilibrium. The competition between the interactions and the expansion is eventually won by the expansion, with so-called *freeze-out* emerging naturally in this description.

In order to investigate the convergence of the 2PI-$1/N$ expansion in the O(N) model, I compare results obtained numerically in $1+1$ dimensions at leading, next-to-leading and next-to-next-to-leading order in $1/N$. Convergence with increasing N, and also with decreasing coupling are discussed. A comparison is also made in the classical statistical field theory limit, where exact numerical results are available. I focus on early-time dynamics and quasi-particle properties far from equilibrium and observe rapid effective convergence already for moderate values of $1/N$ or the coupling strength.

DECLARATION

This work has not previously been accepted in substance for any degree and is not being concurrently submitted in candidature for any degree.

Signed ... . (candidate)

Date: 30th September 2008

STATEMENT 1

This thesis is the result of my own investigations, except where otherwise stated. Where correction services have been used, the extent and nature of the correction is clearly marked in a footnote(s).

Other sources are acknowledged by footnotes giving explicit references. A bibliography is appended.

Signed .... (candidate)

Date: 30th September 2008

STATEMENT 2

I hereby give consent for my thesis, if accepted, to be available for photocopying and for inter-library loan, and for the title and summary to be made available to outside organisations.

Signed .... (candidate)

Date: 30th Spetember 2008

Contents

List of Figures

Chapter 1

Introduction

As I write this, the most ambitious scientific experiment of our time has, after €5bn and 8 years of construction, been switched on. An experiment designed not to meet commercial or military goals, but solely for the advancement of human knowledge. The Large Hadron Collider (LHC) at Cern in Geneva has the potential to transform our understanding of the natural world, expanding our knowledge regarding the deepest questions in science, from the nature of the fundamental forces governing sub-atomic particles to the identity of the mysterious dark matter that pervades our universe.

The detectors situated around the LHC's 27km circular tunnel are designed with a few key questions in mind. The general purpose ATLAS and CMS detectors will study collisions between beams of protons, accelerated to within a fraction of the speed of light, in order to search for new particles including the elusive Higgs boson. The LHCb will seek to shed light on the matter-antimatter asymmetry in the universe through the study of b-mesons. Finally, the ALICE detector will study, instead of protons, high energy collisions between lead nuclei.

This study of collisions of ultrarelativistic heavy ions is key to our understanding of quantum chromodynamics (QCD) in extreme conditions. The collisions offer us the unique possibility of producing unconfined quark-gluon matter (a quark-gluon plasma (QGP) in its thermalised form) and studying in detail the transition from this state to that of ordinary (confined) matter. They also promise to recreate the conditions of extremely high temperature and pressure similar to those present a fraction of a second after the big bang, offering us an insight into the evolution of the universe from its chaotic beginnings into the calm uniformity we see today.

Understanding these collisions requires a thorough study of the various stages

of the thermalisation process: from the far-from-equilibrium initial state present in the immediate aftermath of the collision, to an equilibrated QGP that undergoes a confinement transition, through to the freeze-out where the dilution of the system due to the expansion of the collision fireball is so great that the particles effectively cease to interact.

Various methods can be used to study particular features of this evolution. Descriptions based on hydrodynamics make the assumption that deconfined matter behaves as a strongly interacting perfect fluid; its evolution can then be studied through equations based on the conservation of energy-momentum and other conserved charges. At some point however these hydrodynamical descriptions must break down, since the dilution of the expanding system inevitably leads to violation of the assumption of a continuous medium. Alternatively, kinetic theory, based on the solution of Boltzmann-type equations for the evolution of particle number distributions, can provide us with a description in terms of on-shell partonic degrees of freedom. Both of these approaches however, are unsuitable for dealing with the far-from-equilibrium dynamics at very early times.

The aim of this thesis is to bypass the limitations of these models, by employing a first-principles approach based on the underlying quantum field theory. This method will encompass the evolution in its entirety, including the far-from-equilibrium dynamics at early times, and will also naturally reproduce freeze-out, a feature that has to be placed *ad hoc* into hydrodynamic descriptions.

Chapter 2 constitutes a review of quantum field theory out of equilibrium. It will introduce the two-particle-irreducible (2PI) effective action formalism for a scalar $O(N)$ model, with equations derived in an arbitrary space-time metric, as a method for studying nonequilibrium dynamics. Truncations of the 2PI effective action via the loop-expansion and the $1/N$-expansion will be introduced and discussed. Chapter 3 comprises the *raison d'être* of the thesis. A reparameterisation of Minkowski space-time is introduced in order to model the longitudinal expansion present shortly after a heavy ion collision. The consequences of this expansion are investigated firstly in a non-interacting system, and subsequently in an interacting system via the 2PI effective action. Results are presented from a numerical analysis implemented for both the loop- and $1/N$-expansions at next-to-leading order (NLO). The effective convergence of truncations of the 2PI effective action is investigated in Chapter 4. Building on work done for the case of $0 + 1$ dimensions (i.e. quantum mechanics) results are

presented comparing NLO and next-to-next-to-leading order (N^2LO) truncations in $1+1$ dimensional quantum field theory. Results are also presented in the classical limit, and compared with exact numerical results from classical statistical field theory. Finally, a summary and outlook will be given in chapter 5.

Chapter 2

The two-particle-irreducible effective action

2.1 Nonequilibrium dynamics

2.1.1 What is nonequilibrium field theory?

Nonequilibrium field theory is a branch of quantum field theory that seeks to describe, from first principles, the time evolution of a system of dynamical fields that may be initially arbitrarily far from thermal equilibrium. One of the main challenges it seeks to overcome is to connect far-from-equilibrium dynamics at early times with the approach to quantum thermal equilibrium at late times. Since the process of equilibration results in substantial loss of information about the initial conditions of a system, a full theoretical description of the connection between early and late time dynamics from which this memory loss emerges naturally is essential for an understanding of nonequilibrium phenomena[1].

The motivation for this study arises from the huge influx of data from relativistic heavy-ion collision experiments, as well as from applications in Cosmology. In describing the early post-collision stage of a heavy-ion collison it is necessary to consider extreme nonequilibrium dynamics. Subsequently one hopes to understand the equilibration process that likely leads to the formation of a thermal quark-gluon plasma. A recent avenue of study aims for an understanding of the discrepancy between the very

[1] Of course, one could also argue that since we have memory loss, the connection with the initial conditions is unimportant!

early thermalisation time as measured in experiments [1, 2, 3, 4] at the Relativistic Heavy Ion Collider (RHIC) and that predicted by current theoretical models. Part of its resolution involves the possibility of different quantities equilibrating on different timescales, for example an almost time independent equation of state (fixed relationship between the pressure p and energy density ε) may emerge very early, even whilst particle numbers deviate substantially from their equilibrium distributions. Cosmological phenomena requiring a thorough understanding of nonequilibrium quantum fields include inflationary dynamics, for example the generation of density fluctuations during inflation and the reheating (thermalisation) of the universe at the end of the inflationary phase.

2.1.2 An initial value problem

In order to describe quantum fields out of equilibrium it is first of all necessary to specify an initial state at some time t_0. This may be provided either via the specification of an initial density matrix $\rho_D(t_0)$, or equivalently by specification of all initial n-point correlation functions of the form

$$\mathrm{Tr}\{\rho_D(t_0)\varphi(\mathbf{x}_1,t_0)\ldots\varphi(\mathbf{x}_n,t_0)\}, \tag{2.1}$$

where $\varphi(\mathbf{x},t)$ denotes a Heisenberg field operator. Often, for simplicity, the form of $\rho_D(t_0)$ is restricted to being Gaussian, in which case knowledge of only the one- and two-point correlation functions and their time derivatives at t_0 is required.

In contrast to equilibrium field theory, the density matrix is time dependent (in the Schroedinger picture), and may deviate significantly from a thermal equilibrium density matrix of the form $\rho_D^{eq} \sim e^{-\beta H}$, where the Hamiltonian H is time independent and β is the inverse temperature.

In equilibrium then, the expectation value of an operator $O(t)$ is given by

$$\begin{aligned}\langle O(t)\rangle &= \mathrm{Tr}e^{-\beta H}O(t)\\ &= \mathrm{Tr}e^{-\beta H}e^{iHt}O(0)e^{-iHt}.\end{aligned} \tag{2.2}$$

where in the second line the time dependence is explicitly factored out. Since the time evolution operator e^{iHt} commutes with the density matrix, we can use the cyclicity of the trace to bring the time evolution operators together, resulting in an expectation

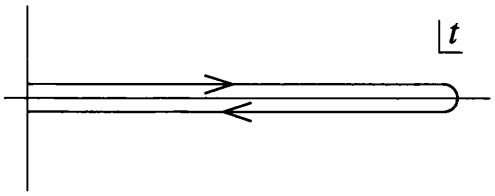

Figure 2.1: Keldysh contour $\mathscr{C}$ in the complex time plane.

value $\langle O \rangle$ that is time independent. Performing the same steps for an expectation value of the form $\langle O(t)O(t') \rangle$ we find that it depends only on $(t' - t)$. Out of equilibrium, the time evolution operator does not in general commute with the density matrix and we are required to consider the full time dependence of expectation values.

Thus nonequilibrium field theory is an initial value problem, the program being to evolve the initial correlation functions forward in time allowing us to extract the time evolution of various observables. The time evolution is completely governed by the Hamiltonian or, equivalently, by a path integral formulation with the classical action S (see below).

Since time-translation invariance is immediately broken by specifying an initial time, nonequilibrium field theory inherently differs from equilibrium theory. One consequence of this is that we cannot perform a fourier transform in time, and hence we must work in a real-time formulation. Nonequilibrium dynamics is distinguished by the fact that it retains memory of its time history, and whilst there is not technically any information loss during the evolution, the approach to thermal equilibrium manifests itself through an effective memory-loss of details of the initial state.

2.1.3 The Schwinger-Keldysh contour

An important technical feature of nonequilibrium field theory emerges naturally when we consider the calculation of an arbitrary correlation function (i.e. the expectation value of a time ordered product of Heisenberg fields) for times later than the initial time t_0. Take the time-ordered two-point function

$$\begin{aligned} \langle T\varphi(x)\varphi(y) \rangle &= \mathrm{Tr}\{\rho_D(t_0) T\varphi(\mathbf{x},t)\varphi(\mathbf{y},t')\} \\ &= \mathrm{Tr}\{\rho_D(t_0) T e^{-i(t_0-t)H}\varphi(\mathbf{x},t_0) e^{-i(t-t')H}\varphi(\mathbf{y},t_0) e^{-i(t'-t_0)H}\}, \quad (2.3) \end{aligned}$$

where again we have explicitly extracted the time evolution (governed by the Hamiltonian) of the Heisenberg fields. The time evolution operator $e^{-i(t-t')H}$ evolves the system from t' to t. Writing it in this way makes clear that the time evolution proceeds along a *finite, closed real-time contour* $\mathscr{C}$ (see Fig. 2.1), on which time ordering is considered to be normal along the forward section $\mathscr{C}^+$ and anti-temporal on the backward section $\mathscr{C}^-$, and all times on $\mathscr{C}^-$ are considered later than any time on $\mathscr{C}^+$ [6, 5]. For the example given, if we take $t > t'$, the time evolution proceeds from $t_0 \to t' \to t$ and finally back to t_0. We therefore introduce the notation $T_{\mathscr{C}}$ and $\int_{\mathscr{C}} dt$ to denote time ordering and integration along the contour respectively.

2.1.4 Simple approximation schemes do not work

There have been various methods employed to attempt a description of far-from-equilibrium quantum dynamics. If the coupling can be guaranteed to be small, a perturbative loop expansion may be attempted; however, ideally one should look for a non-perturbative approximation scheme such as the $1/N$-expansion (where N denotes the number of field components), which imposes no such restriction on the coupling strength. A naive approach to this would be a leading-order large-N, mean field type approximation [7, 8, 9]. Approaches of this type amount to the inclusion of a time-dependent effective mass in the dynamics of the one- and two-point functions but, since no scattering effects are included, they are known to be unable to describe the approach to thermal equilibrium. This failure to exhibit early-time damping of correlations, memory loss and equilibration can be traced to the presence of an infinite number of conserved quantities in the underlying dynamics, and to the existence of a nonthermal fixed point. In order to introduce higher order corrections to the mean field, we may look to a $1/N$-expansion of the one-particle-irreducible (1PI) effective action beyond leading order, but here we encounter another problem: *secularity*. We find so-called secular terms appearing in the expansion of the 1PI effective action, terms which grow with time and therefore render the expansion incapable of describing late-time behaviour, even at weak coupling. Secularity aside, the key deficiency of these approximation schemes is their failure to exhibit *universality*, i.e. the insensitivity of the late-time behaviour to details of the initial conditions. Universality is essential to a successful description of thermalisation where it manifests itself in the loss of memory of the initial state, leading to a late-time result that depends only on globally conserved quantities. It requires an inherent nonlinearity in the underlying

dynamics that places a strong restriction on the approximation being considered.

The issues of secularity and nonlinearity are resolved when we consider the *two-particle-irreducible (2PI) effective action.*

The 2PI effective action, when combined with a systematic coupling- or $1/N$-expansion, provides a description from first principles and without further assumptions, of far-from-equilibrium dynamics and subsequent thermalisation (for a review, see Ref. [10]). The 2PI effective action $\Gamma[\phi, G]$ takes as its independent dynamical variables the *classical field* $\phi(x) \equiv \langle\varphi(x)\rangle$ and the *connected two-point function* $G(x,y) \equiv \langle T_{\mathscr{C}}\varphi(x)\varphi(y)\rangle - \phi(x)\phi(y)$. Derived via a Legendre transform of the generating functional for connected Green's functions, Γ furnishes us with self-consistent equations of motion for ϕ and G that, before truncation, contain the complete information about the system, including quantum fluctuations. The equations are self-consistent in the sense that the expansion of the full propagator $G(x,y)$ is written in terms of G itself. This effectively gives an infinite resummation of diagrams at each order, and provides the nonlinearity required to describe thermalisation[2].

2.2 The $O(N)$ model

The 2PI effective action has largely been studied in the context of $O(N)$ invariant actions comprised of scalar and fermion fields. An $O(4)$ model has, for example, been used as a low-energy effective theory for a scalar σ-field and a triplet of pions π^a $(a = 1,2,3)$, where the mesons are organised in an $O(4)$ vector $\varphi = (\sigma, \pi^a)$. It has also been used in the context of inflation, to describe the nonequilibrium interaction of N scalar boson fields with a scalar 'inflaton' field.

From a practical standpoint, the $O(N)$ model serves as a useful toy model for investigating quantum field dynamics without the presence of gauge symmetry, and also provides the option of a nonperturbative expansion in powers of $1/N$ allowing us to study systems with relatively large coupling strengths.

We now proceed with a review of the construction of the 2PI effective action[3], formulated in an arbitrary metric $g_{\mu\nu}$ for later convenience. We consider a quantum field theory for a real, N-component scalar field φ_a $(a = 1, ..., N)$, with a φ^4 interac-

[2]Contrast this with the 1PI effective action, where ϕ is the only independent variable, and the perturbative expansion of G is written in terms of the free propagator $G_0(x,y;\phi)$.

[3]The discussion to follow is largely based on Refs. [11, 17], but here we work in an arbitrary space-time metric.

tion. We work on the closed time path $\mathscr{C}$ for the reasons discussed earlier. In $d+1$ dimensions, the classical action reads[4]

$$S[\varphi] = \int_x \left(\frac{1}{2} g^{\mu\nu}(x) \partial_\mu \varphi_a(x) \partial_\nu \varphi_a(x) - \frac{m^2}{2} \varphi_a(x) \varphi_a(x) - \frac{\lambda}{4!N} \left[\varphi_a(x) \varphi_a(x) \right]^2 \right), \quad (2.4)$$

where repeated indices are summed over, and the full integral measure is[5]

$$\int_x = \int_{\mathscr{C}} \mathrm{d}x^0 \int \mathrm{d}^d x \sqrt{-g(x)}, \quad (2.5)$$

with $g \equiv \det g_{\mu\nu}$. Integrating by parts we can write this more concisely as

$$S[\varphi] = \int_x \left(\frac{1}{2} \varphi_a(x) (-\Box_x - m^2) \varphi_a(x) - \frac{\lambda}{4!N} \left[\varphi_a(x) \varphi_a(x) \right]^2 \right), \quad (2.6)$$

where

$$\Box_x \equiv \frac{1}{\sqrt{-g(x)}} \partial_\mu \left(\sqrt{-g(x)}\, g^{\mu\nu}(x) \partial_\nu \right) \quad (2.7)$$

is the d'Alembertian operator in a general coordinate system.

The starting point for a derivation of the 2PI effective action is the generating functional for Green's functions in the presence of local and nonlocal source terms

$$\begin{aligned} Z[J,R] &= \int \mathscr{D}\varphi \exp\left(i \left[S[\varphi] + \int_x J_a(x) \varphi_a(x) + \frac{1}{2} \int_{xy} R_{ab}(x,y) \varphi_a(x) \varphi_b(y) \right] \right) \\ &= \exp(iW[J,R]), \end{aligned} \quad (2.8)$$

where $W[J,R]$ is the generating functional for *connected* Green's functions.

At this point we note that, in order to maintain the defining relation of the delta-function in an arbitrary metric, we must include a factor of $(-g)^{-1/2}$, giving

$$\int_x \frac{\delta_{\mathscr{C}}(x-y)}{\sqrt{-g(y)}} = 1, \quad (2.9)$$

where $\delta_{\mathscr{C}}(x-y) = \delta_{\mathscr{C}}(x^0 - y^0) \delta(\mathbf{x} - \mathbf{y})$. Using this, we may take functional derivatives

[4]Technically here, the phi-derivatives should be covariant derivatives since we are working in an arbitrary coordinate system. For scalar fields however, the covariant derivative $\varphi_{;\mu}$ is equivalent to the non-covariant derivative $\varphi_{,\mu} = \partial_\mu \varphi$.

[5]The factor of $\sqrt{-g(x)}$ ensures that the measure is invariant under general coordinate transformations. A similar factor ensures the same invariance for the delta function $\delta_{\mathscr{C}}(x-y)$.

of $W[J,R]$ with respect to the sources, giving

$$\frac{\delta W[J,R]}{\delta J_a(x)} = \langle\varphi_a(x)\rangle = \phi_a(x), \tag{2.10}$$

$$\frac{\delta W[J,R]}{\delta R_{ab}(x,y)} = \frac{1}{2}\langle\varphi_a(x)\varphi_b(x)\rangle = \frac{1}{2}\left(\phi_a(x)\phi_b(y) + G_{ab}(x,y)\right), \tag{2.11}$$

where ϕ_a is the *classical field* (the expectation value of φ_a) and G_{ab} is the *connected two-point function.* We can now obtain the 2PI effective action through a simultaneous Legendre transform of W with respect to the sources J and R:

$$\begin{aligned}\Gamma[\phi,G] &= W[J,R] - \int_x \frac{\delta W[J,R]}{\delta J_a(x)} J_a(x) - \int_{xy} \frac{\delta W[J,R]}{\delta R_{ab}(x,y)} R_{ab}(x,y) \\ &= W[J,R] - \int_x \phi_a(x) J_a(x) \\ &\quad -\frac{1}{2}\int_{xy} \left(R_{ab}(x,y)\phi_a(x)\phi_b(y) + R_{ab}(x,y)G_{ab}(x,y)\right).\end{aligned} \tag{2.12}$$

Note here that if we put the bilocal source to zero we recover the standard expression for the 1PI effective action.

From here we can vary $\Gamma[\phi,G]$ to obtain the *stationarity* conditions:

$$\begin{aligned}\frac{\delta\Gamma[\phi,G]}{\delta\phi_a(x)} &= -J_a(x) - \int_y R_{ab}(x,y)\phi_b(y), \\ \frac{\delta\Gamma[\phi,G]}{\delta G_{ab}(x,y)} &= -\frac{1}{2}R_{ab}(x,y).\end{aligned} \tag{2.13}$$

In the absence of the sources J and R (corresponding to physical processes), these equations give the *equations of motion* for ϕ and G.

2.2.1 Equations of motion

With a view to solving (2.13) we use the following parameterisation of the effective action [12]

$$\Gamma[\phi,G] = S[\phi] + \frac{i}{2}\mathrm{Tr}\ln G^{-1} + \frac{i}{2}\mathrm{Tr}\, G_0^{-1}G + \Gamma_2[\phi,G] + const. \tag{2.14}$$

This may be conveniently viewed as the classical action, plus a one-loop expression, plus higher order contributions (Γ_2). Here

$$iG^{-1}_{0,ab}(x,y) \equiv \frac{\delta^2 S[\phi]}{\delta\phi_a(x)\delta\phi_b(y)} \tag{2.15}$$

$$= -\left(\Box_x + m^2 + \frac{\lambda}{6N}\phi_c(x)\phi_c(x)\right)\delta_{ab}\frac{\delta_{\mathscr{C}}(x-y)}{\sqrt{-g(y)}} - \frac{\lambda}{3N}\phi_a(x)\phi_b(x)\frac{\delta_{\mathscr{C}}(x-y)}{\sqrt{-g(y)}} \tag{2.16}$$

is the inverse classical propagator.

By varying $\Gamma[\phi, G]$ with respect to ϕ and G we can now obtain dynamical equations of motion for the classical field and the full propagator

$$-\left(\Box_x + m^2 + \frac{\lambda}{6N}\left[\phi^2(x) + G_{bb}(x,x)\right]\right)\phi_a(x) = \frac{\lambda}{3N}\phi_b(x)G_{ba}(x,x) - \frac{\delta\Gamma_2[\phi,G]}{\delta\phi_a(x)}, \tag{2.17}$$

and

$$G^{-1}_{ab}(x,y) = G^{-1}_{0,ab}(x,y) - 2i\frac{\delta\Gamma_2[\phi,G]}{\delta G_{ab}(x,y)}, \tag{2.18}$$

which we recognise as the Schwinger-Dyson equation for the propagator, with the self energy given by

$$\Sigma_{ab}(x,y;\phi,G) \equiv 2i\frac{\delta\Gamma_2[\phi,G]}{\delta G_{ab}(x,y)}. \tag{2.19}$$

The exact[6] self energy $\Sigma_{ab}(x,y;\phi,G)$ is equivalent to the 'proper' self energy derived from the 1PI effective action, $\Sigma_{ab}(x,y;\phi)$. However, a particular diagram contributing to $\Sigma_{ab}(x,y;\phi,G)$ contains lines representing the full propagator G. Each diagram therefore effectively performs an infinite resummation of diagrams. Since propagator lines in $\Sigma_{ab}(x,y;\phi)$ are associated only with the classical propagator G_0, making a truncation of these (1PI- and 2PI-) self energies breaks the equivalence between them. Also, the fact that Σ only contains 1PI contributions tells us that Γ_2 only contains diagrams that are 2PI. That is, diagrams that remain connected upon cutting a single propagator line.

[6]At this point the self energy is exact. When performing a numerical solution, we expand the self energy either in powers of the coupling or of the field number parameter N, before making a truncation at the desired order.

To bring this into a form suitable for an initial value problem, we use the following relation to perform a convolution

$$\int_z G^{-1}(x,z)G(z,y) = \frac{\delta_{\mathscr{C}}(x-y)}{\sqrt{-g(y)}}. \tag{2.20}$$

Applying this to (2.18) gives

$$-(\Box_x + m^2)G(x,y) = i\int_z \Sigma(x,z)G(z,y) + i\frac{\delta_{\mathscr{C}}(x-y)}{\sqrt{-g(y)}}. \tag{2.21}$$

At this point the equations of motion are exact, in that Γ_2 and Σ sum diagrams at all orders. In order to perform a numerical analysis we will require that Γ_2 be truncated, the most common ways to organise such a truncation being a loop (coupling) expansion or a $1/N$-expansion.

Whilst the formalism described so far is perfectly suitable for performing a loop-expansion, a $1/N$-expansion is much more efficiently implemented using the *auxiliary-field formalism.* This will provide us with an efficient way of summing diagrams that are the same order in $1/N$, but of different orders in a loop-expansion.

2.2.2 Auxiliary field formalism

From this point on we will work, for simplicity, in the symmetric regime where we assume a vanishing macroscopic field

$$\phi_a(x) = \langle\varphi_a(x)\rangle = 0, \tag{2.22}$$

i.e. there is no symmetry breaking.

To derive equations in the auxiliary field formulation, we begin with the following classical action

$$S[\varphi,\chi] = -\int_x \left[\frac{1}{2}\varphi_a\left(\Box_x + m^2\right)\varphi_a - \frac{3N}{2\lambda}\chi^2 + \frac{1}{2}\chi\varphi_a\varphi_a\right]. \tag{2.23}$$

Integrating out χ yields the original action (2.4). The 2PI effective action is now written in terms of the one-point function $\bar{\chi} = \langle\chi(x)\rangle$ and the two-point functions

$$G_{ab}(x,y) = \langle T_{\mathscr{C}}\phi_a(x)\phi_b(y)\rangle, \qquad D(x,y) = \langle T_{\mathscr{C}}\chi(x)\chi(y)\rangle - \langle\chi(x)\rangle\langle\chi(y)\rangle, \tag{2.24}$$

and reads

$$\Gamma[G,D,\bar{\chi}] = S[0,\bar{\chi}] + \frac{i}{2}\mathrm{Tr}\ln G^{-1} + \frac{i}{2}\mathrm{Tr}\,G_0^{-1}\,(G-G_0) \\ +\frac{i}{2}\mathrm{Tr}\ln D^{-1} + \frac{i}{2}\mathrm{Tr}\,D_0^{-1}\,(D-D_0) + \Gamma_2[G,D], \qquad (2.25)$$

where we have $S[0,\bar{\chi}]$ since we are in the symmetric regime. The free inverse propagators read

$$G^{-1}_{0,ab}(x,y) = i\left[\Box_x + m^2 + \bar{\chi}(x)\right]\delta_{ab}\frac{\delta_{\mathscr{C}}(x-y)}{\sqrt{-g(y)}}, \qquad D_0^{-1}(x,y) = \frac{3N}{i\lambda}\frac{\delta_{\mathscr{C}}(x-y)}{\sqrt{-g(y)}}.$$

To obtain the evolution equations for the propagators G and D and the one-point function $\bar{\chi}$ we extremise (2.25) as before, giving

$$-\left[\Box_x + m^2 + \bar{\chi}(x)\right]G_{ab}(x,y) = i\int_z \Sigma_{ac}(x,z)G_{cb}(z,y) + i\delta_{ab}\frac{\delta_{\mathscr{C}}(x-y)}{\sqrt{-g(x)}}, \\ \frac{3N}{\lambda}D(x,y) = i\int_z \Pi(x,z)D(z,y) + i\frac{\delta_{\mathscr{C}}(x-y)}{\sqrt{-g(y)}}, \qquad (2.26)$$

and

$$\bar{\chi}(x) = \frac{\lambda}{6N}G_{cc}(x,x). \qquad (2.27)$$

The self energies are defined by

$$\Sigma_{ab} = 2i\frac{\delta\Gamma_2[G,D]}{\delta G_{ab}}, \qquad \Pi = 2i\frac{\delta\Gamma_2[G,D]}{\delta D}. \qquad (2.28)$$

As in the standard formalism, the Σ and Π self energies here are exact.

2.3 Dynamical equations in real time

There are numerous two-point functions that may be of interest to us, all of which can be decomposed in terms of the (non time-ordered) Wightman functions

$$G_>(x,y) = \langle\phi(x)\phi(y)\rangle, \qquad G_<(x,y) = \langle\phi(y)\phi(x)\rangle. \qquad (2.29)$$

These functions have the property $G_>(x,y) = G_<(y,x)$, and in the case of a real scalar field $G^*_>(x,y) = G_<(x,y)$. As an example, the time-ordered propagator is

decomposed as

$$G(x,y) = G_>(x,y)\Theta_{\mathscr{C}}(x^0 - y^0) + G_<(x,y)\Theta_{\mathscr{C}}(y^0 - x^0), \tag{2.30}$$

where $\Theta_{\mathscr{C}}$ is the step function defined on the contour.

For our real scalar field theory there are two independent, explicitly real-valued two-point functions, given by the real and imaginary parts of the complex function $G_>(x,y)$,

$$\begin{aligned} F(x,y) &= \frac{1}{2}\langle\{\phi(x),\phi(y)\}\rangle = \frac{1}{2}[G_>(x,y) + G_>^*(x,y)] \equiv \mathrm{Re}[G_>(x,y)], \\ \rho(x,y) &= i\langle[\phi(x),\phi(y)]\rangle = i[G_>(x,y) - G_>^*(x,y)] \equiv -2\mathrm{Im}[G_>(x,y)]. \end{aligned} \tag{2.31}$$

These are known as the *statistical function* and the *spectral function* respectively. To understand the significance of these particular two-point functions, it may be instructive to briefly consider them in thermal equilibrium.

Thermal equilibrium. Consider for a moment the two-point function G in thermal equilibrium. It is described exactly by (2.21) if the Schwinger-Keldysh contour is replaced by the imaginary time path $\mathscr{C} = [0, -i\beta]$, with β the inverse temperature. This leads to the periodicity, or Kubo-Martin-Schwinger (KMS), condition for the two-point function in imaginary time, $G(x,y)|_{x^0=0} = G(x,y)|_{x^0=i\beta}$ [13, 14]. Since in equilibrium we can Fourier transform in time this leads to, for example:

$$G_>^{(eq)}(\omega,\mathbf{p}) = e^{\beta\omega}G_<^{(eq)}(\omega,\mathbf{p}). \tag{2.32}$$

This translates into the following equilibrium relations for the statistical and spectral functions

$$F^{(eq)}(\omega,\mathbf{p}) = -i\left(n_B(\omega) + \frac{1}{2}\right)\rho^{(eq)}(\omega,\mathbf{p}), \tag{2.33}$$

with $n_B(\omega) = (e^{\beta\omega} - 1)^{-1}$. While $\rho^{(eq)}$ encodes information about the spectrum of the theory, we observe that $F^{(eq)}$ encodes statistical information through its dependence on the particle distribution function n_B.

Returning now to general, nonequilibrium considerations, we note that the statistical and spectral functions have the symmetry properties $F(x,y) = F(y,x)$ and

$\rho(x,y) = -\rho(y,x)$. Inverting equations (2.31) gives

$$G_>(x,y) = F(x,y) - \frac{i}{2}\rho(x,y), \qquad G_<(x,y) = F(x,y) + \frac{i}{2}\rho(x,y), \tag{2.34}$$

which can be directly substituted into (2.30). Noticing that

$$\begin{aligned}
&\Theta_{\mathscr{C}}(x^0 - y^0) + \Theta_{\mathscr{C}}(y^0 - x^0) = 1, \\
&\Theta_{\mathscr{C}}(x^0 - y^0) - \Theta_{\mathscr{C}}(y^0 - x^0) = \mathrm{sign}_{\mathscr{C}}(x^0 - y^0),
\end{aligned} \tag{2.35}$$

gives us the decomposition of the two-point function G into statistical and spectral components

$$G(x,y) = F(x,y) - \frac{i}{2}\mathrm{sign}_{\mathscr{C}}(x^0 - y^0)\rho(x,y). \tag{2.36}$$

This manoeuvre affords us numerous benefits. We obtain coupled evolution equations for F and ρ that are fully equivalent to the equation for G but have a simple physical interpretation. The resultant equations will be shown to be causal, and feature characteristic *memory integrals* that run over the time history of the system. In addition, the statistical and spectral functions are real, and possess useful symmetry properties that can be handily exploited during a numerical solution of the equations.

2.3.1 Statistical and spectral equations in the standard formalism

Returning for a moment to the standard (not auxiliary field) formalism, we wish to make a similar decomposition of the self-energy into statistical and spectral components. To achieve this we first separate the self-energy into a local and non-local part,

$$\Sigma(x,y) = -i\Sigma^{(0)}(x)\frac{\delta_{\mathscr{C}}(x-y)}{\sqrt{-g(y)}} + \bar{\Sigma}(x,y). \tag{2.37}$$

We can combine $\Sigma^{(0)}$ with the mass as follows

$$M^2(x) = m^2 + \Sigma^{(0)}(x), \tag{2.38}$$

from which we see that the local part of the self-energy is just a space-time dependent mass correction.

Now we can decompose $\bar{\Sigma}$ in a similar way to G

$$\bar{\Sigma}(x,y) = \Sigma_F(x,y) - \frac{i}{2}\Sigma_\rho(x,y)\mathrm{sign}_{\mathscr{C}}(x^0 - y^0). \tag{2.39}$$

After making these decompositions in (2.21) and comparing real and imaginary parts, we obtain the following exact coupled equations of motion for F and ρ,

$$[\Box_x + M^2(x)]\rho(x,y) = -\int_{y^0}^{x^0} \mathrm{d}z\, \Sigma_\rho(x,z)\rho(z,y), \tag{2.40}$$

$$\begin{aligned}[\Box_x + M^2(x)]F(x,y) = &-\int_0^{x^0} \mathrm{d}z\, \Sigma_\rho(x,z)F(z,y) \\ &+\int_0^{y^0} \mathrm{d}z\, \Sigma_F(x,z)\rho(z,y),\end{aligned} \tag{2.41}$$

where

$$\int_{y^0}^{x^0} \mathrm{d}z = \int_{y^0}^{x^0} \mathrm{d}z^0 \int \mathrm{d}^d z\sqrt{-g(z)} \tag{2.42}$$

2.3.2 Statistical and spectral equations in the auxiliary field formalism

In the auxiliary field formalism we proceed slightly differently since there is no local part to either the Σ or Π self energies. It is however convenient to separate out the local part of D and write

$$D(x,y) = \frac{\lambda}{3N}\left[i\frac{\delta_{\mathscr{C}}(x-y)}{\sqrt{-g(y)}} + \hat{D}(x,y)\right], \tag{2.43}$$

which, upon substitution into (2.26) gives the following equation for $\hat{D}$

$$\hat{D}(x,y) = -\frac{\lambda}{3N}\Pi(x,y) + \frac{i\lambda}{3N}\int_z \Pi(x,z)\hat{D}(z,y). \tag{2.44}$$

Now we once again decompose into statistical and spectral components (this time decomposing G, $\hat{D}$, Σ and Π), giving

$$[\Box_x + M^2(x)]\rho(x,y) = -\int_{y^0}^{x^0} \mathrm{d}z\, \Sigma_\rho(x,z)\rho(z,y), \tag{2.45}$$

$$\begin{aligned}[\Box_x + M^2(x)]F(x,y) = &-\int_0^{x^0} \mathrm{d}z\, \Sigma_\rho(x,z)F(z,y) \\ &+\int_0^{y^0} \mathrm{d}z\, \Sigma_F(x,z)\rho(z,y),\end{aligned} \tag{2.46}$$

where

$$M^2(x) = m^2 + \lambda\frac{N+2}{6N}F(x,x), \tag{2.47}$$

and

$$\frac{3N}{\lambda}D_\rho(x,y) = -\Pi_\rho(x,y) + \int_{y^0}^{x^0} \mathrm{d}z\, \Pi_\rho(x,z)D_\rho(z,y), \tag{2.48}$$

$$\begin{aligned}\frac{3N}{\lambda}D_F(x,y) = &-\Pi_F(x,y) + \int_0^{x^0} \mathrm{d}z\, \Pi_\rho(x,z)D_F(z,y) \\ &-\int_0^{y^0} \mathrm{d}z\, \Pi_F(x,z)D_\rho(z,y).\end{aligned} \tag{2.49}$$

2.4 The 2PI-loop expansion

The simplest approximation scheme available to us is a loop expansion. Ultimately it is valid for small values of the coupling, however, since the expansion self consistently resums diagrams at all orders one can stretch this validity somewhat [16, 22, 34].

In order to draw the diagrams that contribute to Γ_2 we need to know what types of vertices can occur. We find this by taking the interaction term of the action,

$$S_{int}[\varphi] = -\frac{\lambda}{4!N}\int_x \varphi^4, \tag{2.50}$$

where we use φ^4 as shorthand for $\left[\varphi_a(x)\varphi_a(x)\right]^2$. Shifting this by the classical field we get

$$S_{int}[\varphi+\phi] = -\frac{\lambda}{4!N}\int_x (\varphi^4 + 4\varphi^3\phi + 6\varphi^2\phi^2 + 4\varphi\phi^3 + \phi^4). \tag{2.51}$$

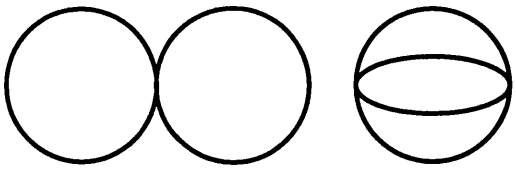

Figure 2.2: The two diagrams that contribute to Γ_2 up to 3-loop level in the symmetric regime $\langle\varphi\rangle = 0$.

Looking only at terms higher than quadratic in the fluctuating field φ we find

$$S_{int}[\varphi,\phi] = -\frac{\lambda}{4!N}\int_x \left[\varphi_a(x)\varphi_a(x)\right]^2 - \frac{\lambda}{6N}\int_x \phi_a(x)\varphi_a(x)\varphi_b(x)\varphi_b(x). \tag{2.52}$$

Since we are calculating Γ_2 in the symmetric regime ($\phi = 0$), there is only a 4-point interaction, and the only $O(N)$ symmetric tensor available to us is $G_{ab} = \delta_{ab}G$. Recalling that Γ_2 only contains 2PI diagrams, we find that up to 3-loop order only the two diagrams shown in Fig. 2.2 contribute.

Summing these diagrams leads to the following expression for $\Gamma_2^{(3-\text{loop})}$

$$\Gamma_2^{(3-\text{loop})}[G] = -\frac{\lambda}{8}\frac{N+2}{3}\int_x G^2(x,x) + i\frac{\lambda^2}{48}\frac{N+2}{3N}\int_x\int_y G^4(x,y). \tag{2.53}$$

This gives for the self energy[7]

$$\Sigma^{(2-\text{loop})}(x,y) = -i\frac{\lambda}{2}\frac{N+2}{3N}G(x,x)\frac{\delta_{\mathscr{C}}(x-y)}{\sqrt{-g(y)}} - \frac{\lambda^2}{6}\frac{N+2}{3N^2}G^3(x,y). \tag{2.54}$$

From this we can read off the local and non-local parts

$$\Sigma^{(0)}(x) = \frac{\lambda}{2}\frac{N+2}{3N}G(x,x) \tag{2.55}$$

and

$$\bar{\Sigma}(x,y) = -\frac{\lambda^2}{6}\frac{N+2}{3N^2}G^3(x,y). \tag{2.56}$$

By making the decomposition of $G(x,y)$ into statistical and spectral components in

[7]The extra factor of $1/N$ in this expression comes from the fact that, as we are effectively making a 'cut' in the diagrams, there is one less trace over the field indices, and hence both terms lose a factor of N.

(2.55) and (2.56), and then comparing with (2.39), we find

$$\Sigma^{(0)}(x) = \frac{\lambda}{2}\frac{N+2}{3N}F(x,x), \tag{2.57}$$

$$\Sigma_F(x,y) = -\frac{\lambda^2}{6}\frac{N+2}{3N^2}\Big[F^3(x,y) - \frac{3}{4}F(x,y)\rho^2(x,y)\Big], \tag{2.58}$$

$$\Sigma_\rho(x,y) = -\frac{\lambda^2}{6}\frac{N+2}{3N^2}\Big[3F^2(x,y)\rho(x,y) - \frac{1}{4}\rho^3(x,y)\Big]. \tag{2.59}$$

2.5 The 2PI-$1/N$ expansion

A useful approximation scheme available to us is the systematic $1/N$-expansion of the 2PI effective action, where the order of a particular diagram is determined according to its scaling with powers of $1/N$ (N being the number of field components). Its importance is clear since it gives us a controlled expansion parameter that does not depend on weak coupling, allowing us to describe physics in cases where a loop- or coupling-expansion is unsuitable. The opportunity to implement the $1/N$-expansion was a motivating factor for choosing a scalar $O(N)$ model, though it may be applied to any bosonic or fermionic theory provided a suitable field number parameter is available.

In the scalar $O(N)$ model, classification of diagrams contributing to the 2PI effective action is accomplished with a scheme based on $O(N)$ invariants. Since $\Gamma[\phi, G]$ is an $O(N)$ singlet parameterised by the fields ϕ_a and G_{ab}, we can write down the possible $O(N)$ invariants that may be constructed from these fields. From the fields ϕ_a, we can only construct one invariant, namely $\phi^2 \equiv \mathrm{tr}\phi\phi \equiv \phi_a\phi_a \sim N$ (which we take to scale proportional to N). The complete set of irreducible invariants, from which all functions of ϕ and G that are $O(N)$ singlets can be constructed, is

$$\phi^2, \quad \mathrm{tr}(G^n) \quad \text{and} \quad \mathrm{tr}(\phi\phi G^n). \tag{2.60}$$

Each of these invariants is taken to scale proportional to N since each contains a single trace over the field indices. When determining the order of a diagram then, we simply count the number of irreducible invariants contributing a factor of N. Additionally, in the loop expansion we see from the original action (2.4) that we must include a factor of $1/N$ for each vertex (in contrast to the $1/N$-expansion where the 3-point

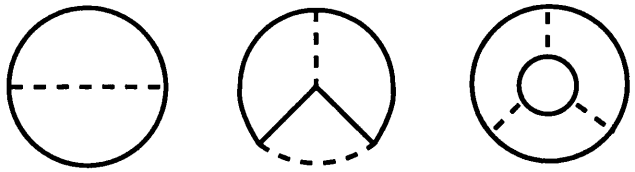

(2) (3) (4)

Figure 2.3: NLO and N^{2}LO contributions to Γ_2 in the $1/N$ expansion. The scalar propagator G is denoted with a full line and the auxiliary-field propagator D with a dashed line.

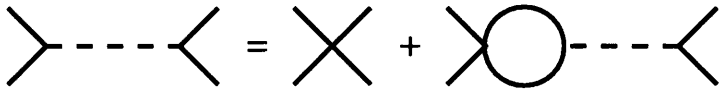

Figure 2.4: Self-consistent equation for the auxiliary propagator D in the 2PI-$1/N$ expansion at NLO.

vertex has no factor of $1/N$, instead this factor is contained within the D propagator itself).

As an example, consider the two-loop diagram in Fig. 2.2. This graph contains two possibilities that contribute at different orders in $1/N$. The first contribution, with the field indices arranged $G_{aa}G_{bb} \equiv (\mathrm{tr}G)^2$, is order N^2 (ignoring the vertex factor); whereas the second contribution, $G_{ab}G_{ab} \equiv \mathrm{tr}(G^2)$, is order N^1. With the vertex factors included these contributions become $\sim N$ (leading order, or LO) and ~ 1 (next-to-leading order, or NLO) respectively. At NLO, there are contributions from an infinite series of diagrams that can be summed. This can be done either in the standard formalism or, more efficiently, in the auxiliary field formalism where all NLO contributions are contained in a single diagram.

To evaluate the order of a diagram in the auxiliary-field formalism, we take the scaling of a closed scalar propagator $G \sim N$ (as above), and the scaling of the auxiliary-field propagator $D \sim 1/N$ (this is clear from (2.26) for instance). Also note that there is no factor of $1/N$ accompanying the three-point vertex. The entire NLO contribution to $\Gamma_2[G, D]$ is contained in the single 2-loop diagram shown in Fig. 2.3, which also shows the NNLO (next-to-next-to-leading order) contributions coming from the 3- and 4-loop diagrams.

As a brief aside it is interesting to see what the auxiliary propagator lines actually

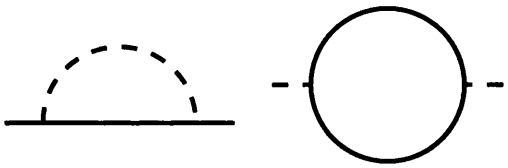

Figure 2.5: Self energy Σ and auxiliary self energy Π at NLO in the $1/N$ expansion.

represent. The equation of motion for the auxiliary propagator D reads[8]

$$D_0^{-1} = D^{-1} + \Pi, \tag{2.61}$$

which can be inverted to give

$$D = D_0 + D_0 \Pi D. \tag{2.62}$$

The effect of the auxiliary propagator at NLO can be seen then in Fig. 2.4 as summing a chain of 'bubbles', all of the same order in N but with each additional contribution suppressed by λ.

The explicit expression for the NLO diagram is then

$$\Gamma_2^{\mathrm{NLO}}[G, D] = \frac{i}{4} \int_{xy} G_{ab}^2(x, y) D(x, y). \tag{2.63}$$

The self energy Σ and the auxiliary-field self energy Π at NLO follow (Fig. 2.5)

$$\Sigma(x, y) = -G(x, y) D(x, y), \qquad \Pi(x, y) = -\frac{N}{2} G^2(x, y). \tag{2.64}$$

Decomposing G and D into statistical and spectral components, then yields

$$\begin{aligned}
\Sigma_F(x, y) &= -\frac{\lambda}{3N} \left[F(x, y) D_F(x, y) - \frac{1}{4} \rho(x, y) D_\rho(x, y) \right], \\
\Sigma_\rho(x, y) &= -\frac{\lambda}{3N} \left[\rho(x, y) D_F(x, y) + F(x, y) D_\rho(x, y) \right], \\
\Pi_F(x, y) &= -\frac{N}{2} \left[F(x, y) F(x, y) - \frac{1}{4} \rho(x, y) \rho(x, y) \right], \\
\Pi_\rho(x, y) &= -N F(x, y) \rho(x, y).
\end{aligned} \tag{2.65}$$

[8]The precise expression is given in (2.26), which, when convoluted with D^{-1}, leads to the equation stated.

2.6 Review of 2PI developments

In recent years the 2PI effective action approach outlined in the previous sections has been applied to a variety of problems in nonequilibrium physics. Thermalisation in a scalar quantum field theory was first demonstrated in Ref. [15], employing a 3-loop truncation of the 2PI effective action in $1+1$ dimensions and in the symmetric phase. Three different nonequilibrium initial conditions with the same energy density were used. For these initial conditions it was shown that modes of the propagator $F(t,t;p)$, with equal momenta p but very different initial values, converge to the same late-time value. Furthermore these late-time values were found to agree with those calculated for a system in thermal equilibrium. This demonstrated the emergence of memory loss and late-time universality (lack of dependence on initial conditions) from the 2PI 3-loop expansion.

The validity of the 2PI-$1/N$ expansion at NLO, and its convergence properties with increasing N in the classical statistical field theory limit, was investigated in Ref. [16]. The (early) time evolution of the unequal-time statistical function $F(t,0;p=0)$, calculated from the classical limit[9] of the 2PI equations of motion, was compared with the exact classical evolution calculated via a Monte Carlo (MC) approach. It was observed that the NLO 2PI-$1/N$ solution showed reasonably good agreement with the exact solution even for small values of N, whilst the two were practically indistinguishable for $N=20$. Results were also presented, this time using a next-to-leading order $1/N$ expansion, showing the evolution and equilibration of the modes of the equal-time statistical function. The initial state used was that of a peaked wave (or "tsunami"), in a thermal background. The quantum evolution of this nonequilibrium initial state to one of thermal equilibrium at late-time was shown to be accurately described by classical physics for sufficiently high initial occupation numbers.

The equations of motion from the 2PI effective action were extended to the more general case of a nonvanishing field expectation value (i.e. $\langle\varphi\rangle \neq 0$) in Ref. [17], which also introduced the auxiliary field formalism described in this chapter. An extension of these methods to fermions was presented in Ref. [18] and applied to a chiral quark-meson model with two fermion flavors coupled to a scalar σ-field and a triplet of pseudoscalar "pions" π^a $(a=1,2,3)$. Late time thermalisation and memory loss was demonstrated for both the bosonic and fermionic correlators, using a variety of initial conditions with the same initial energy density. First steps in the extension

[9] See section 4.2.2 for a discussion of the classical limit.

to gauge theories can be found in Refs. [19, 20, 21], focusing on formal aspects such as renormalisation, Ward identities and a calculation of pressure in the context of QED. As yet there are no nonequilibrium results from gauge theory. Equilibration has also been observed for scalar fields in $3+1$ dimensions [22]. In Ref. [23], the 2PI-$1/N$ expansion was studied at NLO in the context of a search for topological defects in the two-point function during a symmetry-breaking phase transition. Defects are known to be present for small N (depending on the number of space dimensions), however since the 2PI-$1/N$ expansion is based on a large N expansion, it may not be the appropriate truncation to find topological defects. The systematic renormalisation of the 2PI effective action has also been extensively studied [24, 25, 26].

In an attempt to shed light on the discrepancy between the early thermalisation times indicated by collision experiments and the much longer thermalisation timescale expected from the theoretical understanding of QCD, Ref. [27] focused on the phenomenon of *prethermalisation* - the effective thermalisation of certain quantities whilst the system itself is still far from equilibrium. It was shown that an approximately time-independent equation of state (i.e. an almost fixed relationship between the pressure and the energy density) is such a quantity, forming on an extremely short timescale. A constant equation of state is required to close the set of equations used in hydrodynamic descriptions of heavy ion collisions - these methods may therefore be applicable long before the system has fully thermalised.

The reliability of Boltzmann equations for the study of thermalisation is explored in Refs. [28, 29] via a comparison with the 2PI 3-loop expansion. It was found that there were significant discrepancies between the two approaches, with the Boltzmann approach unable to reproduce the universality that emerges from the 2PI equations. The Boltzmann equation only respects a restricted universality as a result of its quasi-particle approximation implying an additional conserved quantity (the total particle number).

In a study of the convergence properties of the 2PI-$1/N$ expansion, the first results beyond next-to-leading order were presented in Ref. [30]. The evolution equations for the O(N) model were derived to next-to-next-to-leading order, solved in $0+1$ dimensions (quantum mechanics) and compared to both previous approximations and the exact numerical solution of the Schrodinger equation. The 2PI-$1/N$ expansion was found to be rapidly converging, with higher order effects giving only quantitative corrections. For the case of quantum mechanics it was found that instabilities were

present already at NLO, presumably due to the lack of destructive interference, but this was believed to be special to quantum mechanics since the NLO approximation in field theory is known to be well behaved. The extension of this work to the case of $1+1$ dimensional quantum field theory forms the basis of chapter 4 of this thesis [36].

Applications to cosmology focus on the transition of the early universe from the inflationary epoch to a period of reheating. Refs. [31, 32, 33, 34] explore the applicability of the 2PI-1/N expansion to particle production, preheating and other aspects of inflation.

Chapter 3

Nonequilibrium dynamics in an expanding background

3.1 Heavy ion collisions

As a starting point we outline the generally accepted picture of the spacetime and thermal evolution of a collision of two identical nuclei, atomic number A, in the centre of mass or lab frame. The nuclei are highly Lorentz contracted "pancakes" travelling toward each other at close to the speed of light. We choose the z-axis to be along the collision axis. The standard picture is informed by two well known features of nucleon-nucleon collisions: *nuclear transparency* (or the leading particle effect) and the *inside-outside cascade.*

Nuclear transparency refers to the observation that a large fraction of the available energy is carried away from the collision point by two secondary nuclei. The rapidity distribution of the baryonic number is centered around these secondary nuclei in what are known as the fragmentation regions. The area between the fragmentation regions is known as the central region and here the baryonic number averages to zero. In order to have a clear separation of the central and fragmentation regions one probably needs an energy per nucleon in the centre of mass frame of ≥ 100 GeV.

With the secondary nuclei receding from the collision point, the remaining energy manifests itself as a "hot plasma" in the central region. The concept of the inside-outside cascade stems from the idea that an excited system of partons does not decay instantaneously. We take the characteristic decay time of such a system in its rest frame to be τ_d. Considering the central region to comprise a number of such

systems, we realise that slower moving systems must decay earlier (in the lab frame) than faster moving ones due to time dilation. Assuming that a collection of excited partonic systems leave the collision point $z = 0$ at time $t = 0$ and travel freely, they will decay on average on a hyperbola of constant proper time $(t^2 - z^2)^{1/2} = \tau_d$. Points on this hyperbola are parameterised by the coordinate

$$\eta = \frac{1}{2} \ln \frac{t+z}{t-z} \tag{3.1}$$

which we identify as the rapidity.

The early post-collision stage is characterised by the drive towards thermal equilibrium that, if it occurs quickly enough and at high enough temperature, results in a quark-gluon plasma. However, the tendency to equilibrate is opposed by the longitudinal expansion of the system along the collision axis. This period of anisotropic expansion is unrelated to the three dimensional radial, isotropic, thermal expansion that occurs when a thermal system expands into a surrounding vacuum. It is instead a remnant of the collision itself, since quanta with higher momenta are found further from the collision point at a particular time t than those with lower momenta.

Experiments suggest that thermalisation does indeed occur on a very short timescale, despite the longitudinal expansion. Expansion of the thermalised system into the vacuum results in rapid cooling, leading to the hadronisation transition when some critical value of the energy density is reached. Once the average separation of the hadrons becomes larger than the range of strong interactions, scattering processes cease and the hadrons decouple, a process known as freeze-out [37].

An important observation from collision experiments is the existence of a "central plateau" structure in the particle production as a function of rapidity. This suggests that in the central region there is an approximate *boost invariance* [38] i.e. the system looks essentially the same if we make a Lorentz boost of moderate rapidity along the collision axis. This phenomenon is well established for $p\bar{p}$ and p-α collisions, and I will assume it holds for collisions of heavier nuclei.

The various stages of the collision process have been studied using a number of methods. Fortunately for theorists, at these extreme energies, simplicity can emerge since we are dealing directly with the degrees of freedom in terms of which the fundamental theory is written. A fundamental question that has been addressed is that of the structure of the wave function of the nucleus at high energy densities. This is directly relevant to heavy ion collisions since the asymptotic form of the wavefunction

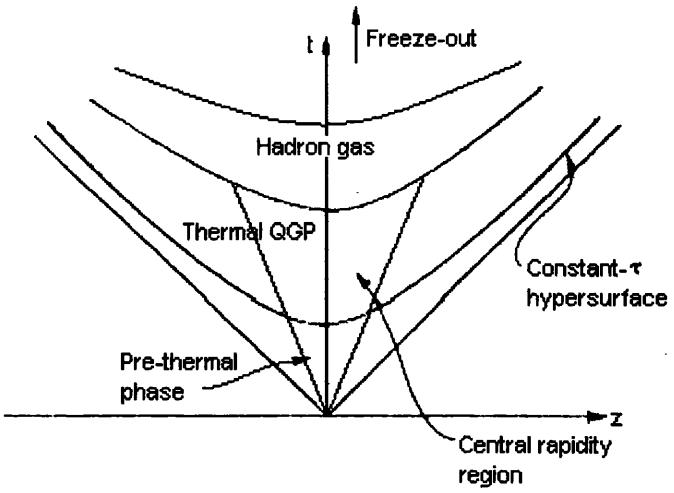

Figure 3.1: Longitudinal space-time evolution after a heavy ion collision

determines the initial conditions for the creation of matter and its subsequent evolution. Theory (supported by data from HERA and RHIC [39, 40]) suggests that the relevant degrees of freedom in the early stages of a collision are partons (rather than nucleons), mainly gluons, whose density grows as energy increases. It is suggested that in the case of such large numbers of quanta, classical field approximations may be valid, leading to an initial collision state known as a "colour glass condensate" [41].

The evolution of the post-collision plasma has been studied using hydrodynamical descriptions [42, 43, 44]. These have been successful in describing the phenomenon of *elliptic flow* [45, 46, 47, 48, 49], the experimental observation that if a nuclei-nuclei collision is non-central[1] the hydrodynamical expansion of the system will take place predominantly along the directions with the largest gradients. This effect leads to predictions that the produced matter thermalises at very early times. The process of thermalisation might also be affected by the presence of plasma instabilities leading to highly nonlinear dynamics of low-momentum degrees of freedom [51, 52, 53, 54, 55, 56, 57].

Much theoretical work has been devoted to studying the properties of the quark-gluon plasma in thermal equilibrium, with reliable information coming from lattice calculations at vanishing chemical potential. More recently, methods have been de-

[1]In a non-central collision, the approaching nuclei don't overlap perfectly when viewed along the collision axis, resulting in an 'almond' shaped, spatially asymmetric collision zone.

veloped that allow calculations at non-vanishing, albeit small chemical potentials, in an attempt to shed light on the phase diagram of QCD. The focus of the lattice calculations is to study the transition from the QGP to confined hadronic matter.

In this work we aim to study the evolution of the system in the longitudinal expansion phase, with nonequilibrium initial conditions specified at some initial time τ_0 shortly after the collision event. As hinted at previously, natural variables for describing the system in this phase are the proper time τ and the rapidity η

$$\tau = (t^2 - z^2)^{1/2}, \qquad \eta = \frac{1}{2} \ln \frac{t+z}{t-z}, \tag{3.2}$$

along with the transverse coordinates (x, y). From these definitions we see that τ and η are only defined inside the light cone (i.e. for $|t| > |z|$).

3.2 Boost invariant dynamics

3.2.1 Coordinate system

Inverting equations (3.2) we find

$$t = \tau \cosh \eta, \qquad z = \tau \sinh \eta. \tag{3.3}$$

Transforming the usual Minkowski line element, we get

$$\mathrm{d}s^2 = \mathrm{d}\tau^2 - \mathrm{d}x_\perp^2 - \tau^2 \mathrm{d}\eta^2, \tag{3.4}$$

where $\mathrm{d}x_\perp^2 = \mathrm{d}x^2 + \mathrm{d}y^2$. We can now simply read off the metric tensor

$$g_{\mu\nu} = \begin{pmatrix} 1 & 0 & 0 & 0 \\ 0 & -1 & 0 & 0 \\ 0 & 0 & -1 & 0 \\ 0 & 0 & 0 & -\tau^2 \end{pmatrix}; \qquad g^{\mu\nu} = \begin{pmatrix} 1 & 0 & 0 & 0 \\ 0 & -1 & 0 & 0 \\ 0 & 0 & -1 & 0 \\ 0 & 0 & 0 & -1/\tau^2 \end{pmatrix}. \tag{3.5}$$

The determinant is

$$g \equiv \det g_{\mu\nu} = -\tau^2, \tag{3.6}$$

and we can now write out the d'Alembertian operator explicitly

$$\Box \equiv \frac{1}{\sqrt{-g}}\,\partial_\mu\left(\sqrt{-g}\,g^{\mu\nu}\partial_\nu\right) = \frac{1}{\tau}\,\partial_\tau\left(\tau\,\partial_\tau\right) - \partial_\perp^2 - \frac{1}{\tau^2}\,\partial_\eta^2, \tag{3.7}$$

where $\partial_\perp^2 = \partial_x^2 + \partial_y^2$.

3.2.2 Covariant conservation of energy-momentum

In order to derive the equations for conservation of energy and momentum in an arbitrary metric, it is necessary to take the *covariant* derivative of the energy-momentum tensor, and set it equal to zero. To do this we require the non-zero Christoffel symbols for the metric (3.5). To obtain the Christoffel symbols from the metric we use

$$\Gamma_{ijk} = \frac{1}{2}\left(g_{ij,k} + g_{ki,j} - g_{jk,i}\right). \tag{3.8}$$

In our particular case, the only space-time dependent component of the metric is g_{33}, and it is a function of τ only. Therefore the only derivative that contributes to (3.8) is

$$\partial g_{33}/\partial x^0 = -2\tau, \tag{3.9}$$

which in turn leads to only three non-zero Christoffel symbols

$$\Gamma^3{}_{03} = 1/\tau = \Gamma^3{}_{30}, \tag{3.10}$$

and

$$\Gamma^0{}_{33} = \tau. \tag{3.11}$$

Now we can take the covariant derivative of $T^{\mu\nu}$,

$$\begin{aligned} T^{\mu\nu}{}_{;\mu} &= \partial_\mu T^{\mu\nu} - \Gamma^{\rho\mu}{}_{\mu} T_\rho{}^\nu - \Gamma^{\rho\nu}{}_{\mu} T^\mu{}_\rho \\ &= \partial_\mu T^{\mu\nu} - g^{\alpha\mu}\Gamma^\rho{}_{\alpha\mu} T_\rho{}^\nu - g^{\alpha\nu}\Gamma^\rho{}_{\alpha\mu} T^\mu{}_\rho \\ &= 0. \end{aligned} \tag{3.12}$$

Upon substitution of the Christoffel symbols, we find

$$\partial_0 T^{00} + \partial_i T^{i0} + \frac{T_0{}^0}{\tau} - \frac{T^3_3}{\tau} = 0, \tag{3.13}$$

$$\partial_0 T^{0j} + \partial_i T^{ij} + \frac{T_0{}^j}{\tau} - g^{3j}\tau\left(T^3{}_0 + \frac{1}{\tau^2}T^0{}_3\right) = 0. \tag{3.14}$$

In order to analyse these equations further we can examine the structure of $T_{\mu\nu}$, given by[2]

$$T_{\mu\nu}(x) = \partial_\mu\varphi(x)\partial_\nu\varphi(x) - g_{\mu\nu}\mathscr{L}. \tag{3.15}$$

Firstly, notice that the second term vanishes for any off-diagonal element of $T_{\mu\nu}$ through our choice of metric. When taking the expectation value $\langle T_{\mu\nu}\rangle$, off-diagonal terms lead to expectation values of the form $\langle\partial_0\varphi\partial_j\varphi\rangle$ and $\langle\partial_i\varphi\partial_j\varphi\rangle$, with $i \neq j$. Since we only consider ensembles that are translationally invariant in space, with $\langle O(\mathbf{x},t)O(\mathbf{y},t')\rangle = G(\mathbf{x}-\mathbf{y};t,t')$, it is useful to transform to momentum space. In that case, these expectation values result in integrals of the form $\int_{-\infty}^{\infty}\mathrm{d}k k^i f(|k|)$ which are odd, and therefore identically zero. It follows that $\langle T_{\mu\nu}\rangle$ is diagonal.

Secondly, since we have assumed spatial translational invariance, elements of $\langle T_{\mu\nu}\rangle$ must be independent of position, and spatial derivatives of the form $\partial_i\langle T^{\mu\nu}\rangle$ must vanish. With these considerations in mind, when we take expectation values of every term in (3.14) we find that each vanishes, and hence this equation is trivially satisfied.[3]

If we then consider (3.13), and take expectation values of every term, we find

$$\partial_0\langle T^{00}\rangle + \partial_i\langle T^{i0}\rangle = -\frac{1}{\tau}\left(\langle T_{00}\rangle + \frac{\langle T_{33}\rangle}{\tau^2}\right). \tag{3.16}$$

For the reasons discussed, the second term vanishes and we finally obtain

$$\dot{\varepsilon} = -\frac{1}{\tau}\left(\varepsilon + P_\eta\right), \tag{3.17}$$

where we have identified the energy density $\varepsilon = \langle T^{00}\rangle$ and the longitudinal pressure $P_\eta = \langle T_{33}\rangle/\tau^2$.

This equation governs the time evolution of the energy density as a function of the longitudinal pressure[4]. Note that this derivation was independent of many details of the system, and specifically doesn't depend on whether the system is inter-

[2]This expression is obtained by varying the action S with respect to the metric tensor $g^{\mu\nu}$.

[3]Note that our coordinate system is anisotropic. Whilst there is isotropy in the transverse (x,y) plane, it does not extend to the longitudinal (η) axis.

[4]We can compare this to the FRW space-time, where the conservation equation is $\dot{\varepsilon}+3H\left(\varepsilon+P\right) = 0$. H is the Hubble function $(= 1/\tau$ in our case) and the factor 3 relates to the isotropic 3-dimensional expansion.

acting/noninteracting, or close to/far from equilibrium.

3.3 Free evolution

3.3.1 Scalar field dynamics

To gain some insight into how the longitudinal expansion affects the dynamics of quantum fields, we will first look at the case of a scalar field theory with no interaction term. For a free scalar field in an arbitrary space-time the action is

$$S = \int \mathrm{d}^4x\sqrt{-g}\,\mathscr{L}, \tag{3.18}$$

with Lagrangian density

$$\mathscr{L} = \frac{1}{2}\left(g^{\mu\nu}\phi_{;\mu}\phi_{;\nu} - m^2\phi^2\right), \tag{3.19}$$

where a semi-colon indicates a covariant derivative. The equation of motion obtained by varying the action is

$$\left(\Box + m^2\right)\phi(\tau, x, y, \eta) = 0\,, \tag{3.20}$$

with $\Box$ given by (3.7). We will solve this equation by first looking for a set of solutions (analogous to plane wave solutions in Minkowski space-time) of the form[5]

$$u_{\mathbf{k}}(\tau, \mathbf{x}) = \frac{e^{i\mathbf{k}\cdot\mathbf{x}}}{(2\pi)^{3/2}}\frac{1}{\tau^{1/2}}f_{\mathbf{k}}(\tau), \tag{3.21}$$

where $\mathbf{x} = (x, y, \eta)^T$, $\mathbf{k}\cdot\mathbf{x} = \mathbf{k}_\perp\cdot\mathbf{x}_\perp + k_\eta\eta$ and we use the notation $\mathbf{x}_\perp = (x, y)^T$ for the transverse coordinates. Substituting this into (3.20) gives an equation for the mode functions $f_{\mathbf{k}}(\tau)$,

$$\ddot{f}_{\mathbf{k}} + \left(\frac{k_\eta^2 + 1/4}{\tau^2} + k_\perp^2 + m^2\right)f_{\mathbf{k}} = 0, \tag{3.22}$$

[5]See, for example, N. Birrell and P. Davies, "Quantum fields in curved space," chapter 5.

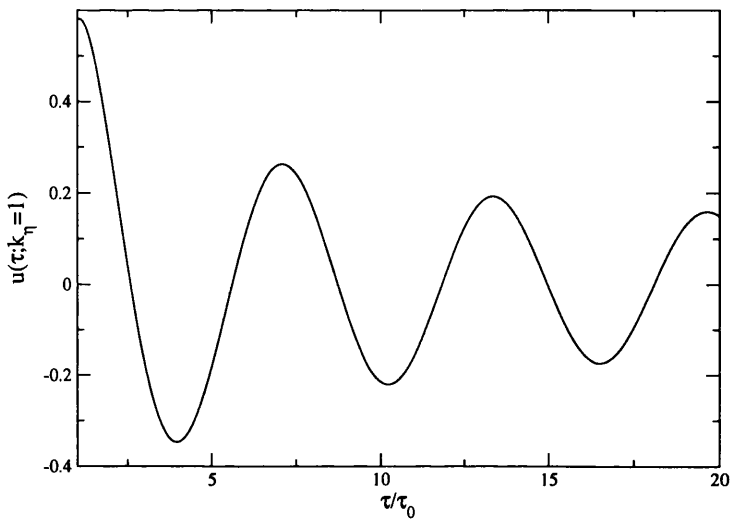

Figure 3.2: Time evolution of the free field solution $u(\tau, k_\eta = 1)$ in $1+1$ dimensions.

where an overdot denotes a proper-time derivative. This equation may be solved by either Bessel or Hankel functions[6]

$$\bar{f}_{\mathbf{k}}(\tau) = A\,\tau^{1/2} J_{-ik_\eta}\left(\sqrt{k_\perp^2 + m^2}\;\tau\right), \tag{3.23}$$

$$f_{\mathbf{k}}(\tau) = B\,\tau^{1/2} H^{(2)}_{ik_\eta}\left(\sqrt{k_\perp^2 + m^2}\;\tau\right), \tag{3.24}$$

where A and B are constants that may, without loss of generality, be taken to be real. It is also useful to know the complex conjugate mode functions,

$$\bar{f}^*_{\mathbf{k}}(\tau) = A\,\tau^{1/2} J_{ik_\eta}\left(\sqrt{k_\perp^2 + m^2}\;\tau\right), \tag{3.25}$$

$$f^*_{\mathbf{k}}(\tau) = \frac{B\,\tau^{1/2}}{\sinh \pi k_\eta}\left[J_{ik_\eta} - e^{-\pi k_\eta} J_{-ik_\eta}\right]. \tag{3.26}$$

Now we can write a general solution to (3.20) as

$$\begin{aligned}\phi(\tau, \mathbf{x}_\perp, \eta) &= \int \mathrm{d}^3\mathbf{k}\left[a_{\mathbf{k}} u_{\mathbf{k}}(\tau, \mathbf{x}_\perp, \eta) + a^\dagger_{\mathbf{k}} u^*_{\mathbf{k}}(\tau, \mathbf{x}_\perp, \eta)\right] \\ &= \int \mathrm{d}^3\mathbf{k}\left[\bar{a}_{\mathbf{k}} \bar{u}_{\mathbf{k}}(\tau, \mathbf{x}_\perp, \eta) + \bar{a}^\dagger_{\mathbf{k}} \bar{u}^*_{\mathbf{k}}(\tau, \mathbf{x}_\perp, \eta)\right].\end{aligned} \tag{3.27}$$

[6]In these expressions, k_η should be thought of as $\sqrt{k_\eta^2}$.

The solutions (3.21) can be plotted easily. In Fig. 3.2 we show the time evolution of $u(\tau; k_\eta = 1)$ (transformed to momentum space and plotted in $1+1$ dimensions). The envelope of oscillations is found to decrease $\sim \tau^{-1/2}$. This behaviour can also be seen analytically by examining the asymptotic form of the Hankel function,

$$H_\alpha^{(2)}(\tau) \to \sqrt{\frac{2}{\pi\tau}}\, e^{-i(\tau - \alpha\pi/2 - \pi/4)}, \tag{3.28}$$

valid for $\tau \gg |\alpha^2 - 1/4|$.

3.3.2 Quantisation

We now wish to quantise the theory on a $\tau = const$ hypersurface, so we will promote the coefficients $a_{\mathbf{k}}$ and $a_{\mathbf{k}}^\dagger$ to operators and impose the following equal proper-time commutation relations

$$[\phi(\tau, \mathbf{x}), \pi(\tau, \mathbf{x}')] = i\delta^3(\mathbf{x} - \mathbf{x}'), \tag{3.29}$$

where $\pi = \delta S/\delta(\partial_0\phi) = \sqrt{-g}\, g^{0\nu}\phi_{,\nu} = \tau\partial_\tau\phi$. Substituting (3.27) and (3.21) into (3.29), and taking the usual relations, $\left[a_{\mathbf{k}}, a_{\mathbf{k}'}^\dagger\right] = \delta_{\mathbf{k}\mathbf{k}'}$, gives the Wronskian condition for the mode functions

$$f_{\mathbf{k}}\dot{f}_{\mathbf{k}}^* - \dot{f}_{\mathbf{k}} f_{\mathbf{k}}^* = i\,, \tag{3.30}$$

which in turn tells us the constants A and B in the expressions for the mode functions

$$A = \left[\frac{2}{\pi}\sinh(\pi k_\eta)\right]^{-1/2}, \qquad B = \frac{\sqrt{\pi}}{2}\, e^{\pi k_\eta/2}. \tag{3.31}$$

The two sets of mode functions are related by a Bogoliubov transformation

$$\bar{f}_{\mathbf{k}} = \alpha_{\mathbf{k}} f_{\mathbf{k}} + \beta_{\mathbf{k}} f_{\mathbf{k}}^*, \tag{3.32}$$

with the coefficients $\alpha_{\mathbf{k}}$ and $\beta_{\mathbf{k}}$ given by

$$\alpha_{\mathbf{k}} = \left[\frac{e^{\pi k_\eta}}{2}\sinh\pi k_\eta\right]^{1/2}, \qquad \beta_{\mathbf{k}} = \left[\frac{e^{-\pi k_\eta}}{2}\sinh\pi k_\eta\right]^{1/2}. \tag{3.33}$$

Using (3.27) and (3.32) it is easy to show that the operators $a_{\mathbf{k}}$, $a_{\mathbf{k}}^\dagger$ and $\bar{a}_{\mathbf{k}}, \bar{a}_{\mathbf{k}}^\dagger$ are also related by a Bogoliubov transformation. From this we can see that the vacuum

state $|\,\bar{0}\rangle$ defined with respect to the operator $\bar{a}_{\mathbf{k}}$ will be inequivalent to the state $|\,0\rangle$ defined with respect to the operator $a_{\mathbf{k}}$. This leads to a choice of which vacuum state (i.e. which mode functions) to use in our calculations.

There exists an integral representation of the Hankel function [50]

$$H^{(2)}_{ik_\eta}(\gamma\tau) = \frac{i}{\pi}\, e^{-\pi k_\eta/2} \int_{-\infty}^{\infty} \mathrm{d}\rho\; e^{-i\gamma\tau\cosh\rho} e^{-ik_\eta\rho}, \tag{3.34}$$

from which, upon transforming back to Minkowski coordinates, we find

$$u_{\mathbf{k}}(t,\mathbf{x}) \propto \int_{-\infty}^{\infty} \mathrm{d}\rho\; e^{-i\omega_{\mathbf{p}}(\rho)t} e^{i\mathbf{p}(\rho)\cdot\mathbf{x}} e^{-ik_\eta\rho}, \tag{3.35}$$

where now $\mathbf{x} = (x,y,z)^T$, and

$$\begin{aligned} \omega_{\mathbf{p}}(\rho) &= \sqrt{k_\perp^2 + m^2}\cosh\rho, \\ p_1 = k_1, \quad p_2 = k_2, \quad p_3(\rho) &= -\sqrt{k_\perp^2 + m^2}\sinh\rho. \end{aligned} \tag{3.36}$$

From (3.35) we can see that the solutions involving $H^{(2)}$ are superpositions of purely positive frequency plane waves with respect to Minkowski time. Therefore the vacuum $|\,0\rangle$ defined with respect to the modes $f_{\mathbf{k}}$ is the usual Minkowski vacuum and the one we will calculate with[7].

3.3.3 Components of the energy-momentum tensor

If we define the expectation value of the particle number operator

$$\mathrm{Tr}\rho\, a^\dagger_{\mathbf{k}} a_{\mathbf{k}} = \langle a^\dagger_{\mathbf{k}} a_{\mathbf{k}}\rangle = \langle a_{\mathbf{k}} a^\dagger_{\mathbf{k}}\rangle - 1 = n_{\mathbf{k}}, \tag{3.37}$$

then we can calculate the four non-zero components of $\langle T_{\mu\nu}\rangle$ explicitly by substituting the expansions (3.27) and (3.21) into (3.15), giving

$$\langle T_{\tau\tau}\rangle \overset{\text{def}}{=} \varepsilon = \frac{1}{\tau}\int \frac{\mathrm{d}^3\mathbf{k}}{(2\pi)^3}\,(n_{\mathbf{k}} + 1/2)\left[|\dot{f}_{\mathbf{k}}|^2 - \frac{1}{\tau}\mathrm{Re}(\dot{f}_{\mathbf{k}} f^*_{\mathbf{k}})\right.$$

[7]Also, this vacuum is agreed upon by all comoving observers, i.e. observers who are moving *with* the expansion, as these observers live on worldlines of constant rapidity, and therefore experience a proper time $\tau \propto t$.

$$+\left(\frac{k_\eta^2+1/4}{\tau^2}+k_\perp^2+m^2\right)|f_{\mathbf{k}}|^2\Bigg], \tag{3.38}$$

$$\langle T_{11}\rangle \stackrel{\text{def}}{=} P_1 = \frac{1}{\tau}\int\frac{\mathrm{d}^3\mathbf{k}}{(2\pi)^3}(n_{\mathbf{k}}+1/2)\Bigg[|\dot{f}_{\mathbf{k}}|^2-\frac{1}{\tau}\mathrm{Re}(\dot{f}_{\mathbf{k}}f_{\mathbf{k}}^*) + \left(\frac{k_\eta^2-1/4}{\tau^2}-(k_1^2-k_2^2)+m^2\right)|f_{\mathbf{k}}|^2\Bigg], \tag{3.39}$$

$$\langle T_{22}\rangle \stackrel{\text{def}}{=} P_2 = \frac{1}{\tau}\int\frac{\mathrm{d}^3\mathbf{k}}{(2\pi)^3}(n_{\mathbf{k}}+1/2)\Bigg[|\dot{f}_{\mathbf{k}}|^2-\frac{1}{\tau}\mathrm{Re}(\dot{f}_{\mathbf{k}}f_{\mathbf{k}}^*) + \left(\frac{k_\eta^2-1/4}{\tau^2}-(k_2^2-k_1^2)+m^2\right)|f_{\mathbf{k}}|^2\Bigg], \tag{3.40}$$

$$\frac{\langle T_{\eta\eta}\rangle}{\tau^2} \stackrel{\text{def}}{=} P_\eta = \frac{1}{\tau}\int\frac{\mathrm{d}^3\mathbf{k}}{(2\pi)^3}(n_{\mathbf{k}}+1/2)\Bigg[|\dot{f}_{\mathbf{k}}|^2-\frac{1}{\tau}\mathrm{Re}(\dot{f}_{\mathbf{k}}f_{\mathbf{k}}^*) + \left(\frac{k_\eta^2+1/4}{\tau^2}-(k_\perp^2+m^2)\right)|f_{\mathbf{k}}|^2\Bigg]. \tag{3.41}$$

Notice that if $n_{\mathbf{k}} = n(\sqrt{k_1^2+k_2^2}, k_\eta)$ then we can let $k_1 \leftrightarrow k_2$ in (3.40), and we find that P_1 and P_2 are equal. This is equivalent to saying that the transverse momentum space is isotropic[8].

3.3.4 Connection between the mode functions and the statistical/spectral functions

Recall that the statistical function is defined in terms of the fields as

$$F(x,y) = \frac{1}{2}\langle\{\phi(x),\phi(y)\}\rangle. \tag{3.42}$$

[8]This will only be the case for precisely head-on collisions between the nuclei. In general collisions will not be head-on, and there will be real space transverse anisotropy which will result in a similar anisotropy in momentum space.

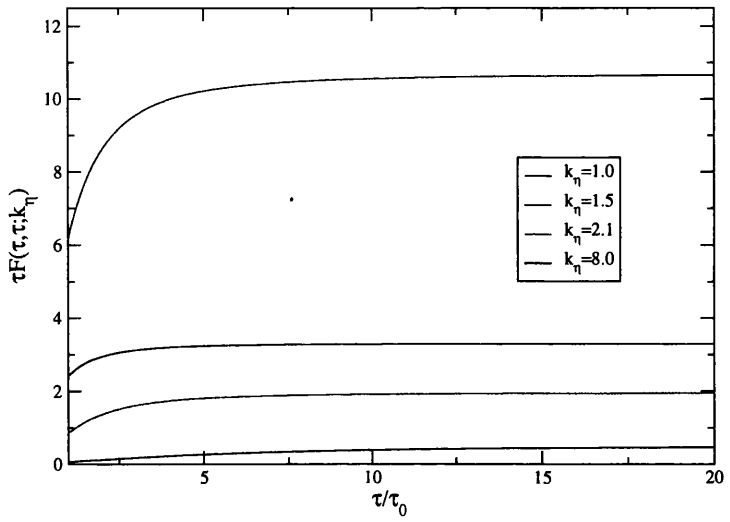

Figure 3.3: Time evolution of the equal-time statistical function $\tilde{F}(\tau,\tau;k_\eta)$ in $1+1$ dimensions for various momenta.

Explicitly, that is

$$F(\tau,\tau';\mathbf{x},\mathbf{x}') = \frac{1}{2}\langle\phi(\tau,\mathbf{x})\phi(\tau',\mathbf{x}') + \phi(\tau',\mathbf{x}')\phi(\tau,\mathbf{x})\rangle. \tag{3.43}$$

Substituting in the decomposition of the field given in (3.27), and defining the expectation value of the particle number operator $\mathrm{Tr}\rho\, a_{\mathbf{k}}^\dagger a_{\mathbf{k}} = \langle a_{\mathbf{k}}^\dagger a_{\mathbf{k}}\rangle = \langle a_{\mathbf{k}} a_{\mathbf{k}}^\dagger\rangle - 1 = n_{\mathbf{k}}$, this becomes

$$F(\tau,\tau';\mathbf{x},\mathbf{x}') = \int \mathrm{d}^3\mathbf{k}(n_{\mathbf{k}}+1/2)\left[u_{\mathbf{k}}(\tau,\mathbf{x})u_{\mathbf{k}}^*(\tau',\mathbf{x}') + u_{\mathbf{k}}(\tau',\mathbf{x}')u_{\mathbf{k}}^*(\tau,\mathbf{x})\right]. \tag{3.44}$$

Finally, substituting in (3.21) gives us an expression in terms of the mode functions

$$F(\tau,\tau';\mathbf{x}-\mathbf{x}') = \int \frac{\mathrm{d}^3\mathbf{k}}{(2\pi)^3}(n_{\mathbf{k}}+1/2)\frac{1}{\sqrt{\tau\tau'}}\left[\mathrm{e}^{i\mathbf{k}\cdot(\mathbf{x}-\mathbf{x}')}f_{\mathbf{k}}(\tau)f_{\mathbf{k}}^*(\tau') + \mathrm{conj.}\right], \tag{3.45}$$

which in momentum space reads simply

$$\tilde{F}(\tau,\tau';\mathbf{k}) = (n_{\mathbf{k}}+1/2)\left[f_{\mathbf{k}}(\tau)f_{\mathbf{k}}^*(\tau') + \mathrm{conj.}\right], \tag{3.46}$$

where $\tilde{F} = \sqrt{\tau\tau'}F$ (this rescaling will be discussed below). The evolution of this free

statistical function from 'tsunami' initial conditions[9] is shown in Fig. 3.3 for various momentum modes.

3.4 2PI evolution equations in an expanding background

Now that we are more familiar with Bjorken's coordinate system, we can specialise the equations of motion derived from the 2PI effective action in chapter 2 to this metric (we work in $3+1$ dimensions).

In order to manipulate the equations into the optimal form for numerical solution we will do two things. Firstly, assume that we have translational invariance in both the η-direction (a valid assumption that follows from the boost invariance described in section 3.1 provided we are working in the central rapidity region) and the directions perpendicular to the collision axis, and fourier transform the equations into momentum space. Secondly, we can rescale the propagators as follows[10]

$$\begin{aligned}\tilde{F}(\tau,\tau';\mathbf{x}-\mathbf{y}) &= \sqrt{\tau\tau'}F(\tau,\tau';\mathbf{x}-\mathbf{y})\\ \tilde{\rho}(\tau,\tau';\mathbf{x}-\mathbf{y}) &= \sqrt{\tau\tau'}\rho(\tau,\tau';\mathbf{x}-\mathbf{y})\end{aligned} \tag{3.47}$$

and the self energies

$$\begin{aligned}\tilde{\Sigma}_F(\tau,\tau';\mathbf{x}-\mathbf{y}) &= (\tau\tau')^{3/2}\Sigma_F(\tau,\tau';\mathbf{x}-\mathbf{y})\\ \tilde{\Sigma}_\rho(\tau,\tau';\mathbf{x}-\mathbf{y}) &= (\tau\tau')^{3/2}\Sigma_\rho(\tau,\tau';\mathbf{x}-\mathbf{y}).\end{aligned} \tag{3.48}$$

This gives the final form of the equations of motion

$$\begin{aligned}&\left[\partial_\tau^2+\frac{1/4+k_\eta^2}{\tau^2}+\mathbf{k}_\perp^2+M^2(\tau)\right]\tilde{\rho}(\tau,\tau';\mathbf{k})\\ &\qquad=-\frac{1}{\tau}\int_{\tau'}^{\tau}\frac{\mathrm{d}\tau''}{\tau''}\tilde{\Sigma}_\rho(\tau,\tau'';\mathbf{k})\tilde{\rho}(\tau'',\tau';\mathbf{k}),\end{aligned} \tag{3.49}$$

[9] See section 3.5.

[10] At late times we know that, due to the expansion, this system effectively becomes free. We found in the free field analysis that the late time behaviour of the mode function solutions was $\sim 1/\tau^{1/2}$, so this is a 'natural' rescaling of F and ρ that explicitly factors out this time dependence.

$$\left[\partial_\tau^2 + \frac{1/4 + k_\eta^2}{\tau^2} + \mathbf{k}_\perp^2 + M^2(\tau)\right]\tilde{F}(\tau,\tau';\mathbf{k})$$
$$= -\frac{1}{\tau}\int_{\tau_0}^{\tau}\frac{\mathrm{d}\tau''}{\tau''}\tilde{\Sigma}_\rho(\tau,\tau'';\mathbf{k})\tilde{F}(\tau'',\tau';\mathbf{k})$$
$$+\frac{1}{\tau}\int_{\tau_0}^{\tau'}\frac{\mathrm{d}\tau''}{\tau''}\tilde{\Sigma}_F(\tau,\tau'';\mathbf{k})\tilde{\rho}(\tau'',\tau';\mathbf{k}) \qquad (3.50)$$

where $\mathbf{k} = (k_\eta, \mathbf{k}_\perp)$, and

$$M^2(\tau) = m^2 + \delta m^2(\tau), \qquad (3.51)$$

with

$$\delta m^2(\tau) = \frac{\lambda}{2}\Big(\frac{N+2}{3N}\Big)\frac{1}{\tau}\int\frac{\mathrm{d}^3\mathbf{p}}{(2\pi)^3}\tilde{F}(\tau,\tau;\mathbf{p}). \qquad (3.52)$$

A few features of these equations can immediately be noted. Firstly, consider the longitudinal "momentum" k_η. I put "momentum" in quotes since it is not dimensionally/physically a momentum. Since the longitudinal coordinate η is dimensionless, so is its momentum-space counterpart k_η. However, in the equations of motion it appears as k_η/τ - a quantity we will consider to be the 'physical momentum'. Physically then, the longitudinal wave number of every mode decreases linearly with time, an effective red-shift as a consequence of the linear expansion of the background spacetime. At late times, the k_η-dependence (the term $(1/4 + k_\eta^2)/\tau^2$) drops out from the equations of motion.

Secondly consider the terms containing the interactions. Both the local interaction term included in $M^2(\tau)$ and the nonlocal memory integrals (right hand sides of (3.49) and (3.50)) are preceded by a factor of $1/\tau$. This factor suggests, as we might expect, that there will be a suppression of interactions as the system evolves in time. This consequence of the expanding background is necessary if the equations are to successfully reproduce the freeze-out observed in heavy ion collision experiments, where we expect interactions to be suppressed as the system becomes more and more dilute.

The same manipulations in the auxiliary-field formalism yield the rescalings

$$\tilde{D}_\rho(\tau,\tau';\mathbf{k}) = \tau\tau'\hat{D}_\rho(\tau,\tau';\mathbf{k}),$$
$$\tilde{D}_F(\tau,\tau';\mathbf{k}) = \tau\tau'\hat{D}_F(\tau,\tau';\mathbf{k}) \qquad (3.53)$$

for the auxiliary-field propagators, and for the self energies

$$\begin{aligned}\tilde{\Pi}_\rho(\tau,\tau';\mathbf{k}) &= \tau\tau'\Pi_\rho(\tau,\tau';\mathbf{k}),\\ \tilde{\Pi}_F(\tau,\tau';\mathbf{k}) &= \tau\tau'\Pi_F(\tau,\tau';\mathbf{k}).\end{aligned} \tag{3.54}$$

This leads to equations (3.50) and (3.49) for $\tilde{F}$ and $\tilde{\rho}$, and the additional equations of motion for the auxiliary-field propagators

$$\tilde{D}_\rho(\tau,\tau';\mathbf{k}) = -\tilde{\Pi}_\rho(\tau,\tau';\mathbf{k}) + \int_{\tau'}^{\tau}\frac{\mathrm{d}\tau''}{\tau''}\tilde{\Pi}_\rho(\tau,\tau'';\mathbf{k})\tilde{D}_\rho(\tau'',\tau';\mathbf{k}), \tag{3.55}$$

$$\begin{aligned}\tilde{D}_F(\tau,\tau';\mathbf{k}) = -\tilde{\Pi}_F(\tau,\tau';\mathbf{k}) &+ \int_{\tau_0}^{\tau}\frac{\mathrm{d}\tau''}{\tau''}\tilde{\Pi}_\rho(\tau,\tau'';\mathbf{k})\tilde{D}_F(\tau'',\tau';\mathbf{k})\\ &- \int_{\tau_0}^{\tau'}\frac{\mathrm{d}\tau''}{\tau''}\tilde{\Pi}_F(\tau,\tau'';\mathbf{k})\tilde{D}_\rho(\tau'',\tau';\mathbf{k}).\end{aligned} \tag{3.56}$$

The same observations about the red-shifting of the physical longitudinal momenta, and the suppression of interactions at late times apply equally to these auxilliary-field equations of motion.

We have now arrived at a set of self consistent, coupled equations for the propagators $\tilde{F}$ and $\tilde{\rho}$. The equations are inherently causal, in that at any given time τ_f all quantities can be obtained by integration over explicitly known functions for times $\tau < \tau_f$.

3.4.1 Energy and pressure

We can also calculate expressions for the energy density and longitudinal pressure of the system. The energy-momentum tensor is given by

$$T_{\mu\nu} = \partial_\mu\varphi_a(x)\partial_\nu\varphi_a(x) - g_{\mu\nu}\mathscr{L}. \tag{3.57}$$

The T_{00} component for our interacting theory reads

$$\begin{aligned}T_{00} = \frac{1}{2}\Big[&\partial_\tau\varphi_a(x)\partial_{\tau'}\varphi_a(x') + \partial_x\varphi_a(x)\partial_{x'}\varphi_a(x') + \partial_y\varphi_a(x)\partial_{y'}\varphi_a(x')\\ &+\frac{1}{\tau^2}\partial_\eta\varphi_a(x)\partial_{\eta'}\varphi_a(x') + m^2\varphi_a(x)\varphi_a(x')\Big]\Big|_{x=x'}\end{aligned}$$

$$+\frac{\lambda}{4!N}(\varphi_a(x)\varphi_a(x))^2. \tag{3.58}$$

Taking expectation values this becomes

$$\begin{aligned}\langle T_{00}\rangle \equiv \varepsilon &= \frac{N}{2}\Big[\partial_\tau\partial_{\tau'}F(x,x') + \partial_\perp^2 F(x,x') + \frac{1}{\tau^2}\partial_\eta\partial_{\eta'}F(x,x') + m^2F(x,x')\Big]|_{x=x'} \\ &\quad +\frac{\lambda}{4!N}\langle\varphi_a(x)\varphi_a(x)\varphi_b(x)\varphi_b(x)\rangle \\ &= \frac{N}{2}\Big[\partial_\tau\partial_{\tau'} + \partial_\perp^2 + \frac{1}{\tau^2}\partial_\eta\partial_{\eta'} + m^2 + \frac{\lambda}{12}\frac{N+2}{N}F(x,x)\Big]F(x,x')|_{x=x'} \\ &\quad +\frac{N}{4}\int_0^{x^0}\mathrm{d}z\Big[\Sigma_\rho(x,z)F(x,z) + \Sigma_F(x,z)\rho(x,z)\Big],\end{aligned} \tag{3.59}$$

where $\partial_\perp^2 = \partial_x\partial_{x'} + \partial_y\partial_{y'}$. Similarly, for the T_{33} component

$$\begin{aligned}\frac{\langle T_{33}\rangle}{\tau^2} \equiv P_\eta &= \frac{N}{2}\Big[\partial_\tau\partial_{\tau'}F(x,x') + \partial_\perp^2 F(x,x') + \frac{1}{\tau^2}\partial_\eta\partial_{\eta'}F(x,x') - m^2F(x,x')\Big]|_{x=x'} \\ &\quad -\frac{\lambda}{4!N}\langle\varphi_a(x)\varphi_a(x)\varphi_b(x)\varphi_b(x)\rangle \\ &= \frac{N}{2}\Big[\partial_\tau\partial_{\tau'} + \partial_\perp^2 + \frac{1}{\tau^2}\partial_\eta\partial_{\eta'} - m^2 - \frac{\lambda}{12}\frac{N+2}{N}F(x,x)\Big]F(x,x')|_{x=x'} \\ &\quad -\frac{N}{4}\int_0^{x^0}\mathrm{d}z\Big[\Sigma_\rho(x,z)F(x,z) + \Sigma_F(x,z)\rho(x,z)\Big].\end{aligned} \tag{3.60}$$

These equations can now be Fourier transformed and rescaled so they are written in terms of the same variables as the equations of motion (3.49) and (3.50). After these steps, the final expressions are

$$\begin{aligned}\langle T_{00}\rangle \equiv \varepsilon = \frac{N}{2}\frac{1}{\tau}\int\frac{\mathrm{d}^3\mathbf{k}}{(2\pi)^3}\Bigg(&\Big[\partial_\tau\partial_{\tau'} - \frac{1}{2}\Big(\frac{\partial_\tau}{\tau'} + \frac{\partial'_\tau}{\tau}\Big) + \frac{1/4+k_\eta^2}{\tau^2} + k_\perp^2 + m^2 \\ &+\frac{\lambda}{12}\Big(\frac{N+2}{N}\Big)\frac{1}{\tau}\int\frac{\mathrm{d}^3\mathbf{p}}{(2\pi)^3}\tilde{F}(\tau,\tau;\mathbf{p})\Big]\tilde{F}(\tau,\tau';\mathbf{k})|_{\tau=\tau'} \\ &+\frac{1}{2\tau}\int_{\tau_0}^{\tau}\mathrm{d}\tau''\frac{1}{\tau''}\Big[\tilde{\Sigma}_\rho(\tau,\tau'';\mathbf{k})\tilde{F}(\tau,\tau'';\mathbf{k}) + \tilde{\Sigma}_F(\tau,\tau'';\mathbf{k})\tilde{\rho}(\tau,\tau'';\mathbf{k})\Big]\Bigg),\end{aligned}$$

$$\frac{\langle T_{33}\rangle}{\tau^2} \equiv P_\eta = \frac{N}{2}\frac{1}{\tau}\int\frac{\mathrm{d}^3\mathbf{k}}{(2\pi)^3}\Bigg(\Big[\partial_\tau\partial_{\tau'} - \frac{1}{2}\Big(\frac{\partial_\tau}{\tau'} + \frac{\partial'_\tau}{\tau}\Big) + \frac{1/4+k_\eta^2}{\tau^2} + k_\perp^2 - m^2$$

$$-\frac{\lambda}{12}\Big(\frac{N+2}{N}\Big)\frac{1}{\tau}\int\frac{\mathrm{d}^3\mathbf{p}}{(2\pi)^3}\tilde{F}(\tau,\tau;\mathbf{p})\Big]\tilde{F}(\tau,\tau';\mathbf{k})|_{\tau=\tau'}$$
$$-\frac{1}{2\tau}\int_{\tau_0}^{\tau}\mathrm{d}\tau''\frac{1}{\tau''}\Big[\tilde{\Sigma}_\rho(\tau,\tau'';\mathbf{k})\tilde{F}(\tau,\tau'';\mathbf{k})+\tilde{\Sigma}_F(\tau,\tau'';\mathbf{k})\tilde{\rho}(\tau,\tau'';\mathbf{k})\Big]\Bigg),$$

where $k_\perp^2 = k_x^2 + k_y^2$. These expressions are related by the covariant conservation equation (3.17) (a numerical check of this statement will be discussed below).

3.5 Numerical solution

What does the solution to the problem look like when interactions are introduced? We are now equipped to perform and examine a numerical solution of the equations of motion derived from the 2PI effective action, using a truncation of either the loop- or the $1/N$-expansion[11].

We approach a numerical solution via discretisation on a space-time lattice, with the memory integrals calculated at every timestep (see appendix A for details of the numerical method). In order to evaluate the memory integrals, the NLO self energies should be calculated in position-space where they are simple products of the two-point functions. A fast-fourier transform routine is thus required to switch between the position- and momentum-space propagators and self energies.

The equations are perfectly suited to numerical solution; we begin by specifying correlation functions at τ_0, and then all correlators at a later time τ_f are obtained by integrating over known functions for times $\tau_0 \leq \tau < \tau_f$.

Since the computation time required to solve the full 3+1 dimensional theory is significant, we now restrict ourselves to the 1+1 dimensional case. In doing this, all previous expressions remain unchanged provided we replace $\mathbf{k}$ with k_η, and drop the $\mathbf{k}_\perp$ terms in (3.49) and (3.50) (and similar for the auxiliary field equations of motion),

$$\tilde{F}_{ab}(\tau,\tau';\mathbf{k}) \to \tilde{F}_{ab}(\tau,\tau';k_\eta), \tag{3.61}$$
$$\tilde{\rho}_{ab}(\tau,\tau';\mathbf{k}) \to \tilde{\rho}_{ab}(\tau,\tau';k_\eta), \tag{3.62}$$

and similarly for $\tilde{D}_F$, $\tilde{D}_\rho$ and the self energies.

We discretise the times in the equation as $\tau = na_\tau + \tau_0$, $\tau' = ma_\tau + \tau_0$ where

[11]Note that the rescalings introduced in section 3.4 have no effect on the self energy expressions derived in sections 2.4 and 2.5.

m and n are integers and a_τ is the time-step size[12], so that $\rho(\tau,\tau';p) \to \rho(n,m;p)$, $F(\tau,\tau';p) \to F(n,m;p)$ and the time derivatives/integrals are discretised as follows

$$\partial_\tau^2 F(\tau,\tau') \to \frac{1}{a_\tau^2}\Big[F(n+1,m)+F(n-1,m)-2F(n,m)\Big], \tag{3.63}$$

$$\int_{\tau_0}^{\tau} \mathrm{d}\tau F(\tau,\tau') \to a_\tau\Big[F(0,m)/2+\sum_{l=1}^{n-1}F(l,m)+F(n,m)/2\Big]. \tag{3.64}$$

For the spatial discretisation we use $\eta/a_\eta = 0,1,\ldots,N_s-1$ so that $p_\eta = 2\pi k/N_s a_\eta$, with $k=-N_s/2+1,\ldots,0,\ldots,N_s/2$. This leads to the following discretisation of the momentum integral

$$\int \frac{\mathrm{d}p_\eta}{2\pi}F(\tau,\tau';p_\eta) \to \frac{1}{N_s a_\eta}\Big[F(n,m;0)+2\sum_{k=1}^{N_\eta-2}F(n,m;k)+F(n,m;N_\eta-1)\Big] \tag{3.65}$$

where $N_\eta = N_s/2+1$ is the number of independent modes. Also, we find for the square of the momentum

$$p_\eta^2 \to \frac{4}{a_\eta^2}\sin^2(\frac{\pi k}{N_s}). \tag{3.66}$$

At late times, the extent of the time integrals ("memory integrals") on the right hand side of (3.50) becomes increasingly large, as they sum over the entire history of the evolution. This slows down the numerical evaluation dramatically at late time. Fortunately, the dependence of late time behaviour on early times is suppressed through the $1/\tau$ factor preceding the memory integrals. Thus, at late times, we will only integrate over a certain recent history of the system. The error introduced by leaving out early time information can be checked by performing a series of runs with an increasingly larger memory time.

In order to solve equations (3.49)-(3.50) and (3.55)-(3.56) we need to specify the initial state of the system. This may be done by providing an initial density matrix $\rho_D(\tau_0)$, or alternatively, by specifying all quantum correlation functions at the initial time. Here we will consider a general Gaussian density matrix which, in the symmetric regime, means that we only need to specify the initial 2-point correlation functions to fully specify the initial state[13].

[12]We include the initial time $\tau_0 \neq 0$ as there are factors of $1/\tau$ in the equations that would diverge were we to start from $\tau_0 = 0$.

[13]For a Gaussian density matrix, all higher correlation functions are given in terms of the 2-point

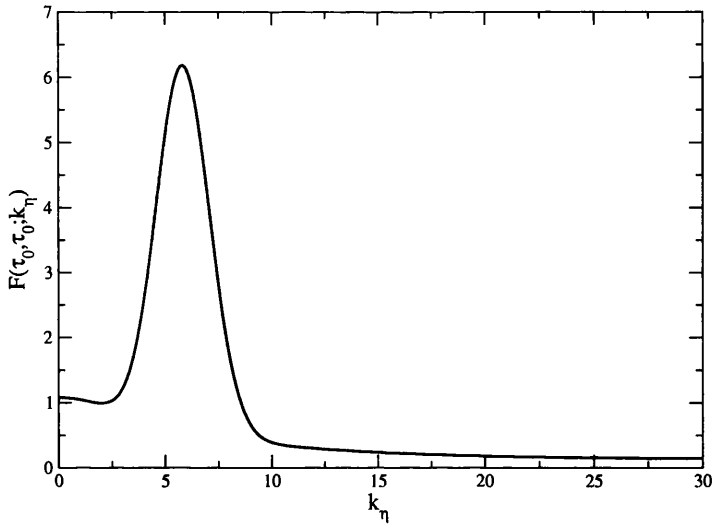

Figure 3.4: Tsunami initial conditions for $\tilde{F}(\tau_0, \tau_0; k_\eta)$.

The initial conditions for the spectral function are fixed by the equal-time commutation relations of the theory, which read (in $3+1$ dimensions)

$$[\phi(\tau, \mathbf{x}), \phi(\tau', \mathbf{y})]|_{\tau=\tau'} = 0, \tag{3.67}$$

$$[\pi(\tau, \mathbf{x}), \phi(\tau', \mathbf{y})]|_{\tau=\tau'} = -i\delta(\mathbf{x}-\mathbf{y}) \tag{3.68}$$

where $\pi = \delta S/\delta(\partial_0\phi) = \sqrt{-g}\, g^{0\nu}\phi_{,\nu} = \tau\partial_\tau\phi$. This leads to the following momentum space initial conditions for the rescaled spectral function

$$\tilde{\rho}(\tau, \tau'; k_\eta)|_{\tau=\tau'} = 0, \quad \partial_\tau\tilde{\rho}(\tau, \tau'; k_\eta)|_{\tau=\tau'} = 1. \tag{3.69}$$

For the statistical function and its derivatives we take the following form for the initial conditions, chosen in analogy with the free field case such that the statistical function and its second derivative differ by a factor of $\omega_{k_\eta}^2$,

$$\tilde{F}(\tau, \tau'; k_\eta)|_{\tau=\tau'=\tau_0} = \frac{1}{\omega_{k_\eta}}\Big[n_0(k_\eta) + \frac{1}{2}\Big], \quad \partial_\tau\tilde{F}(\tau, \tau'; k_\eta)|_{\tau=\tau'=\tau_0} = 0,$$
$$\partial_\tau\partial_{\tau'}\tilde{F}(\tau, \tau'; k_\eta)|_{\tau=\tau'=\tau_0} = \omega_{k_\eta}\Big[n_0(k_\eta) + \frac{1}{2}\Big], \tag{3.70}$$

functions (and also the 1-point functions, though these are equal to zero in the symmetric regime).

where the initial particle number $n_0(k_\eta) = n_{ts}(k_\eta) + n_B(k_\eta)$ describes a peaked "tsunami" $n_{ts}(k_\eta) = A\exp[-\frac{1}{2\sigma^2}(|k_\eta| - |k_{ts}|)^2]$ in a thermal background $n_B(k_\eta) = [\exp(\omega_{k_\eta}/T_0) - 1]^{-1}$. Note that this is a far-from-equilibrium initial condition, illustrated in Fig. 3.4. The initial mode energy $\omega_{k_\eta} = (k_\eta^2/\tau_0^2 + M^2)^{1/2}$, is calculated using the one-loop renormalised mass M, determined self consistently from the mean field mass gap equation. From the action we see that the coupling constant λ has dimension 2, accordingly we take λ/m^2 as a dimensionless coupling. The results in the next section were generated with $a_\tau/a_\eta = 0.1$, lattice spacing $am = 0.4$, and the number of 'rapidity modes' $L_\eta = 30$. We use $N = 4$ and set $m\tau_0 = 1$ throughout.

The initial conditions for $\hat{D}_\rho$ and $\hat{D}_F$ are determined by eqs. (3.55) and (3.56).

3.6 Results

I begin this section by presenting, in Fig. 3.5, a typical result obtained from a 3-loop truncation of the loop-expansion of the 2PI effective action in an expanding background. Fig. 3.5 was generated with a moderate value of the coupling strength ($\lambda/m^2 = 10$) and shows the time evolution of the equal-time statistical function[14] $\tilde{F}(\tau, \tau; k_\eta)$ for various modes k_η.

This plot illustrates some basic features common to results generated at various coupling strengths from both the loop- and $1/N$-expansions (to be presented below). The first feature of note is the behaviour at very early times ($m\tau \lesssim 10$). This initial rise in the occupation numbers, evident particularly in the modes near the peak of the tsunami (modes with high initial occupation numbers), will be shown to be described by a mean-field approximation. The mean-field approach exhibits a non-thermal fixed point, towards which the system heads at early times (before the influence of the memory integrals has had time to build up).

The next feature we notice is the rapid reduction in occupation number of the (initially) highly populated modes, and the contemporaneous increase in occupation of the (initially) less populated modes. This behaviour occurs over an intermediate time period and is indicative of the system's drive towards a state of thermal equilibrium. When the equations are solved in a nonexpanding background there is nothing to inhibit this drive towards equilibrium - the evolution progresses until the modes

[14] In a Minkowski space-time analysis, where the system is effectively defined in a box, one may define a particle number and study its evolution. However, there is no straightforward definition of particle number in our expanding coordinate system.

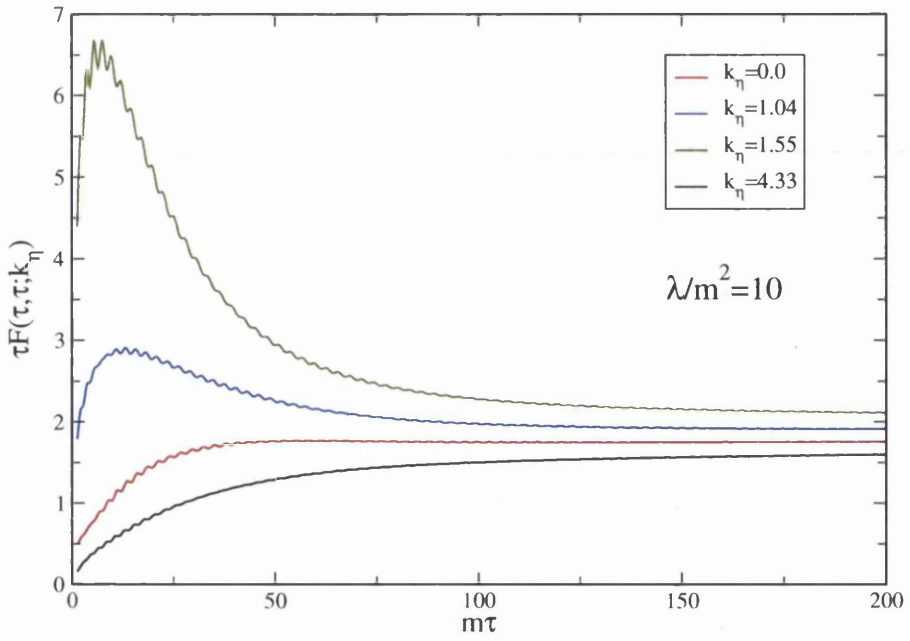

Figure 3.5: Time evolution of the equal-time statistical function $\tilde{F}(\tau, \tau; k_\eta)$, calculated from the loop-expansion at NLO, with $\lambda/m^2 = 10$.

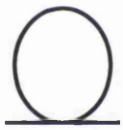

Figure 3.6: One-loop tadpole diagram that is included in the mean field approximation as a local, time-dependent mass correction.

reach their equilibrium occupation numbers (as demonstrated for scalar fields [15] and fermionic fields [18]) at late time.

In the results I present however, the tendency of the system to equilibrate is opposed by the expansion of the system. At late times, say $m\tau \gtrsim 100$ in Fig. 3.5, the effect of interactions in the system is diminished to the point that occupation numbers settle to fixed values and the subsequent evolution is essentially that of a free theory. This is the natural emergence of the phenomenon of freeze-out described in Sect. 3.1.

In the sections to follow I will discuss the early- intermediate- and late-time regimes in more detail, including an investigation into how changing the coupling strength affects the prospects of the system reaching equilibrium.

3.6.1 Early time mean-field evolution

The mean field approximation can be obtained from the exact evolution equations (3.49) and (3.50) simply by setting the integrals on the RHS of those equations to zero. The only place where interactions enter then is in the time-dependent mass $M^2(\tau)$ (see equation (3.52)), a local mass correction represented by the one-loop tadpole diagram (Fig. 3.6). In this approximation the equations for F and ρ decouple and describe the evolution of on-shell quasiparticles with a mass $M^2(\tau)$ determined from the gap equation.

An equivalent method for deriving the mean field approximation will make clear the existence of a non-thermal fixed point. Starting from the classical equation of motion for one scalar field $\phi(\tau, \mathbf{x}, \eta)$ in an expanding background, we have

$$\Big(\partial_\tau^2 + \frac{1}{\tau}\partial_\tau - \partial_\perp^2 - \frac{1}{\tau^2}\partial_\eta^2 + m^2 + \frac{\lambda}{6}\phi^2\Big)\phi = 0. \tag{3.71}$$

To be consistent with the formalism developed so far in this chapter, we make a rescaling $\tilde{\phi} = \sqrt{\tau}\phi$. The equation for $\tilde{\phi}$ is then

$$\Big(\partial_\tau^2 - \partial_\perp^2 - \frac{1}{\tau^2}\Big(\partial_\eta^2 - \frac{1}{4}\Big) + m^2 + \frac{\lambda}{6\tau}\tilde{\phi}^2\Big)\tilde{\phi} = 0. \tag{3.72}$$

We now work in an equal-time formulation, constructing the equal-time correlators ($\mathbf{x} = (\mathbf{x}_\perp, \eta)$),

$$\begin{aligned}
G_{\tilde{\phi}\tilde{\phi}}(\tau, \mathbf{x}-\mathbf{y}) &= \tilde{F}(\tau, \tau; \mathbf{x}-\mathbf{y}) = \langle\tilde{\phi}(\tau, \mathbf{x})\tilde{\phi}(\tau, \mathbf{y})\rangle, \\
G_{\tilde{\phi}\tilde{\pi}}(\tau, \mathbf{x}-\mathbf{y}) &= \partial_\tau\tilde{F}(\tau, \tau'; \mathbf{x}-\mathbf{y})|_{\tau=\tau'} = \frac{1}{2}\langle\tilde{\phi}(\tau, \mathbf{x})\tilde{\pi}(\tau, \mathbf{y}) + \tilde{\pi}(\tau, \mathbf{x})\tilde{\phi}(\tau, \mathbf{y})\rangle, \\
G_{\tilde{\pi}\tilde{\pi}}(\tau, \mathbf{x}-\mathbf{y}) &= \partial_\tau\partial_{\tau'}\tilde{F}(\tau, \tau'; \mathbf{x}-\mathbf{y})|_{\tau=\tau'} = \langle\tilde{\pi}(\tau, \mathbf{x})\tilde{\pi}(\tau, \mathbf{y})\rangle,
\end{aligned} \tag{3.73}$$

where $\tilde{\pi} = \partial_\tau\tilde{\phi}$.

In the mean field approximation, these correlators obey a closed set of equations that read, in momentum space ($\mathbf{k} = (\mathbf{k}_\perp, k_\eta)$),

$$\begin{aligned}
\partial_\tau G_{\tilde{\phi}\tilde{\phi}}(\tau, \mathbf{k}) &= 2G_{\tilde{\phi}\tilde{\pi}}(\tau, \mathbf{k}), \\
\partial_\tau G_{\tilde{\phi}\tilde{\pi}}(\tau, \mathbf{k}) &= G_{\tilde{\pi}\tilde{\pi}}(\tau, \mathbf{k}) - \omega_{\mathbf{k}}^2(\tau)G_{\tilde{\phi}\tilde{\phi}}(\tau, \mathbf{k}), \\
\partial_\tau G_{\tilde{\pi}\tilde{\pi}}(\tau, \mathbf{k}) &= -2\omega_{\mathbf{k}}^2(\tau)G_{\tilde{\phi}\tilde{\pi}}(\tau, \mathbf{k}),
\end{aligned} \tag{3.74}$$

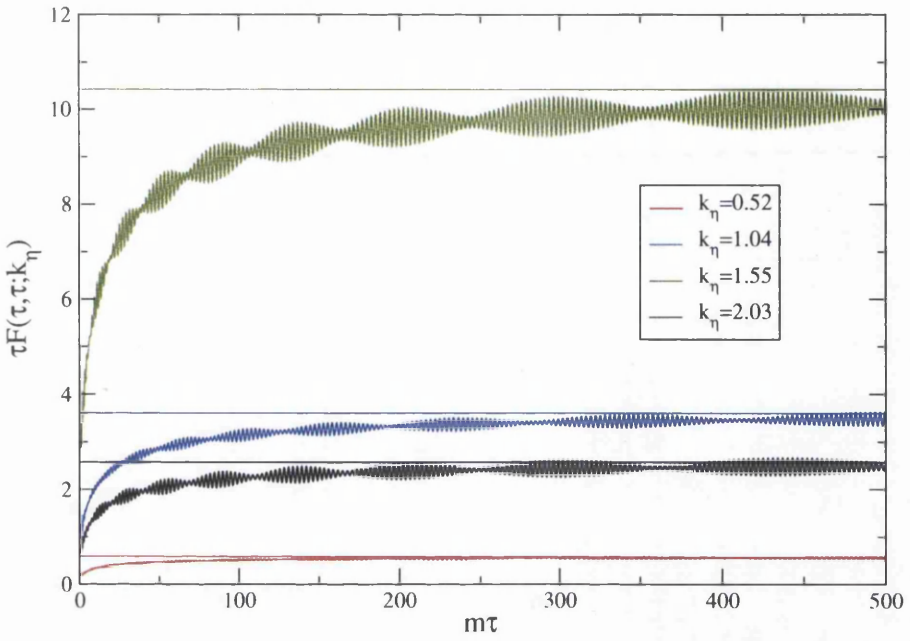

Figure 3.7: Approach to the fixed point in the mean field approximation.

where

$$\omega_{\mathbf{k}}^2(\tau) = \mathbf{k}_\perp^2 + \frac{k_\eta^2 + 1/4}{\tau^2} + m^2 + \frac{\lambda}{2\tau}\frac{(N+2)}{3N}\int_{\mathbf{k}} G_{\tilde{\phi}\tilde{\phi}}(\tau, \mathbf{k}), \tag{3.75}$$

It is straightforward to verify that these equations conserve the following combination

$$C(\mathbf{k}) = G_{\tilde{\phi}\tilde{\phi}}(\tau, \mathbf{k}) G_{\tilde{\pi}\tilde{\pi}}(\tau, \mathbf{k}) - G_{\tilde{\phi}\tilde{\pi}}^2(\tau, \mathbf{k}). \tag{3.76}$$

For a particular value of k_η, $\omega_{\mathbf{k}}$ becomes time independent at sufficiently late times, specifically $\omega_{\mathbf{k}}^2 \to \omega_{\mathbf{k}}^{*2} = \mathbf{k}_\perp^2 + m^2$. The fixed points of the equations are then

$$G_{\tilde{\pi}\tilde{\pi}}^*(\mathbf{k}) = \omega_{\mathbf{k}}^{*2} G_{\tilde{\phi}\tilde{\phi}}^*(\mathbf{k}), \qquad G_{\tilde{\pi}\tilde{\phi}}^*(\mathbf{k}) = 0, \tag{3.77}$$

and

$$C(\mathbf{k}) = G_{\tilde{\phi}\tilde{\phi}}^*(\tau, \mathbf{k}) G_{\tilde{\pi}\tilde{\pi}}^*(\tau, \mathbf{k}), \tag{3.78}$$

or

$$G_{\tilde{\phi}\tilde{\phi}}^*(\mathbf{k}) = \frac{\sqrt{C(\mathbf{k})}}{\omega_{\mathbf{k}}^*}, \qquad G_{\tilde{\pi}\tilde{\pi}}^*(\mathbf{k}) = \sqrt{C(\mathbf{k})}\,\omega_{\mathbf{k}}^*. \tag{3.79}$$

In Fig. 3.7 we solve the mean field equations numerically in 1+1d, with the tsunami

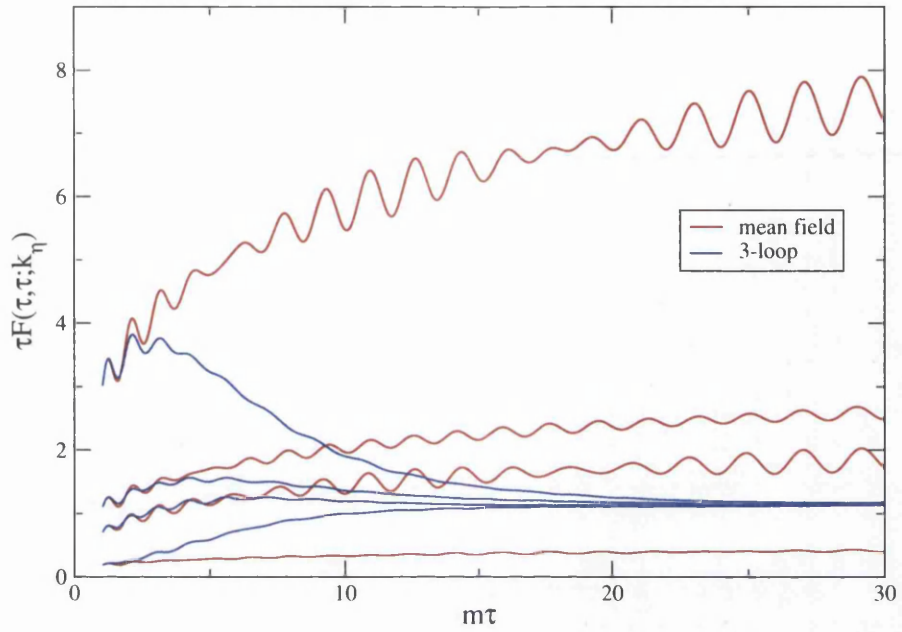

Figure 3.8: Early-time comparison of 3-loop and mean field approximations.

initial conditions described in Sect. 3.5, and $\lambda/m^2 = 30$. The horizontal lines in the figure correspond to the fixed point values $C(k_\eta)$, which we see the modes approaching at late times. The oscillations present in each mode are explained by the fact that there is little interaction between modes, and therefore little damping. In Fig. 3.8 we compare the mean field evolution with the 2PI loop expansion at NLO. The solutions follow each other at very early times, say $m\tau \lesssim 4$, which seems reasonable since the memory integrals in the loop expansion have had little time to 'build up'. The memory integrals are non-zero however, accounting for the small discrepancy between the approximations. Later, we see the solutions deviate significantly - the mean field solution continuing on towards the late-time fixed point, and the NLO solution becoming dominated by the interaction terms on the RHS of the equations of motion.

3.6.2 Intermediate time dynamics

In order to better understand the behaviour of the system in the intermediate time regime (commencing when we see deviation from the mean-field solution), it is instructive to examine the non-expanding case. This case has been extensively studied [15, 16, 17, 18], with results demonstrating that the equal-time statistical functions

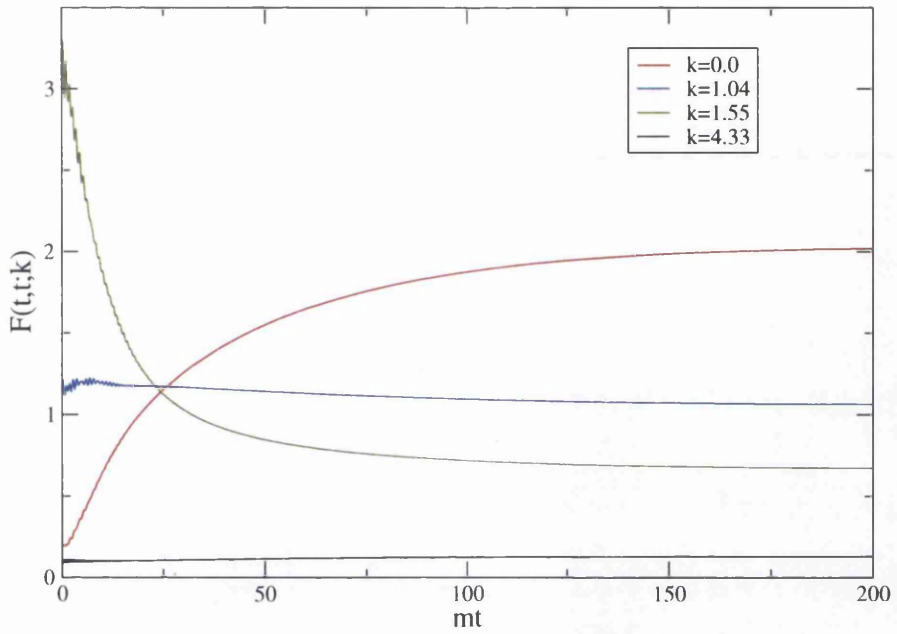

Figure 3.9: Time evolution of $F(t,t;k)$ showing level crossing in a non-expanding system, with $\lambda/m^2 = 30$.

for all modes approach their equilibrium values at late times. A clear indicator of this behaviour is the appearance of "level crossing". This is reproduced in Fig. 3.9 showing the time evolution of the equal time statistical function $F(t,t;k)$, calculated from the NLO loop expansion in Minkowski space-time. Here we observe that the initially highly occupied tsunami modes "decay" with increasing time, while the lower momentum modes increase in population. The distinctive crossing of the low momentum and "tsunami" modes occurs as the initial state in Fig. 3.4 evolves towards a Bose-Einstein equilibrium distribution.

Fig. 3.10 shows the equivalent system evolving in an expanding background (exactly the same parameters were used here as in Fig. 3.9). A few differences from the nonexpanding case are immediately apparent. Firstly, we see that the initial rise in occupation numbers described by the mean field approximation (in the expanding case) is absent in the nonexpanding case. Since the mean field approximation amounts to ignoring the memory integrals, this can be understood by examining the time-dependent mass correction (see equation (3.52)). In the expanding case, the factor of $1/\tau$ appearing in $\delta m^2(\tau)$ naively results in an effective mass that decreases with time. Considering that the equal time correlator, at early times, behaves inversely as a function of the mass (see equation (3.70)), we expect to see the initial rise in

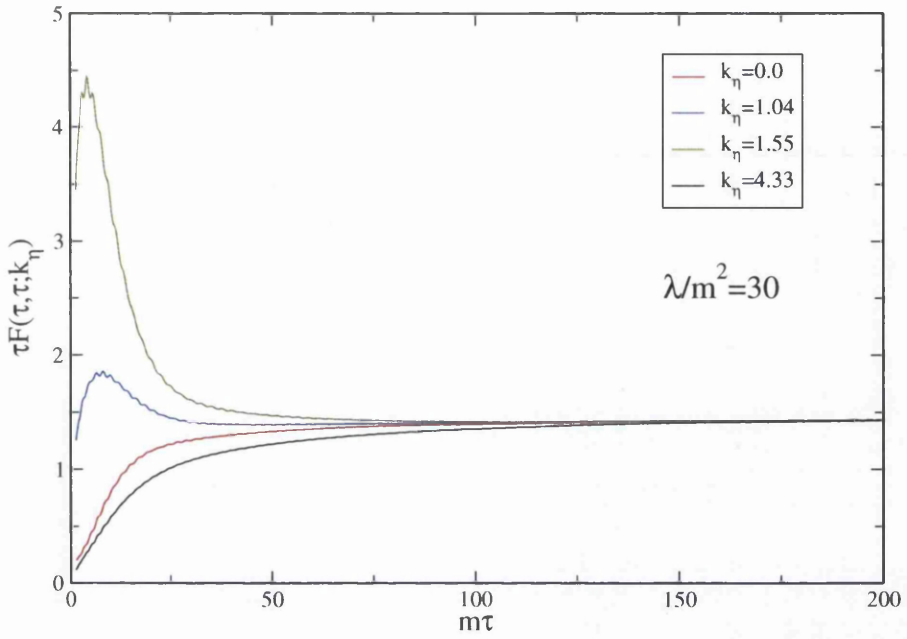

Figure 3.10: Time evolution of the equal-time statistical function $\tilde{F}(\tau, \tau; k_\eta)$, calculated from the loop-expansion at NLO, with $\lambda/m^2 = 30$.

occupation numbers. In the nonexpanding mean field approximation however, no factor of $1/t$ is present in the mass correction, $\delta m^2(t)$, and it follows that we should not expect the same initial rise in occupation numbers.

This difference notwithstanding, we can recognise the subsequent evolution in the expanding case as a drive towards equilibrium. The same rapid decrease in occupation of the tsunami modes, combined with the increase in population of the low momentum modes is seen in both cases.

The major difference then is at late times, where the consequences of the expanding background become all important. The most obvious of these consequences is that no level crossing occurs - the curves corresponding to different k_η either retain their ordering from the initial conditions as in Fig. 3.5, or lie precisely on top of each other at late times as in Fig. 3.10, but they do not cross. Clearly, this behaviour excludes the possibility of the modes reaching the equilibrium occupation numbers seen in the nonexpanding case. To understand this, we must revisit one of the considerations touched upon in Sect. 3.4. The longitudinal "momentum" k_η, being the momentum-space counterpart of the dimensionless quantity η, is not a physical momentum. The dimensionally correct quantity that appears in the equations of motion is k_η/τ which I will call the 'physical momentum'. As the system evolves, the physical momenta

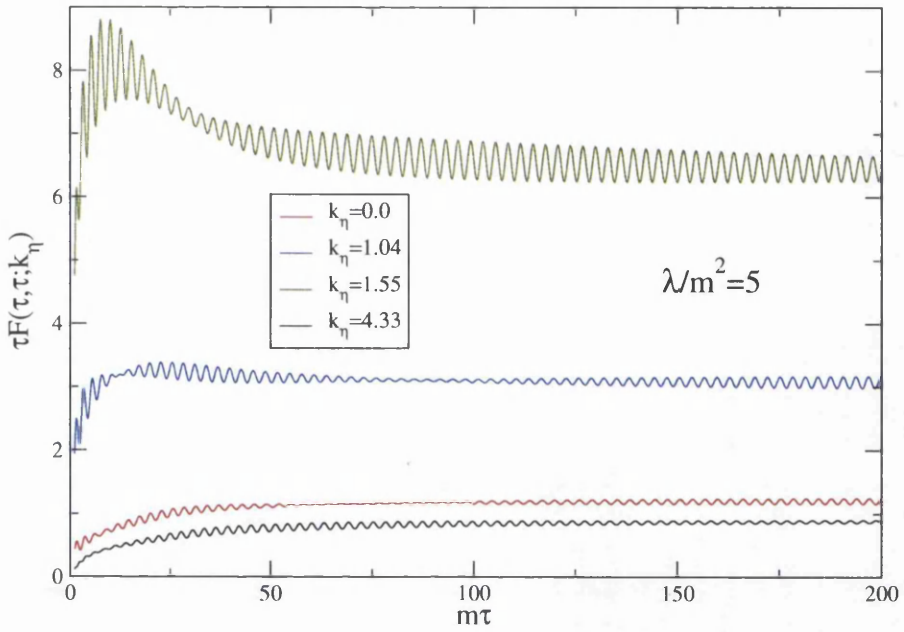

Figure 3.11: Time evolution of the equal-time statistical function $\tilde{F}(\tau, \tau; k_\eta)$, calculated from the loop-expansion at NLO, with $\lambda/m^2 = 5$.

of all modes experience a red-shift as a direct result of the linear expansion of the background space-time. At late times, all initial modes are essentially red-shifted to zero momentum, and therefore would all have the same thermal equilibrium occupation number - that of the zero-mode. It follows that the characteristic 'level crossing' observed in the nonexpanding case is not something we should necessarily expect to see in an expanding background.

The question to ask then is what, if anything, would be an indicator of equilibration for a system in an expanding background?

3.6.3 Late time memory loss and freeze-out

A comparison of Figs. 3.5 and 3.10, with coupling strengths $\lambda/m^2 = 10$ and 30 respectively, illustrates the phenomenon of *memory loss*. That is, in the latter case different modes evolve to reach precisely the same occupation number at late times. In the process, any information about the relative ordering of the modes in the initial state is lost. Conversely in the more weakly coupled case, the modes at late times *do* retain information about the initial conditions since they remain ordered in the same way they were at τ_0. One of the key properties of a system in equilibrium is that, as

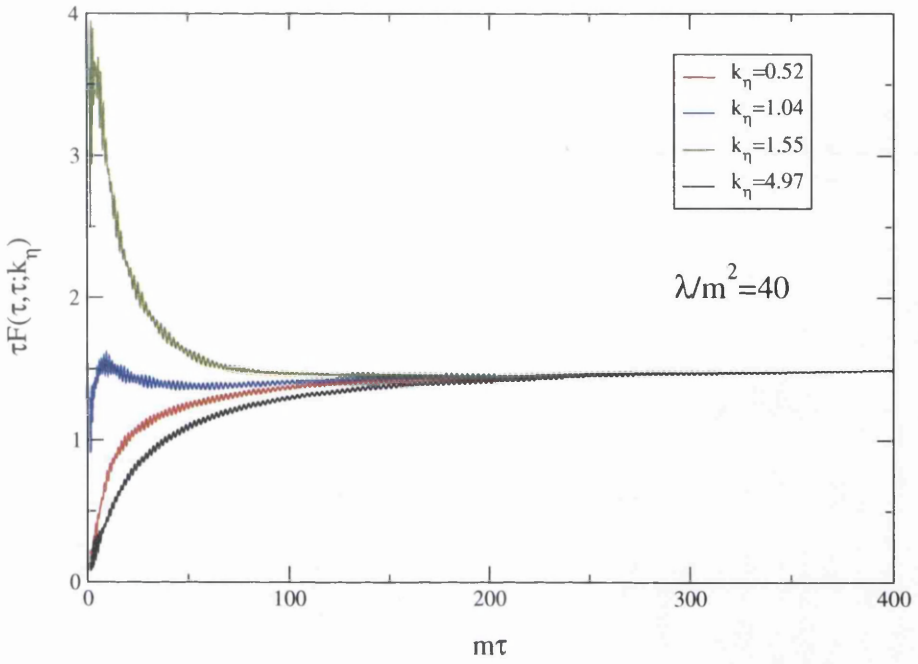

Figure 3.12: Time evolution of the equal-time statistical function $\tilde{F}(\tau, \tau; k_\eta)$, calculated from the $1/N$-expansion at NLO, with $\lambda/m^2 = 40$.

a result of universality, it is independent of (i.e. retains no memory of) details of the initial state, only having a dependence on the initial energy density (this dictates the temperature of the equilibrated system).

Following from this observation then, we can conclude that the more weakly coupled system cannot have equilibrated since 1) level crossing is absent, and 2) memory of the initial state is retained through the ordering of the modes. At stronger coupling, the situation is ambiguous. Level crossing is again absent, but as I have shown, this isn't a guarantee that the system hasn't equilibrated. The fact that the modes all converge to the same value suggests that their physical momenta have been effectively red-shifted to zero momentum, resulting in a loss of details of the initial state.

Having analysed in detail the early- and intermediate-time regimes, we now come to the late-time behaviour. As is clear from the plots that have just been discussed, there comes a point beyond which there is essentially no interaction between different modes (say, for $m\tau \gtrsim 120$). Once this point has been reached, each mode has effectively settled at its 'final' occupation number and will remain there indefinitely. Therefore, examining the evolution for arbitrarily long times will never result in new behaviour, for example the appearance of level crossing. The final occupation num-

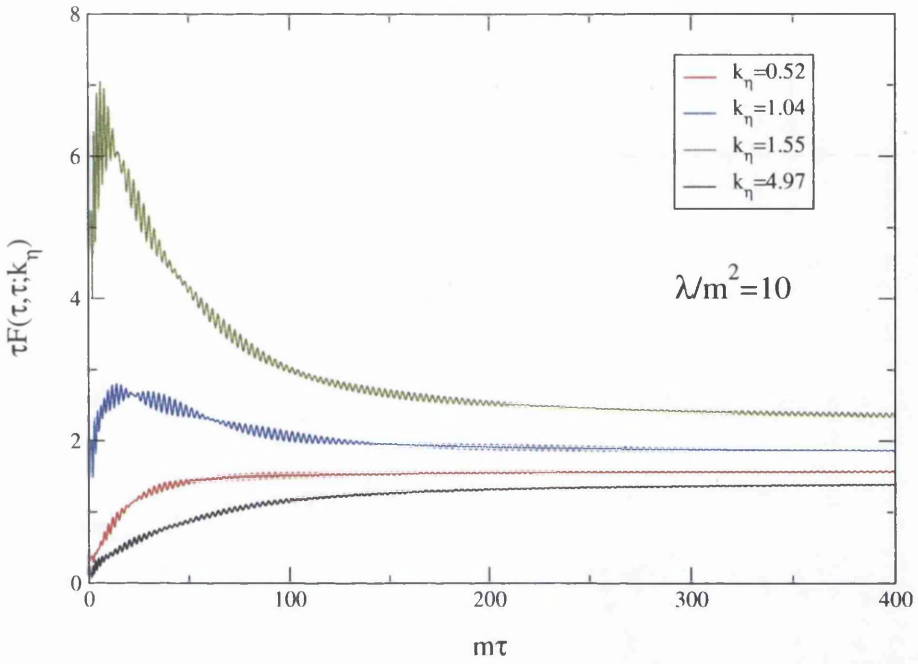

Figure 3.13: Time evolution of the equal-time statistical function $\tilde{F}(\tau, \tau; k_\eta)$, calculated from the $1/N$-expansion at NLO, with $\lambda/m^2 = 10$.

bers reached in Fig. 3.10 are difficult to quantify since occupation numbers are not clearly defined in our continually expanding system. One measure would be the vacuum contribution to the initial occupation numbers (the factor of one-half in (3.70)), with respect to which the final value reached by the statistical function certainly cannot be said to be large.

The suppression of interactions at late time indicates the onset of freeze-out. Physically, this corresponds to the regime where the average distance between particles exceeds the range of strong interactions, resulting in a freely evolving system. I emphasise that freeze-out emerges naturally from the 2PI effective action formalism when formulated in an expanding background. This is in contrast with other formalisms (e.g. hydrodynamics) where freeze-out is an *ad hoc* addition.

Fig. 3.11 shows the evolution at still weaker coupling. Here the modes barely approach each other before the system freezes out. Comparing this with the two previous results at stronger coupling, we can clearly see the 'competition' of interaction *vs.* expansion. In a strongly coupled system the drive towards equilibrium is far more pronounced, whereas a weakly coupled system freezes out long before it approaches an equilibrated state.

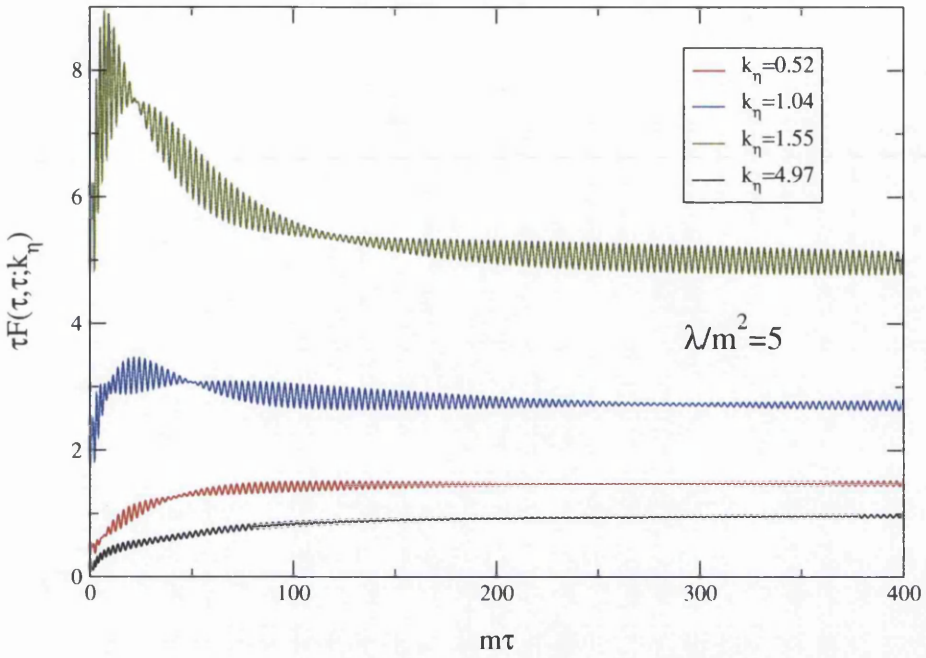

Figure 3.14: Time evolution of the equal-time statistical function $\tilde{F}(\tau, \tau; k_\eta)$, calculated from the $1/N$-expansion at NLO, with $\lambda/m^2 = 5$.

The way by which freeze-out emerges from the 2PI formalism is understood by examining the equations of motion (3.49)-(3.52) at late time, specifically the terms involving factors of $1/\tau$. In the large-τ limit, the memory integrals on the RHS vanish, as do the $(1/4 + k_\eta^2)/\tau^2$ terms, whilst $M^2(\tau) \to m^2$. As a result, the equations of motion reduce to those of a simple harmonic oscillator, with the following solution

$$F(\tau, \tau'; k_\eta) = A(k_\eta)\cos(m\tau)\cos(m\tau') + B(k_\eta)\sin(m\tau)\sin(m\tau') \tag{3.80}$$

which gives for the equal-time correlator

$$F(\tau, \tau; k_\eta) = A(k_\eta) + [B(k_\eta) - A(k_\eta)]\sin^2(m\tau). \tag{3.81}$$

The initial conditions for this free evolution must be determined from the occupation numbers of the modes at the time of freeze-out. The coefficients $A(k_\eta)$ correspond to the final occupation numbers of the modes k_η. At strong enough coupling, such that all modes tend to the same final occupation number, $A(k_\eta)$ will be a k_η-independent constant, A. The combination $B(k_\eta) - A(k_\eta)$ gives the amplitude of

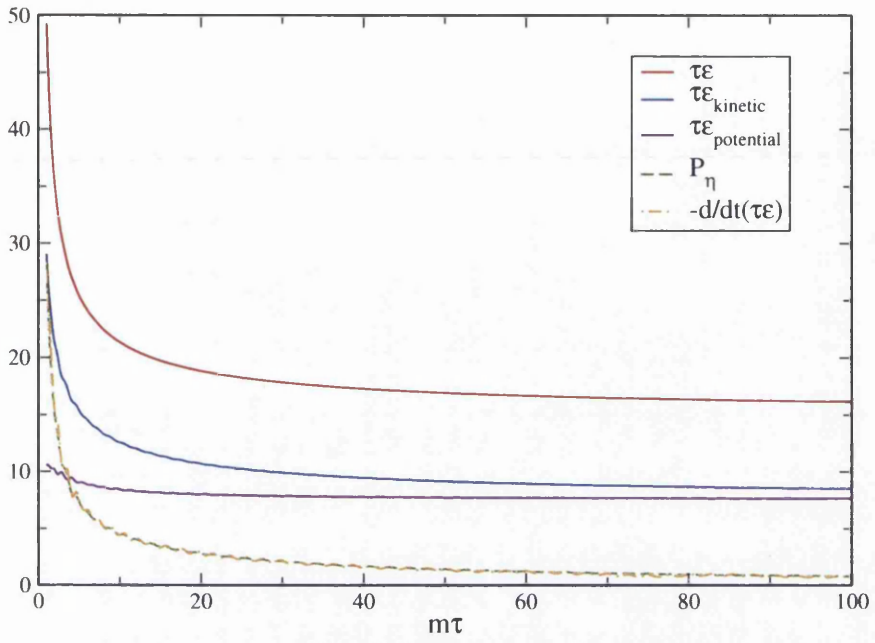

Figure 3.15: Various components of the energy.

oscillations around $A(k_\eta)$ - this is almost zero at stronger coupling, but can become large at weak coupling as a result of less damping, as seen in Fig. 3.11.

In Figs. 3.12, 3.13 and 3.14 I present similar results obtained from the 2PI-$1/N$ expansion at NLO. The general features of the evolution are very similar to those seen in the loop expansion, with early-time mean field-type behaviour, an intermediate time period consisting of a drive towards equilibrium, and the onset of freeze out at late times with strongly coupled systems exhibiting memory loss that isn't present at weaker couplings. We observe less damping of oscillations from the $1/N$-expansion due to the effective coupling being slightly weaker than in the loop-expansion.

In Fig. 3.15 various components of the energy are shown to decrease over time as one would expect for a system in an expanding background. Slightly rearranging the covariant conservation equation (3.17) yields the following equation relating the energy density ε and the longitudinal pressure P_η

$$-\frac{\mathrm{d}}{\mathrm{d}\tau}(\tau\varepsilon) = P_\eta. \tag{3.82}$$

These two quantities are also plotted in Fig. 3.15 and found to agree, verifying that the energy density behaves as expected.

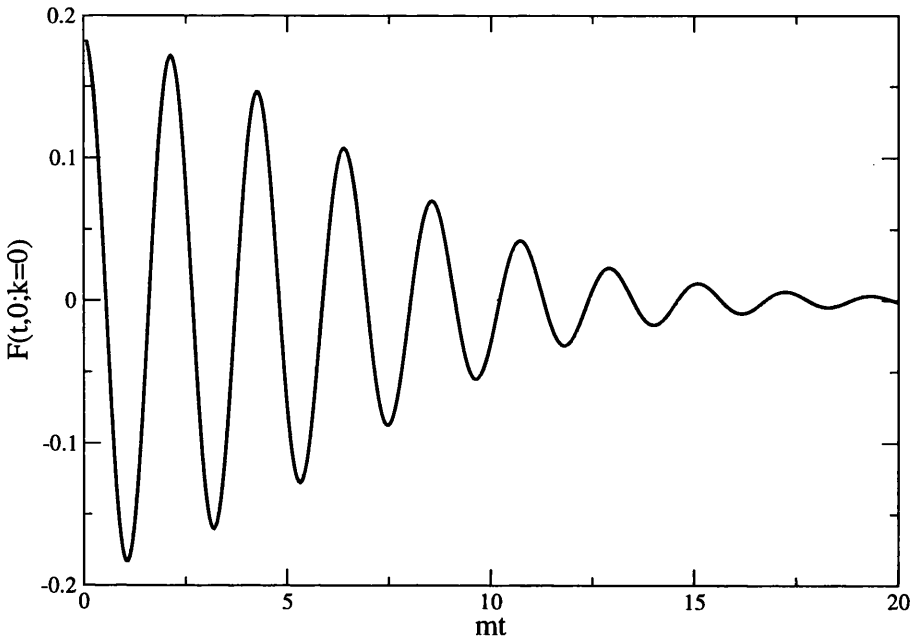

Figure 3.16: Time evolution of the unequal-time statistical function $F(t, 0; k = 0)$ in a non-expanding system.

3.6.4 Unequal-time correlators and memory loss

In Fig. 3.16 I show the time evolution of the unequal-time statistical function $F(t, 0; k = 0)$ for a nonexpanding system. We observe strong damping, such that the amplitude has almost decreased to zero by $mt = 20$. This demonstrates a strong reduction of correlations between the field at time t, and the initial field. This is also indicative of a rapid loss of 'memory' of the initial state, even though at this early time the system may still be far from equilibrium.

The same quantity, for a system in an expanding background, is shown in Fig. 3.17. Again we see damping, however, the damping rate lessens as the evolution progresses until there is essentially no damping at large times. This behaviour is another manifestation of the onset of freeze-out. Once freeze-out has occured and the system is evolving freely there are no longer any of the scattering processes that lead to damping of the unequal-time correlator.

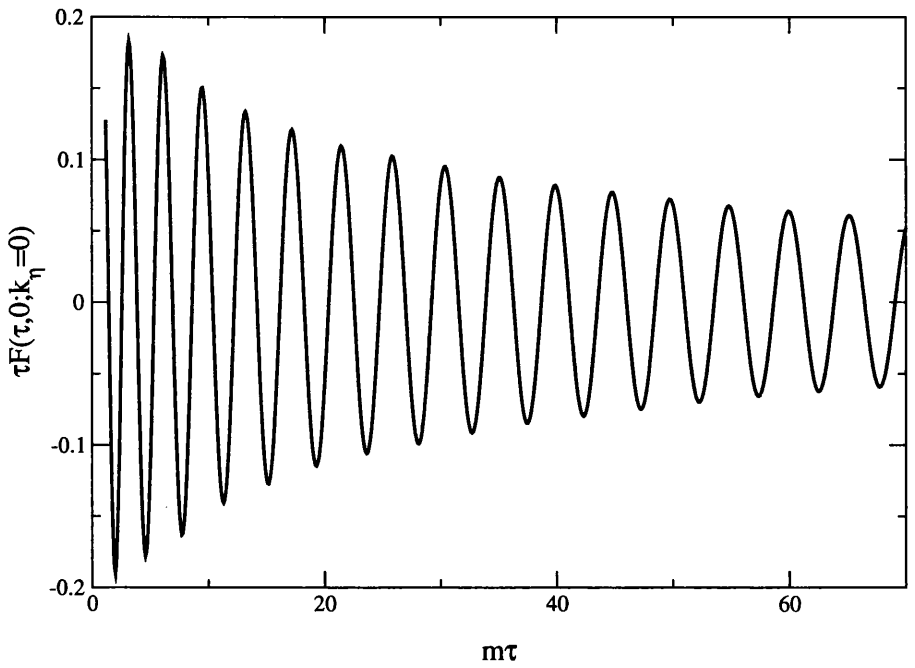

Figure 3.17: Time evolution of the unequal-time statistical function $\tilde{F}(\tau, 0; k_\eta = 0)$ in an expanding system.

3.7 Adding momentum modes

When discretising the system on a space-time lattice for numerical solution, we wrote the momentum k as

$$k = 2\pi n / N_s a \tag{3.83}$$

with $n = -N_s/2 + 1, \ldots, 0, \ldots, N_s/2$. In doing this we introduced a fixed cutoff on comoving momenta at $k_{max} = \pi/a$. This results in a cutoff on physical momenta that decreases linearly with time (since $k_{phys} = k/\tau$).

As we have seen, the fact that physical momenta are effectively shifted to zero as the system evolves makes it hard to discuss equilibration, since at strong couplings all modes approach the same occupation number at late times. In an attempt to retain the influence of higher (physical) momentum modes, one might consider imposing a *fixed cutoff on physical momenta.* Taking a physical momentum cutoff of Λ would then result in a cutoff on comoving momenta that increased as $\Lambda\tau$.

In order to implement this, we have to introduce new momentum modes to the system over time. Modes that initially have $k_{phys} > \Lambda$, should be introduced as and when their physical momenta drop below the cutoff. For initial conditions where the

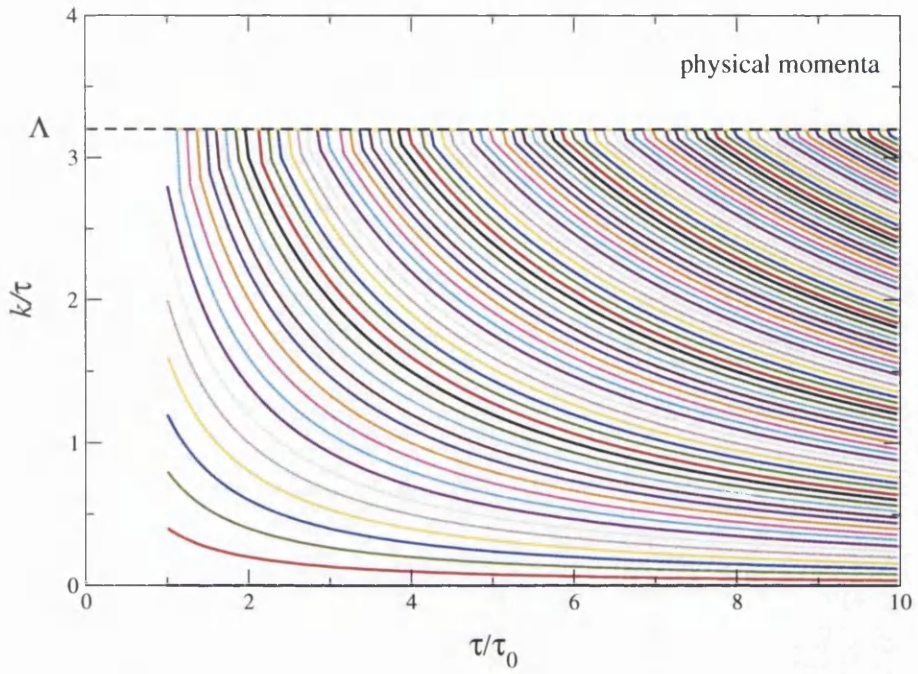

Figure 3.18: The addition of physical momenta at the cutoff, as a function of τ/τ_0.

initial occupation number goes to zero for large momenta (for example, the tsunami initial conditions described in section 3.5), the added modes should be initialised in vacuum. Fig. 3.18 illustrates the addition of physical momentum modes at the cutoff Λ with increasing time.

Adding momentum modes in this fashion places large demands on CPU memory, since every time a mode is added the size of each array increases by a factor of N_τ^2, where N_τ is the size of the memory kernel. The limited availability of CPU memory then translates into a maximal accessible time, τ_{max}. We can write the cutoff on comoving momenta as

$$k_{max}(\tau) = \Lambda\tau/\tau_0 = \Delta k N(\tau), \tag{3.84}$$

where Δk is the spacing between momentum modes (fixed at τ_0), and $N(\tau)$ is the number of modes at time τ. This gives the following expression for $N(\tau)$

$$N(\tau) = \frac{\Lambda}{\Delta k}\frac{\tau}{\tau_0}. \tag{3.85}$$

The initial number of modes is $N_0 = N(\tau_0) = \Lambda/\Delta k$. If we then specify the maximum number of modes, N_{max}, that would fit onto our CPU, we can deduce the maximum

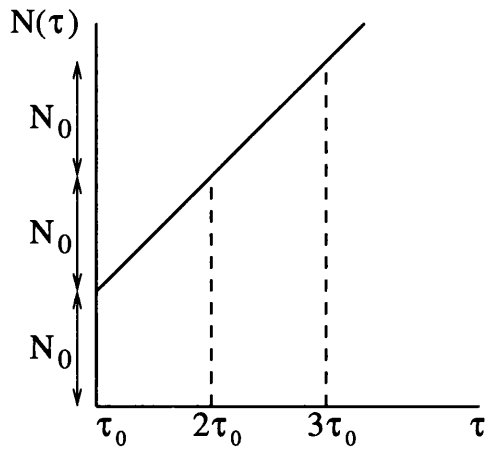

Figure 3.19: Linear addition of momentum modes.

time accessible,

$$\frac{N_{max}}{N_0} = \frac{\tau_{max}}{\tau_0}. \tag{3.86}$$

Fig. 3.19 illustrates the linear addition of momentum modes, spacing Δk, to the system. In each period of time of length τ_0, N_0 modes are added; however, since the time discretisation is much finer than the mode spacing, many time steps pass between each addition of a new mode.

I attempted to implement this technique for very short times in the mean field approximation. The results suggested that the added modes, initialised in vacuum, have little effect on the tsunami modes that are present at $\tau = \tau_0$, though one would want to go to larger times to verify that this is indeed the case.

3.8 Conclusions

The aim of this chapter was to study the real-time evolution of a far-from-equilibrium quantum system in a longitudinally expanding space-time background. We modelled the expansion by implementing a reparameterisation of space-time that replaces the Minkowski coordinates (t, z) with proper time/rapidity coordinates (τ, η), leading to an anisotropic and time-dependent metric. To better understand the consequences of this expanding background the case of a free scalar field was solved analytically in terms of time-dependent mode functions. The free field solutions were found to behave $\sim \tau^{-1/2}$ at late times, and the energy density was found to decrease as dictated by the covariant conservation of the energy-momentum tensor.

We next turned to the 2PI effective action in order to study the nonequilibrium evolution of an $O(N)$ model, with a φ^4 interaction. Exact, causal, real-time evolution equations were derived for the statistical and spectral two-point functions in an expanding background, and NLO truncations of the self-energies in both loop- and $1/N$-expansions were developed.

In performing a numerical solution, starting from highly nonequilibrium initial conditions, we found the evolution of the equal-time statistical function to show three distinct types of behaviour on different time scales:

1. **early-time mean field-type behaviour**

   - evolution well described by a mean-field approximation
   - interactions have a diminished role
   - evolution characterised by the presence of a non-thermal fixed point

2. **intermediate-time drive towards equilibrium**

   - interactions dominate, driving the system towards equilibrium
   - no level crossing observed, even at strong coupling

3. **late-time memory loss and freeze out**

   - interactions suppressed at large times such that the system becomes essentially free, indicating the onset of freeze out
   - strong coupling: modes all settle to the same final occupation number, memory of initial conditions is lost
   - weak coupling: modes settle to different final occupation numbers, memory of initial conditions is retained

The absence of level crossing is understood to be due to the effective red-shift of physical momenta. This behaviour limits our ability to study equilibration in the system, since even at strong coupling, all physical momenta are essentially shifted to zero before level crossing can occur. At strong coupling however, the system exhibits memory loss of details of the initial state. It follows that we cannot rule out the possibility that the system has equilibrated.

The evolution of the unequal-time statistical function exhibits damping that decreases with time, with no damping at late times. This is consistent with the onset

of freeze out, since we expect no damping once the system becomes free. Finally, as in the free field case the energy density and longitudinal pressure of the system are found to evolve such that they covariantly conserve the energy momentum tensor.

An attempt to introduce additional momentum modes to the system over time, in order to have a fixed physical momentum cutoff, can be implemented. However, it places large demands on CPU memory and therefore has only been tested for very short times.

Chapter 4

Effective convergence of the $1/N$ expansion for nonequilibrium field dynamics

Applications of 2PI effective action techniques are based on truncations, employing either a weak coupling or a large N expansion. In work done so far, truncations stop at relatively low order: until now all studies in field theory use next-to-leading order (NLO) truncations in the coupling or $1/N$ [1]. The reason for this situation is clear: beyond NLO the complexity of the equations and the numerical effort required to solve them increases dramatically [30]. In this chapter I will discuss the extension of the evolution equations to next-to-next-to-leading order (N^2LO) and present the first results beyond NLO in field theory.

Remarkably, the lowest order truncations beyond mean field theory include already many of the physical processes necessary to describe quantum field dynamics both far from and close to equilibrium and are capable of capturing effective memory loss, universality of late time evolution, and thermalization. The natural question to ask then is how accurately a truncation at a given order describes the dynamics in the full theory. There are several ways this can be investigated. In the case of a systematic expansion, it should be possible to compare different orders of the expansion, shedding light on the effective convergence. When restricting to LO and NLO truncations

[1] Mean field (leading order $1/N$ or Hartree) approximations will be referred to as leading order (LO). It should also be noted that due to the effective resummation inherent in the 2PI approach, infinite series of perturbative diagrams are included.

(2) (3) (4)

Figure 4.1: NLO and N^{2}LO contributions to Γ_2 in the $1/N$ expansion. The scalar propagator G is denoted with a full line and the auxiliary-field propagator D with a dashed line.

only, the applicability of this approach is limited. The reason is that in LO mean field approximations scattering is absent and there is no notion of equilibration and thermalization, as there is at NLO. It is therefore necessary to consider the N^{2}LO contribution as well. Section 4.2.1 comprises the study of this problem in the $O(N)$ model and compares the dynamics obtained at LO, NLO and (part of) N^{2}LO in the $1/N$ expansion in quantum field theory. In cases where an exact solution is available, a direct comparison can be carried out, this approach having been successfully applied using classical statistical field theory instead of quantum field theory [35, 16]. In the classical limit, the nonperturbative solution can be constructed numerically by direct integration of the field equations of motion, sampling initial conditions from a given probability distribution. Section 4.2.2 uses this approach to further quantify the validity of truncations.

4.1 The 2PI-$1/N$ expansion to next-to-next-to leading order

The exact evolution equations under consideration are equations (2.45) through (2.49), derived from the auxiliary field formalism in Chapter 2. We wish to solve these equations with the self energies Σ and Π truncated at N^{2}LO in $1/N$.

In extending the 2PI-$1/N$ expansion to N^{2}LO we find that Γ_2 contains one diagram at NLO and two diagrams at N^{2}LO as shown in Fig. 4.1. Using the powercounting technique discussed in section 2.5 (i.e. a closed scalar propagator $G \sim N$ and the auxiliary-field propagator $D \sim 1/N$) we see that diagram (2) ~ 1 and diagrams (3)

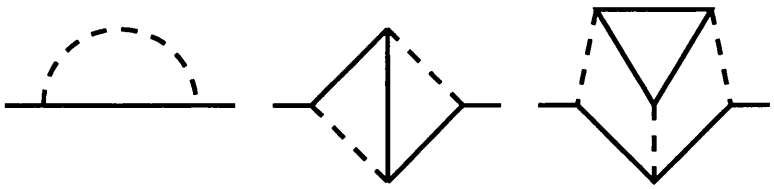

(1) (2) (3)

Figure 4.2: NLO and N^{2}LO contributions to Σ in the $1/N$ expansion. The scalar propagator G is denoted with a full line and the auxiliary-field propagator D with a dashed line.

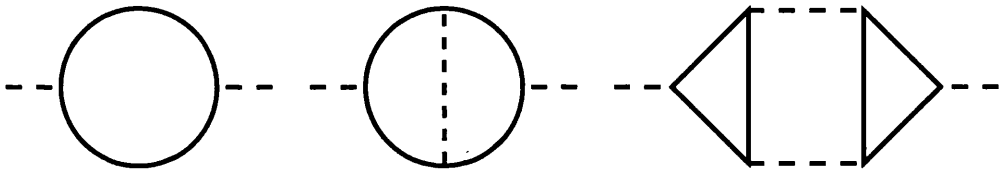

(1) (2) (3)

Figure 4.3: NLO and N^{2}LO contributions to Π in the $1/N$ expansion. The scalar propagator G is denoted with a full line and the auxiliary-field propagator D with a dashed line.

and (4) $\sim 1/N$. The expressions are

$$\Gamma_2^{\rm NLO}[G,D] = \frac{i}{4}\int_{xy} G_{ab}^2(x,y)D(x,y), \tag{4.1}$$

$$\Gamma_2^{\rm NNLO(3)}[G,D] = -\frac{i}{8}\int_{xyzw} G_{ab}(x,y)G_{bc}(y,z)G_{cd}(z,w)G_{da}(w,x)D(x,z)D(y,w),$$

$$\Gamma_2^{\rm NNLO(4)}[G,D] = \frac{i}{12}\int_{xyzx'y'z'} G_{ab}(x,y)G_{bc}(y,z)G_{ca}(z,x) \times G_{a'b'}(x',y')G_{b'c'}(y',z')G_{c'a'}(z',x')D(x,x')D(y,y')D(z,z').$$

The corresponding self energies are shown in Figs. 4.2 and 4.3.

As in chapter 2, we continue in the $O(N)$ symmetric case, such that $G_{ab}(x,y) = G(x,y)\delta_{ab}$ and $\Sigma_{ab}(x,y) = \Sigma(x,y)\delta_{ab}$. Since the self-energy expressions are rather complex, for notational simplicity it helps to label the self energies according to the number of loops, e.g. $\Sigma^{(\ell)}$, where $\ell = 1,2,3$.

At NLO the self energies read

$$\Sigma^{(1)}(x,y) = -G(x,y)D(x,y), \tag{4.2}$$

$$\Pi^{(1)}(x,y) = -\frac{N}{2}G^2(x,y), \tag{4.3}$$

and at N^{2}LO

$$\Sigma^{(2)}(x,y) = \int_{zw} G(x,w)G(w,z)G(z,y)D(x,z)D(w,y), \tag{4.4}$$

$$\Sigma^{(3)}(x,y) = -N\int_{zx'y'z'} G(x,z)G(z,y)G(x',y')G(y',z')G(z',x')D(x,x')D(y,y')D(z,z'),$$

$$\Pi^{(2)}(x,y) = \frac{N}{2}\int_{zw} G(x,w)G(w,y)G(x,z)G(z,y)D(z,w), \tag{4.5}$$

$$\Pi^{(3)}(x,y) = -\frac{N^2}{2}\int_{zz'ww'} G(x,z)G(z,w)G(w,x)G(y,z')G(z',w')G(w',y)D(w,w')D(z,z').$$

The statistical and spectral self energies at NLO were given in section 2.5 and read

$$\begin{aligned}
\Sigma_F^{(1)}(x,y) &= -\frac{\lambda}{3N}\left[F(x,y)\hat{D}_F(x,y) - \frac{1}{4}\rho(x,y)\hat{D}_\rho(x,y)\right], \\
\Sigma_\rho^{(1)}(x,y) &= -\frac{\lambda}{3N}\left[\rho(x,y)\hat{D}_F(x,y) + F(x,y)\hat{D}_\rho(x,y)\right], \\
\Pi_F^{(1)}(x,y) &= -\frac{N}{2}\left[F(x,y)F(x,y) - \frac{1}{4}\rho(x,y)\rho(x,y)\right], \\
\Pi_\rho^{(1)}(x,y) &= -NF(x,y)\rho(x,y).
\end{aligned} \tag{4.6}$$

Going beyond NLO now, we are faced with self energies that have internal vertices and therefore require further contour integrals. Since the CPU time required to solve the full N^{2}LO approximation is prohibitively large, we will be restricting ourselves to the two loop self-energies only[2]. In order to understand the general structure of the N^{2}LO self energies it is instructive to look at $\Sigma^{(2)}(x,y)$ in some detail. Firstly, we separate the local part of D by inserting eq. (2.43) into eq. (4.4). This yields

$$\Sigma^{(2)}(x,y) = \int_{zw} D(x,z)G(x,w)G(y,z)D(y,w)G(z,w)$$

[2]Note that the three loop self-energies are suppressed by factors of the coupling constant relative to the two loop ones. The effect of reducing the coupling strength on the accuracy of the approximation will be discussed in the results section.

$$
\begin{aligned}
&= -g^2 G^3(x,y) \\
&\quad + ig^2 \int_z \left[\hat{D}(x,z) G(x,y) G^2(y,z) + G^2(x,z) G(x,y) \hat{D}(y,z) \right] \\
&\quad + g^2 \int_{zw} \hat{D}(x,z) G(x,w) G(y,z) \hat{D}(y,w) G(z,w), \qquad (4.7)
\end{aligned}
$$

where

$$
g = \frac{\lambda}{3N}. \qquad (4.8)
$$

We can organise this naturally into three contributions, according to the number of $\hat{D}$ propagators. We use the notation $\Sigma^{(2,n)}$ for the contribution with n $\hat{D}$'s. The term with no $\hat{D}$ propagators consists of simple products of the two-point functions and reads

$$
\begin{aligned}
\Sigma_F^{(2,0)}(x,y) &= -g^2 \left[F^2(x,y) - \frac{3}{4}\rho^2(x,y) \right] F(x,y), \\
\Sigma_\rho^{(2,0)}(x,y) &= -g^2 \left[3F^2(x,y) - \frac{1}{4}\rho^2(x,y) \right] \rho(x,y). \qquad (4.9)
\end{aligned}
$$

We proceed to give expressions for the terms with internal vertices, taken from Ref. [30]. For the term with one $\hat{D}$ propagator, we find explicitly

$$
\begin{aligned}
&\frac{1}{g^2} \Sigma_F^{(2,1)}(x,y) = \\
&\quad \int_0^x dz \left[2F(x,z)\rho(x,z)\hat{D}_F(y,z) + \hat{D}_\rho(x,z) \left(F^2(y,z) - \frac{1}{4}\rho^2(y,z) \right) \right] F(x,y) \\
&\quad + \int_0^y dz \left[2\hat{D}_F(x,z)F(y,z)\rho(y,z) + \left(F^2(x,z) - \frac{1}{4}\rho^2(x,z) \right) \hat{D}_\rho(y,z) \right] F(x,y) \\
&\quad + \int_y^x dz \, \frac{1}{2} \left[\hat{D}_\rho(x,z)F(y,z)\rho(y,z) + F(x,z)\rho(x,z)\hat{D}_\rho(y,z) \right] \rho(x,y), \qquad (4.10)
\end{aligned}
$$

and

$$
\begin{aligned}
&\frac{1}{g^2} \Sigma_\rho^{(2,1)}(x,y) = \\
&\quad \int_0^x dz \left[2F(x,z)\rho(x,z)\hat{D}_F(y,z) + \hat{D}_\rho(x,z) \left(F^2(y,z) - \frac{1}{4}\rho^2(y,z) \right) \right] \rho(x,y) \\
&\quad + \int_0^y dz \left[2\hat{D}_F(x,z)F(y,z)\rho(y,z) + \left(F^2(x,z) - \frac{1}{4}\rho^2(x,z) \right) \hat{D}_\rho(y,z) \right] \rho(x,y)
\end{aligned}
$$

$$-\int_y^x dz\, 2\left[\hat{D}_\rho(x,z)F(y,z)\rho(y,z)+F(x,z)\rho(x,z)\hat{D}_\rho(y,z)\right]F(x,y), \qquad (4.11)$$

and for the self energy with two $\hat{D}$ propagators

$$\begin{aligned}
\frac{1}{g^2}\Sigma_F^{(2,2)}(x,y) = &-\int_0^x dz\int_0^x dw\,\rho(x,z)\hat{D}_\rho(x,w)\hat{D}_F(y,z)F(y,w)F(z,w)\\
&-\int_0^y dz\int_0^y dw\,\hat{D}_F(x,z)F(x,w)\rho(y,z)\hat{D}_\rho(y,w)F(z,w)\\
&-\int_0^x dz\int_0^z dw\left[\rho(x,z)\hat{D}_F(x,w)\hat{D}_F(y,z)F(y,w)\right.\\
&\qquad\left.+\hat{D}_F(x,z)F(x,w)F(y,z)\hat{D}_\rho(y,w)\right]\rho(z,w)\\
&-\int_0^y dz\int_0^z dw\left[\hat{D}_F(x,z)F(x,w)\rho(y,z)\hat{D}_F(y,w)\right.\\
&\qquad\left.+F(x,z)\hat{D}_\rho(x,w)\hat{D}_F(y,z)F(y,w)\right]\rho(z,w)\\
&-\int_0^x dz\int_0^y dw\left[\hat{D}_\rho(x,z)F(x,w)F(y,z)\hat{D}_\rho(y,w)\right.\\
&\qquad\left.+\rho(x,z)\hat{D}_F(x,w)\hat{D}_F(y,z)\rho(y,w)\right]F(z,w)\\
&-\int_0^x dz\int_z^y dw\,\frac{1}{4}\left[\hat{D}_\rho(x,z)F(x,w)\rho(y,z)\hat{D}_\rho(y,w)\right.\\
&\qquad\left.+\rho(x,z)\hat{D}_F(x,w)\hat{D}_\rho(y,z)\rho(y,w)\right]\rho(z,w)\\
&-\int_0^y dz\int_z^x dw\,\frac{1}{4}\left[\hat{D}_\rho(x,z)\rho(x,w)\rho(y,z)\hat{D}_F(y,w)\right.\\
&\qquad\left.+\rho(x,z)\hat{D}_\rho(x,w)\hat{D}_\rho(y,z)F(y,w)\right]\rho(z,w)\\
&+\int_y^x dz\int_y^x dw\,\frac{1}{4}\hat{D}_\rho(x,z)\rho(x,w)\rho(y,z)\hat{D}_\rho(y,w)F(z,w), \qquad (4.12)
\end{aligned}$$

and

$$\begin{aligned}
\frac{1}{g^2}\Sigma_\rho^{(2,2)}(x,y) = &\int_y^x dz\int_0^x dw\left[\hat{D}_\rho(x,z)\rho(x,w)\rho(y,z)\hat{D}_F(y,w)\right.\\
&\qquad\left.+\rho(x,z)\hat{D}_\rho(x,w)\hat{D}_\rho(y,z)F(y,w)\right]F(z,w)\\
&+\int_y^x dz\int_0^y dw\left[\hat{D}_\rho(x,z)F(x,w)\rho(y,z)\hat{D}_\rho(y,w)\right.\\
&\qquad\left.+\rho(x,z)\hat{D}_F(x,w)\hat{D}_\rho(y,z)\rho(y,w)\right]F(z,w)
\end{aligned}$$

$$
\begin{aligned}
&+\int_y^x dz \int_0^z dw \Big[\hat{D}_\rho(x,z)F(x,w)\rho(y,z)\hat{D}_F(y,w) \\
&\qquad +\rho(x,z)\hat{D}_F(x,w)\hat{D}_\rho(y,z)F(y,w)\Big]\rho(z,w) \\
&+\int_y^x dz \int_y^z dw \,\frac{1}{2}\Big[\hat{D}_\rho(x,z)F(x,w)F(y,z)\hat{D}_\rho(y,w) \\
&\qquad +\rho(x,z)\hat{D}_F(x,w)\hat{D}_F(y,z)\rho(y,w)\Big]\rho(z,w) \\
&+\int_y^x dz \int_x^z dw \,\frac{1}{2}\Big[F(x,z)\hat{D}_\rho(x,w)\hat{D}_\rho(y,z)F(y,w) \\
&\qquad +\hat{D}_F(x,z)\rho(x,w)\rho(y,z)\hat{D}_F(y,w)\Big]\rho(z,w) \\
&-\int_y^x dz \int_0^y dw \,\frac{1}{4}\Big[\hat{D}_\rho(x,z)\rho(x,w)\rho(y,z)\hat{D}_\rho(y,w) \\
&\qquad +\rho(x,z)\hat{D}_\rho(x,w)\hat{D}_\rho(y,z)\rho(y,w)\Big]\rho(z,w). \qquad (4.13)
\end{aligned}
$$

In a few terms the symmetry of the integrand was used to make some minor simplifications.

For the auxiliary-field self energy we proceed in the same manner and find, at two loops,

$$
\begin{aligned}
\Pi^{(2)}(x,y) &= \frac{N}{2}\int_{zw} G(x,z)G(x,w)G(y,z)G(y,w)D(z,w) \qquad (4.14)\\
&= \frac{i\lambda}{6}\int_z G^2(x,z)G^2(y,z) + \frac{\lambda}{6}\int_{zw} G(x,z)G(x,w)G(y,z)G(y,w)\hat{D}(z,w).
\end{aligned}
$$

Denoting these diagrams again as $\Pi^{(2,n)}$, where n again denotes the number of $\hat{D}$ propagators, we find with $n=0$,

$$
\begin{aligned}
\Pi_F^{(2,0)}(x,y) &= \frac{\lambda}{3}\int_0^x dz\, F(x,z)\rho(x,z)\left(F^2(y,z)-\frac{1}{4}\rho^2(y,z)\right) \\
&\quad +\frac{\lambda}{3}\int_0^y dz\,\left(F^2(x,z)-\frac{1}{4}\rho^2(x,z)\right)F(y,z)\rho(y,z), \\
\Pi_\rho^{(2,0)}(x,y) &= -\frac{2\lambda}{3}\int_y^x dz\, F(x,z)\rho(x,z)F(y,z)\rho(y,z), \qquad (4.15)
\end{aligned}
$$

and with one $\hat{D}$ propagator

$$
\frac{6}{\lambda}\Pi_F^{(2,1)}(x,y) = -\int_0^x dz\int_0^x dw\,\rho(x,z)\rho(x,w)F(y,z)F(y,w)\hat{D}_F(z,w)
$$

$$
\begin{aligned}
&- \int_0^y dz \int_0^y dw\, F(x,z)F(x,w)\rho(y,z)\rho(y,w)\hat{D}_F(z,w) \\
&- \int_0^x dz \int_0^z dw\, 2\rho(x,z)F(x,w)F(y,z)F(y,w)\hat{D}_\rho(z,w) \\
&- \int_0^y dz \int_0^z dw\, 2F(x,z)F(x,w)\rho(y,z)F(y,w)\hat{D}_\rho(z,w) \\
&- \int_0^x dz \int_0^y dw\, 2\rho(x,z)F(x,w)F(y,z)\rho(y,w)\hat{D}_F(z,w) \\
&+ \int_y^x dz \int_y^x dw\, \frac{1}{4}\rho(x,z)\rho(x,w)\rho(y,z)\rho(y,w)\hat{D}_F(z,w) \\
&- \int_0^x dz \int_z^y dw\, \frac{1}{2}\rho(x,z)F(x,w)\rho(y,z)\rho(y,w)\hat{D}_\rho(z,w) \\
&- \int_0^y dz \int_z^x dw\, \frac{1}{2}\rho(x,z)\rho(x,w)\rho(y,z)F(y,w)\hat{D}_\rho(z,w), \quad (4.16)
\end{aligned}
$$

and

$$
\begin{aligned}
\frac{6}{\lambda}\Pi_\rho^{(2,1)}(x,y) = &\int_y^x dz \int_0^x dw\, 2\rho(x,z)\rho(x,w)\rho(y,z)F(y,w)\hat{D}_F(z,w) \\
&+ \int_y^x dz \int_0^y dw\, 2\rho(x,z)F(x,w)\rho(y,z)\rho(y,w)\hat{D}_F(z,w) \\
&+ \int_y^x dz \int_y^z dw\, \rho(x,z)F(x,w)F(y,z)\rho(y,w)\hat{D}_\rho(z,w) \\
&+ \int_y^x dz \int_x^z dw\, F(x,z)\rho(x,w)\rho(y,z)F(y,w)\hat{D}_\rho(z,w) \\
&+ \int_y^x dz \int_0^z dw\, 2\rho(x,z)F(x,w)\rho(y,z)F(y,w)\hat{D}_\rho(z,w) \\
&- \int_y^x dz \int_0^y dw\, \frac{1}{2}\rho(x,z)\rho(x,w)\rho(y,z)\rho(y,w)\hat{D}_\rho(z,w). \quad (4.17)
\end{aligned}
$$

4.2 Numerical results

We aim to solve the evolution equations (2.45) through (2.49) numerically by discretisation on a space-time lattice (see appendix A for details of the numerical method). The self energies in the space-time integrals on the RHS of those equations are, at NLO, simple products of F, ρ, $\hat{D}_F$ and $\hat{D}_\rho$. At N^{2}LO however the self energies themselves require space-time integrals to be performed, with the two-loop self energy containing up to two internal vertices, and the three-loop self energy containing up to

four. This structure leads to nested loops over time, dramatically increasing the necessary CPU time. In the following analysis we will restrict ourselves to consideration of the two-loop self energies only. In order to obtain viable runtimes, we distribute the time integrals over multiple processors.

We solve the equations in $1+1$ dimensions via a discretisation with spatial lattice spacing a and temporal spacing a_t, taking $a_t/a = 0.2$. For the initial conditions we restrict ourselves to a Gaussian density matrix[3], resulting in the initial correlation functions

$$F(0,0;k) = F(a_t,a_t;k) = \frac{1}{\omega_k}\Big[n_0(\omega_k) + \frac{1}{2}\Big], \tag{4.18}$$

$$F(a_t,0;k) = F(0,0;k)\left(1 - \frac{a_t^2\omega_k^2}{2}\right), \tag{4.19}$$

where $\omega_k = (k^2 + M_0^2)^{1/2}$, M_0 is the initial mass (determined from the mean field mass gap equation) and n_0 is the initial (nonequilibrium) particle number. For the initial particle number we take a Gaussian distribution $n_0(k) = A\exp[-\frac{1}{2\sigma^2}(|k| - |k_c|)^2]$, centred around k_c with width σ. As in Chapter 3, initial conditions for the spectral function are fixed by the equal-time commutation relations, and those for the auxiliary field correlators are determined from equations (2.48) and (2.49).

4.2.1 Convergence in the quantum theory

We begin by comparing NLO and N^{2}LO truncations of the $1/N$ expansion in the quantum theory. In Fig. 4.4 we show the unequal-time two-point function $F(t,0;k=0)$ for four values of N, with all other parameters kept constant. The coupling is $\lambda/m^2 = 30$, where m is the renormalised mass in vacuum. The lattice spacing is $am = 0.5$ and the volume $Lm = 32$. The memory kernel is preserved for the entire evolution.

At LO (not shown) there is no damping in the unequal-time correlator. At higher order, we observe that the agreement between the NLO and N^{2}LO evolutions of the correlation function improves with increasing N. There is reasonable agreement at early times at $N = 4$, with the two truncations becoming barely distinguishable at

[3]In principle non-Gaussian initial conditions present no problem. A Gaussian density matrix is assumed to simplify the analysis, but this assumption has no impact on the validity of the dynamics.

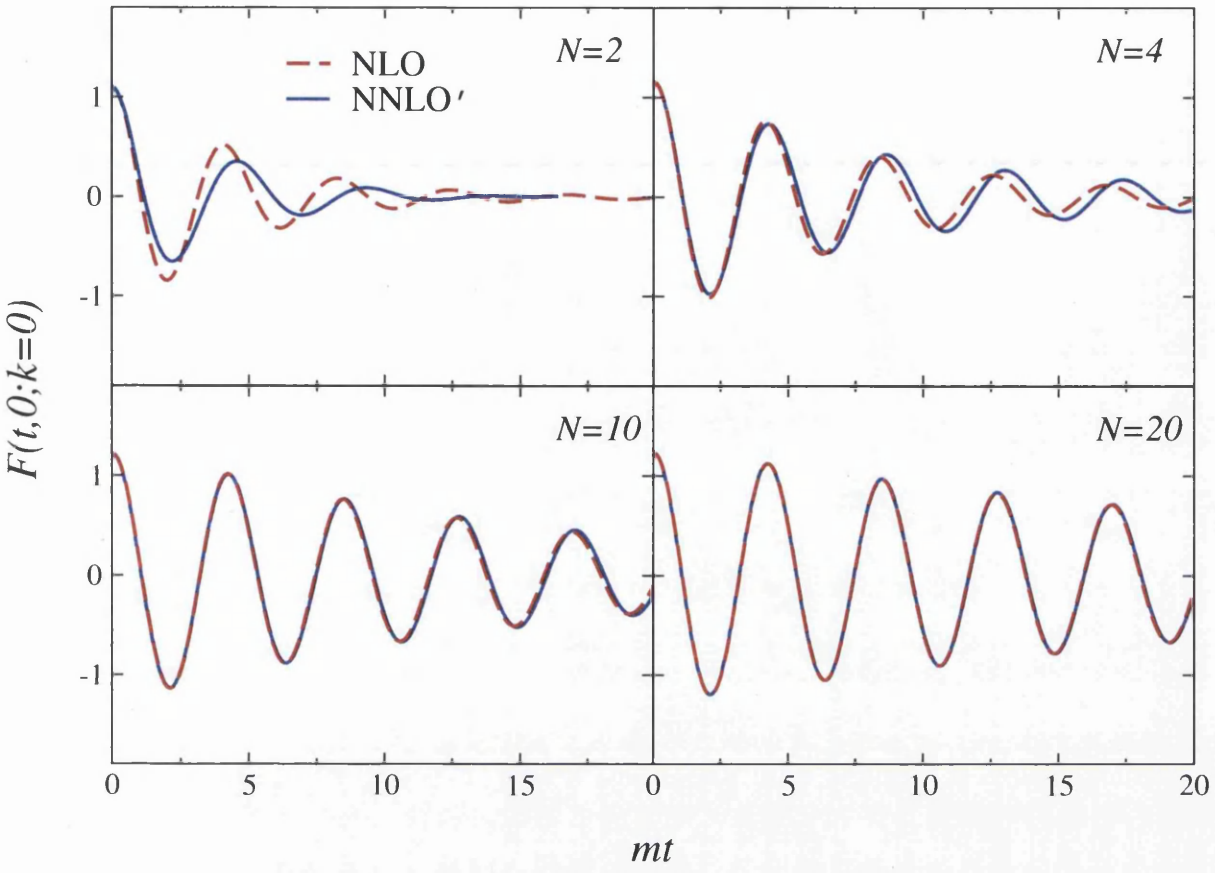

Figure 4.4: Unequal time correlation function $F(t, 0; k = 0)$ at zero momentum for $N = 2, 4, 10, 20$ in the quantum theory. The full lines show results from the N^{2}LO truncation and the dashed lines from NLO.

$N = 10$.[4]

In Fig. 4.5 we compare two quantities, the mass M and the damping rate γ, extracted via a fit of the curves in Fig. 4.4 to an Ansatz of the form $Ae^{-\gamma t}\cos(Mt)$, where M is the quasiparticle mass and γ is the width. Also included here are masses calculated in the mean field approximation, where only the local part of the self-energy is retained as a time-dependent correction to the mass parameter (the damping rate is always zero in the mean field approximation).

From the upper plot we see clearly the convergence of the mean field, NLO and N^{2}LO truncations as the value of N is increased, with the latter two agreeing for $N \gtrsim 10$, though differing slightly from the mean field. The quasiparticle mass converges to

[4]The $N = 2$ NNLO curve is abruptly cut off at around $mt = 16$ since it diverged at this point. Presumably this small value of N led to a numerical instability at late times since larger-N runs behaved well.

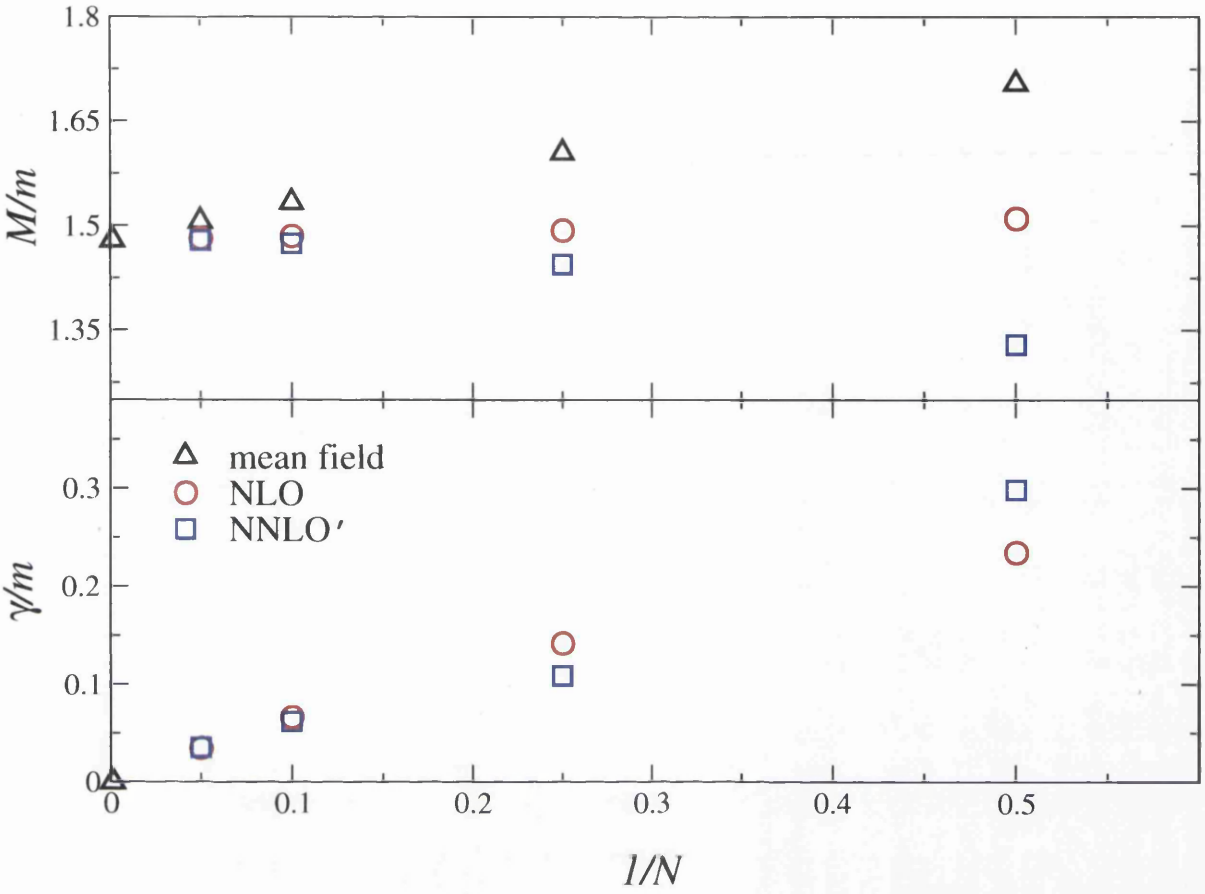

Figure 4.5: Masses and damping rates extracted from the curves in Fig. 4.4, as a function of $1/N$. In addition to NLO and N^{2}LO, masses are shown for the mean field approximation.

the value determined by the nonthermal fixed point of the mean field equations in the large N limit. For the parameters used here we find $M/m = 1.48$ when $N \to \infty$. The lower plot shows the reduction in damping rate as N is increased, vanishing in the large-N limit. Again there is rapid convergence of the NLO and N^{2}LO truncations.

4.2.2 Convergence in the classical approximation

In this section we take the classical limit of the set of 2PI equations in order to compare with the 'exact' solution from classical statistical field theory. In the latter case the nonperturbative evolution can be computed by numerically solving the classical field equations, sampling initial conditions from the Gaussian ensemble.

To take the classical limit of the 2PI equations of motion we note that, in the limit,

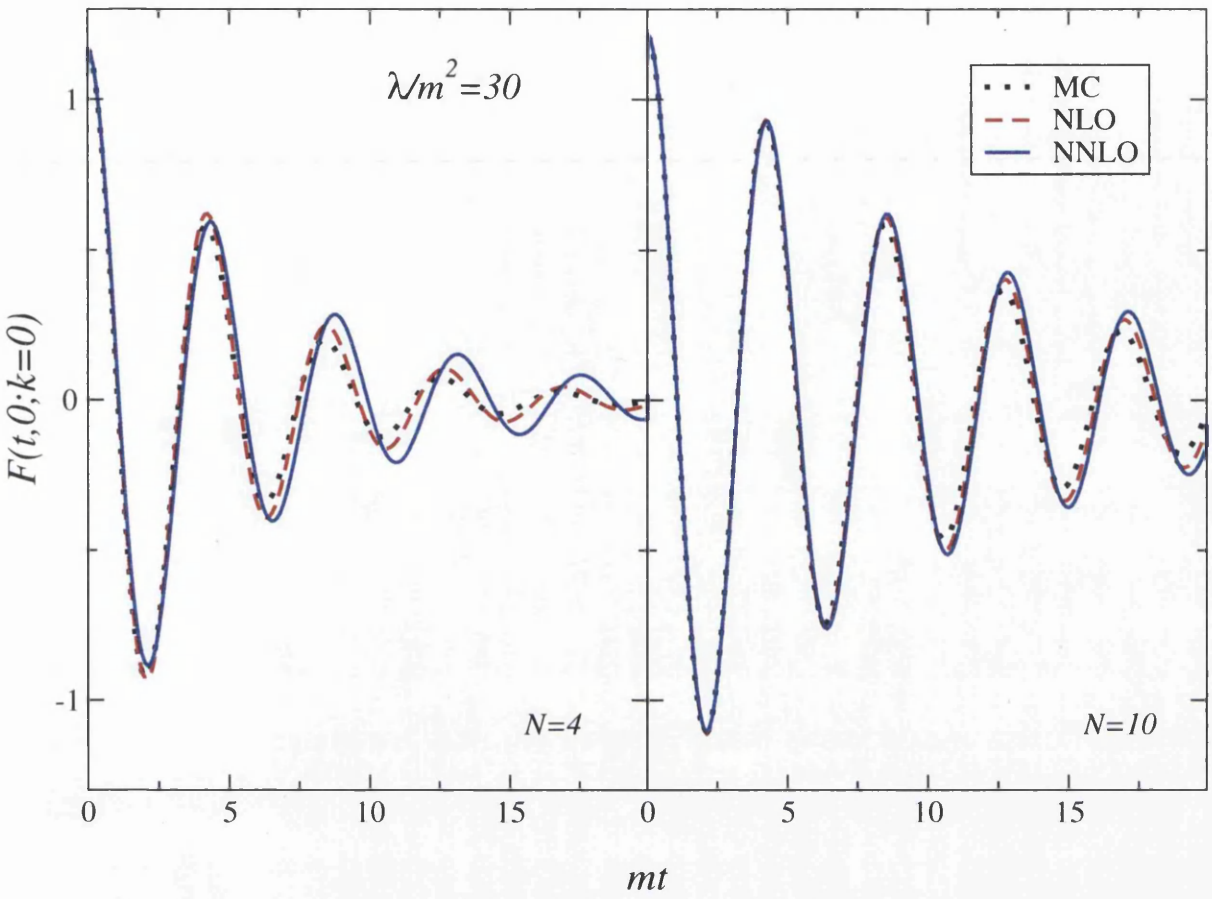

Figure 4.6: Unequal time correlation function $F(t, 0; k = 0)$ at zero momentum for $N = 4, 10$ in the classical theory. Included are the NLO and N^{2}LO results in the classical limit of the 2PI-1/N expansion, and the exact result obtained by Monte Carlo solution of the classical equations of motion.

statistical two-point functions (F) dominate with respect to spectral functions (ρ). This can most easily be seen in equilibrium, where $F(\omega, \mathbf{p})$ and $\rho(\omega, \mathbf{p})$ are related by

$$F^{(eq)}(\omega, \mathbf{p}) = -i\left(n_B(\omega) + \frac{1}{2}\right)\rho^{(eq)}(\omega, \mathbf{p}). \tag{4.20}$$

In equilibrium, $n_B(\omega)$ is given by

$$n_B(\omega) = \frac{1}{e^{\hbar\omega/kT} - 1}. \tag{4.21}$$

Taking the classical limit $\hbar \to 0$ we have

$$n_B^{\mathrm{cl}}(\omega) = \frac{kT}{\hbar\omega}, \tag{4.22}$$

and it follows that $F^{(eq)}(\omega, \mathbf{p}) \gg \rho^{(eq)}(\omega, \mathbf{p})$ in the limit. Equation (4.22) suggests an alternative definition of the classical limit as the presence of very large occupation numbers.

Following from this, terms that are subleading when F is taken to be much larger than ρ are dropped.

In Fig. 4.6 we show the two-point function $F(t, 0; k = 0)$ for $N = 4$ and $N = 10$. As in the quantum case we observe better agreement between NLO and N^{2}LO at the larger value of N, with the two following each other until around $mt = 10$ in the $N = 10$ case. Unexpectedly, at both values of N we see the NLO approximation following the exact evolution more closely than the N^{2}LO .

Since our N^{2}LO approximation includes only the 2- and 3-loop contributions to the 2PI-1/N expansion, a conceivable explanation of this discrepancy might be the absence of the N^{2}LO 4-loop diagram. As this diagram is suppressed by the coupling constant relative to the 3-loop diagram, we expect its influence to be diminished at weaker coupling. To study this we take a relatively small value of $N = 4$, where NLO and N^{2}LO differ noticably at large coupling, and perform simulations at successively weaker coupling. Fig. 4.7 shows the behaviour of the NLO, N^{2}LO and exact (MC for Monte Carlo) solutions as the coupling strength is reduced.

In the top left corner, the coupling constant is $\lambda/m^2 = 30$ and we see less damping at N^{2}LO than at NLO (similar to the quantum case). As noted previously, NLO appears to be closer than N^{2}LO to the exact solution. Decreasing the coupling constant, we observe that the agreement between the two 2PI truncations improves, demonstrating convergence. Furthermore, at weaker coupling we see that the MC result lies between the NLO and N^{2}LO curves. At $\lambda/m^2 = 30/4$ and $30/8$, the N^{2}LO result appears closest to the exact result signalling a well converging expansion. Simulations were carried out at even smaller coupling (not shown) and all curves were found to lie essentially on top of each other, even for $N = 4$.

Since the N^{2}LO approximation is so numerically intensive, an investigation was carried out into whether it might be possible to truncate the N^{2}LO memory kernel earlier than the NLO one, saving considerable computer resources.

Fig. 4.8 shows the evolution of $F(t, 0; k = 0)$ for various truncations of the N^{2}LO

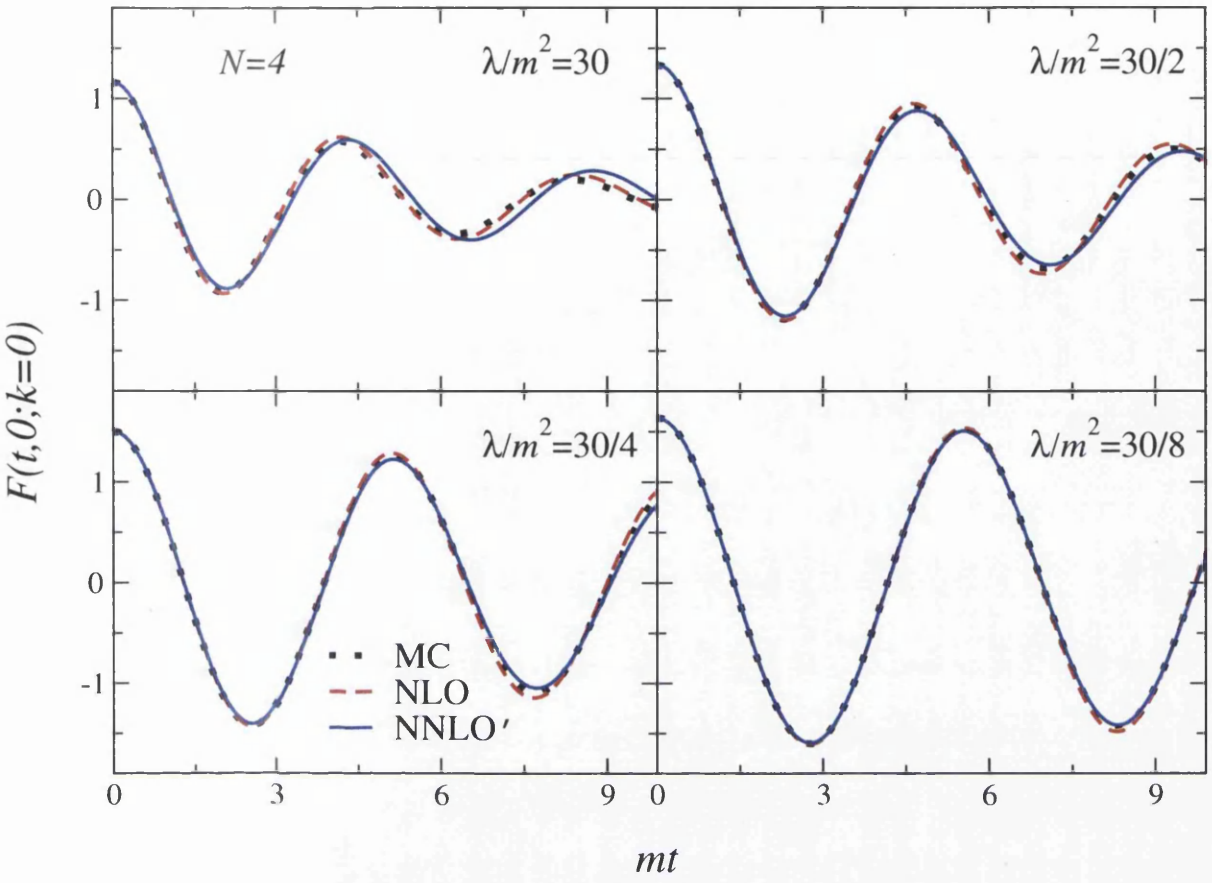

Figure 4.7: NLO, N^{2}LO and MC results for the unequal time propagator $F(t, 0; k = 0)$ at $N = 4$ with coupling strengths $\lambda/m^2 = 30/n$, where $n = 1, 2, 4, 8$.

memory kernel. We find that the curves with truncated memory kernels deviate from the untruncated case as soon as the N^{2}LO is filled. It is therefore necessary to preserve memory kernels over the entire history, which currently prevents us from going to larger times and studying the approach to equilibrium beyond NLO.

4.3 Conclusions

In this chapter we have investigated the convergence properties of the 2PI-1/N expansion for nonequilibrium quantum fields. For the first time in quantum field theory, contributions at N^{2}LO were included, allowing us to compare results obtained at LO, NLO and N^{2}LO in $1/N$. Additionally we studied convergence in the classical statistical field theory limit, where exact numerical results are available. Due to the intensive

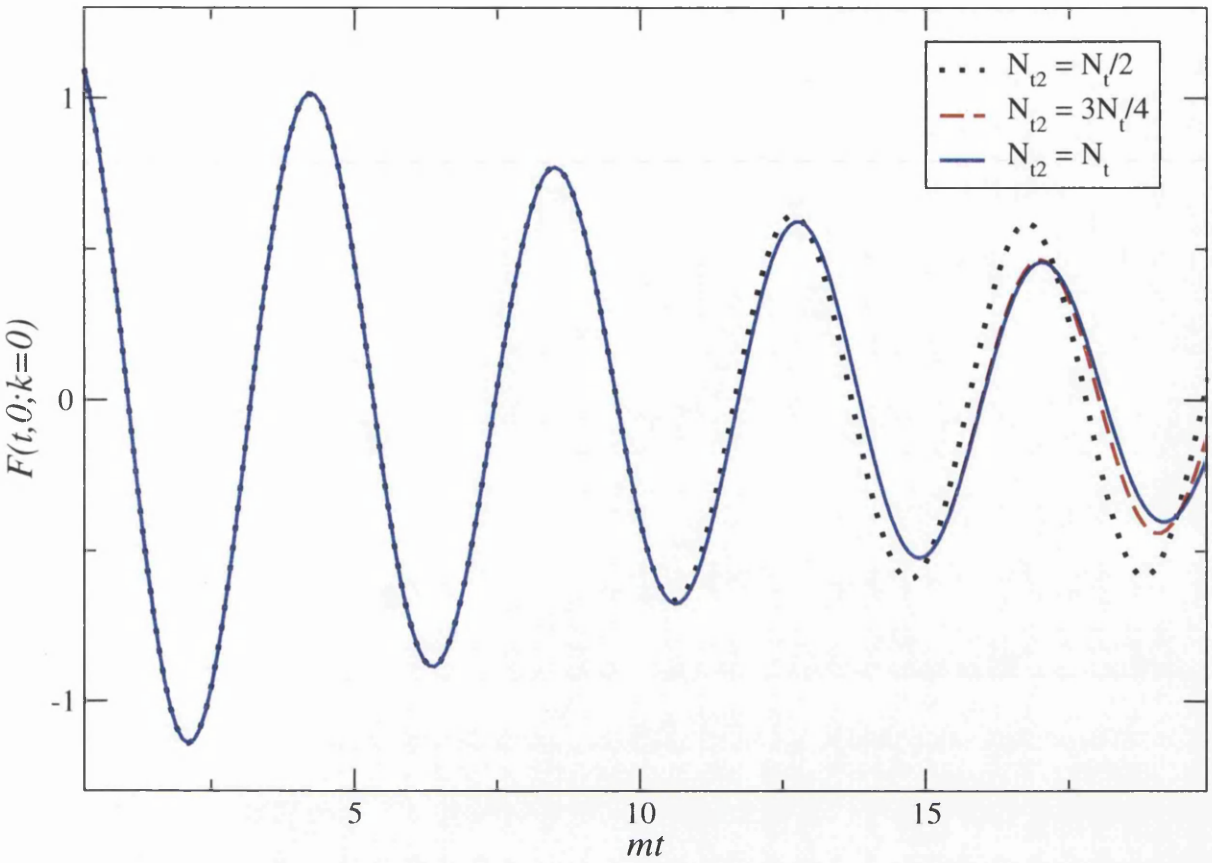

Figure 4.8: Unequal-time correlator with truncations of the N^{2}LO memory kernel. N_t and N_{t2} are the lengths of the NLO and N^{2}LO memory kernels respectively.

numerical demands of simulating at N^{2}LO, we focused on early-time dynamics.

- **Convergence in the quantum theory**

  We included two-loop self-energies at N^{2}LO in $1/N$. Comparing unequal-time statistical functions at NLO and N^{2}LO we found that the expansion is rapidly convergent as N is increased, with the two truncations barely distinguishable at $N = 10$. This confirms that for early-time NLO dynamics in $1 + 1$ dimensions, $N \gtrsim 10$ works very well even at strong coupling.

- **Convergence in the classical limit**

  Again we found convergence of the NLO and N^{2}LO truncations with increasing N. At $N = 4$, where NLO and N^{2}LO differ at large coupling, we found convergence as the coupling strength is reduced. Reducing the coupling effectively diminishes the effect of the N^{2}LO 4-loop diagram (which we did not include due

to the substantial numerical effort required), since it is suppressed by the coupling. Comparing with the exact numerical solution, we found that the 2PI-$1/N$ expansion truncated at NLO already gives quantitatively accurate results for moderate values of N or coupling strength. Similarly to the quantum case, NLO works very well at any coupling with $N = 10$, however for the often used $N = 4$, a trade-off in terms of a smaller coupling is required for precision calculations. At very weak couplings, the 3-loop $\mathrm{N^2LO}$ truncation offers improvement over NLO in better approximating the exact solution.

Chapter 5

Summary and outlook

We have undertaken an investigation into the nonequilibrium dynamics of quantum fields in an expanding space-time background. We studied an O(N)-symmetric scalar quantum field theory in $1+1$ dimensions, using NLO loop- and $1/N$-expansions of the 2PI effective action. Focusing on the real-time evolution of the statistical function we found the early-time behaviour to be described by a mean field approximation, and characterised by a non-thermal fixed point of the mean field equations. At intermediate times we found that interactions dominated the evolution, driving the system towards equilibrium. During this period we observed competition between interactions and expansion in the system, resulting in the absence of level crossing that is a signal of equilibration in the nonexpanding case. In $1+1$ dimensions the momentum dependence of the equations of motion was found to drop out at late times as a result of the effective red-shift of momenta due to the expansion. It would be of great interest to obtain results in $3+1$ dimensions since in this case the equations of motion retain a dependence on the transverse momenta at late times. A study of momentum-space isotropisation in the system would then be possible, that is, to test whether the longitudinal pressure P_η and the (initially different) transverse pressure $P_\perp$ become equal during the evolution. Simulations in $3+1$ dimensions would also allow us to study an anisotropic transverse momentum space - the result of a non-central collision. The initial attempt made in section 3.7 to include a fixed cutoff on physical momenta, thereby retaining some longitudinal momentum dependence at late times, was only implemented for very short times due to CPU memory constraints, and gave inconclusive results. A method for studying such a system over a longer time period would be welcome. It was also found that interaction terms were suppressed

at late times, leading to natural emergence of freeze-out in the model. At strong coupling, we found that the interactions forced all modes to the same final occupation number before the onset of freeze-out. This resulted in a loss of memory of the initial conditions since all modes became indistinguishable. At weak coupling, we found that the modes settled to different final occupation numbers. As there was no level crossing the modes remained in their initial ordering, with the result that the system retained memory of its initial conditions.

In chapter 4 we investigated convergence of the 2PI-1/N expansion by numerically solving a 3-loop N^{2}LO truncation of the effective action. For quantum field theory in $1+1$ dimensions we found rapid convergence of NLO and N^{2}LO results as N was increased, concluding that it is safe to use the 2PI-1/N expansion truncated at NLO for $N \gtrsim 10$ at any coupling strength. Taking the classical limit, we compared NLO and N^{2}LO truncations with exact numerical results from classical statistical field theory. We found the 2PI-1/N expansion to be convergent both as N is increased, and as the coupling is reduced, concluding that for smaller values of N, say $N = 4$, a trade-off in terms of a smaller coupling strength is required for precision calculations. Due to the intensive numerical effort at N^{2}LO we were only able to study the evolution at early times. Going to larger times would be of interest, allowing us to study the approach to equilibrium at N^{2}LO, but would require some clever numerical techniques. Extending the analysis from $1+1$ dimensions to $3+1$ would also be worthwhile - we expect the convergence properties to persist in higher dimensions, but a direct confirmation would be welcome. Finally, inclusion of the 4-loop N^{2}LO diagram would allow for a truer comparison of NLO and N^{2}LO truncations, but the numerical effort involved may be prohibitive.

Appendix A

Numerical method

In order to solve numerically the equations of motion derived in chapter 3, one requires a program that evolves the statistical and spectral propagators, $\tilde{F}(\tau,\tau';k_\eta)$ and $\tilde{\rho}(\tau,\tau';k_\eta)$, forward in time from given initial conditions. In $1+1$ dimensions we must define three-dimensional arrays corresponding to the momentum-space propagators, of size $N_\tau \times N_\tau \times N_\eta$, where N_τ specifies the size of the memory kernel (determining how much of the recent history of the system is to be retained in the memory integrals), and N_η specifies the number of momentum modes. We define two-dimensional arrays corresponding to the self energies $\tilde{\Sigma}_F(\tau,\tau';k_\eta)$ and $\tilde{\Sigma}_\rho(\tau,\tau';k_\eta)$, of size $N_\tau \times N_\eta$, since knowledge of these functions is only ever required at a given time τ. If one is working in the auxiliary field formalism, additional arrays will be required for the auxiliary propagators and self energies.

In order to determine the in-medium mass M, to be used in the initial conditions, we solve the mass gap equation at the initial time τ_0,

$$M^2(\tau_0) = m_B^2 + \frac{\lambda}{2}\Big(\frac{N+2}{3N}\Big)\frac{1}{\tau_0}\int \frac{\mathrm{d}k_\eta}{2\pi}\frac{(n_0(k_\eta)+1/2)}{\sqrt{k_\eta^2+M^2(\tau_0)}}, \tag{A.1}$$

where the 'bare' mass m_B is a specified parameter, and $n_0(k_\eta)$ the initial particle number.

We discretise the times as $\tau = na_\tau + \tau_0$ and $\tau' = n'a_\tau + \tau_0$, where n and n' are integers and a_τ is the time-step size. The statistical propagator is then addressed as `F[n][n']`[k]. The initial conditions given in section 3.5 for the propagators and their derivatives translate (in the discretised system) to a specification of the array elements `F[0][0]`[k], `F[1][0]`[k], `F[1][1]`[k], and ρ[0][0][k], ρ[1][0][k], ρ[1][1][k], for integer $0 \leq$ k $\leq$

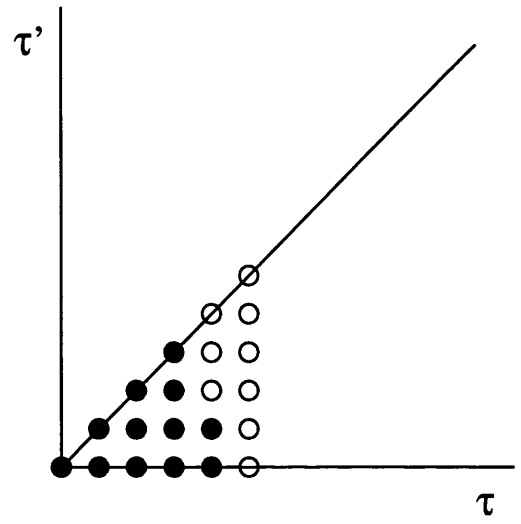

Figure A.1: The order of calculation of discrete points in the $\tau - \tau'$ plane.

$(N_\eta - 1)$. These correspond to the three points in the lower-left corner of Fig. A.1.

The time evolution is implemented by moving one timestep in the τ-direction, and then calculating the propagators for each value $\tau_0 \leq \tau' \leq \tau$ (or $0 \leq \mathtt{n}' \leq \mathtt{n}$). In terms of array elements then, we proceed from the initial conditions to calculate the points [2][0][k], [2][1][k] and [2][2][k], for all k. This approach is illustrated in Fig. A.1, where filled circles denote (τ, τ') points that have been calculated, and empty circles denote points yet to be calculated. We only need calculate the lower triangle in the $\tau - \tau'$ plane since the symmetry properties[1] of $\tilde{F}$ and $\tilde{\rho}$ can be used to fill in the points $\tau' > \tau$ with no additional calculation.

At each timestep then, we are faced with memory integrals containing terms such as

$$\frac{1}{\tau}\int_{\tau_0}^{\tau}\frac{\mathrm{d}\tau''}{\tau''}\tilde{\Sigma}_\rho(\tau,\tau'';k_\eta)\tilde{F}(\tau'',\tau';k_\eta). \tag{A.2}$$

The memory integrals are discretised according to the prescription given in section 3.5. The self energy in this expression is most easily calculated in position space where it is (at NLO) a simple product of statistical and spectral propagators[2]. Thus a routine is required for Fourier transforming the self energies back and forth, a procedure that takes up a large fraction of the CPU time[3]. Once the self energies have been calculated, we can compute the memory integrals and update the equations

[1] See section 2.3.

[2] Exact expressions are given in sections 2.4 and 2.5.

[3] I used the Fastest Fourier Transform in the West (FFTW), available at http://www.fftw.org.

UNIVERSITY OF WALES SWANSEA LIBRARY

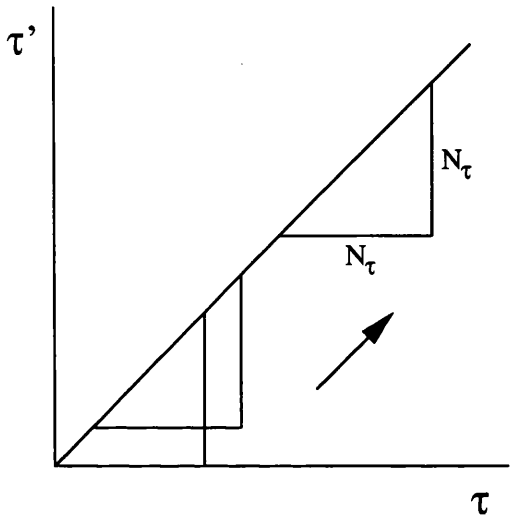

Figure A.2: Retaining a memory kernel of size $N_\tau \times N_\tau$.

of motion for $\tilde{F}$ and $\tilde{\rho}$ (discretised according to section 3.5).

Calculating the time evolution in this manner, the number of terms summed in the memory integrals quickly becomes very large as the area of the triangle increases. In order to improve run times, we can take advantage of the fact that we are at liberty to only integrate over the recent history of the system[4]. This is illustrated in Fig. A.2 where we only integrate over the most recent N_τ points in both the τ and τ' directions.

At next-to-next-to-leading order the situation becomes more complex as the self energies themselves require space-time integrals to be performed. In this case one may define additional four-dimensional arrays (20 in all) for storing the integrals of the various distinct combinations of propagators and auxiliary propagators appearing in the self energy expressions given in section 4.1. Since this dramatically increases the CPU memory requirement, one may distribute the calculation over multiple processors using the MPI (Message Passing Interface) specification. There are various ways to parallelise the calculation. The method we used was to distribute the t' index of all arrays such that when one runs on n processors, each processor stores only every nth timestep in the t' direction[5]. When an integral over t' (i.e. the second time index) is to be performed, all processors send the relevant array elements to a single node,

[4]This results from the fact that the memory integrals at late times are suppressed by a factor $1/\tau$.

[5]For example, when running on 64 processors, the first processor stores the 1st, 65th, 129th etc. timesteps, the second processor stores the 2nd, 66th, 130th etc. timesteps, and so forth.

which can then calculate the sum. For example, the memory integral (A.2) requires a sum over the second (distributed) time index of the self energy Σ_ρ. In this case the node that performs the sum (which I will call processor M) would be the one that stores the 'current' value of t', since it knows $F(t'', t'; k)$ for all values of t''. All other processors would then send their stored values of Σ_ρ to processor M, such that it then knows $\Sigma_\rho(t, t''; k)$ for all t'', and can simply calculate the integral.

Parallelising the computation in this way leads to manageable (though still large) run times.

Acknowledgements

I would like to thank my supervisor, Gert Aarts, for many interesting discussions and useful suggestions, without which this thesis wouldn't have been possible. My thanks also go to Simon Hands for his continued support and encouragement, and to Anders Tranberg for collaborating with me on the material in chapter 4.

I offer my deepest gratitude to my parents, Anita Cadman and Steven Laurie, and to Martin Cadman, for their faith in me and their unbounded support for whatever I have chosen to do. Finally, my warmest thanks to Kim Eun-jung, who was always there for me.

Bibliography

[1] B. B. Back *et al.*, "The PHOBOS perspective on discoveries at RHIC," Nucl. Phys. A **757** (2005) 28 [arXiv:nucl-ex/0410022].

[2] J. Adams *et al.* [STAR Collaboration], "Experimental and theoretical challenges in the search for the quark gluon plasma: The STAR collaboration's critical assessment of the evidence from RHIC collisions," Nucl. Phys. A **757** (2005) 102 [arXiv:nucl-ex/0501009].

[3] I. Arsene *et al.* [BRAHMS Collaboration], "Quark gluon plasma and color glass condensate at RHIC? The perspective from the BRAHMS experiment," Nucl. Phys. A **757** (2005) 1 [arXiv:nucl-ex/0410020].

[4] K. Adcox *et al.* [PHENIX Collaboration], "Formation of dense partonic matter in relativistic nucleus nucleus collisions at RHIC: Experimental evaluation by the PHENIX collaboration," Nucl. Phys. A **757** (2005) 184 [arXiv:nucl-ex/0410003].

[5] L. V. Keldysh, "Diagram Technique For Nonequilibrium Processes," Zh. Eksp. Teor. Fiz. **47** (1964) 1515.

[6] J. Schwinger, "Brownian Motion Of A Quantum Oscillator," J. Math. Phys. **2** (1961) 407;

[7] F. Cooper, S. Habib, Y. Kluger and E. Mottola, "Nonequilibrium dynamics of symmetry breaking in lambda Phi**4 field theory," Phys. Rev. D **55**, 6471 (1997) [arXiv:hep-ph/9610345].

[8] S. Habib, Y. Kluger, E. Mottola and J. P. Paz, "Dissipation and Decoherence in Mean Field Theory," Phys. Rev. Lett. **76**, 4660 (1996) [arXiv:hep-ph/9509413].

[9] F. Cooper, S. Habib, Y. Kluger, E. Mottola, J. P. Paz and P. R. Anderson, "Nonequilibrium quantum fields in the large N expansion," Phys. Rev. D **50**, 2848 (1994) [arXiv:hep-ph/9405352].

[10] J. Berges, "Introduction to nonequilibrium quantum field theory," AIP Conf. Proc. **739** (2005) 3 [arXiv:hep-ph/0409233].

[11] J. Berges, "Controlled nonperturbative dynamics of quantum fields out of equilibrium," Nucl. Phys. A **699** (2002) 847 [arXiv:hep-ph/0105311].

[12] J. M. Cornwall, R. Jackiw and E. Tomboulis, "Effective Action For Composite Operators," Phys. Rev. D **10** (1974) 2428.

[13] R. Kubo, J. Phys. Soc. Japan **12** (1957) 570;

[14] P. C. Martin and J. Schwinger, "Theory Of Many Particle Systems. I," Phys. Rev. **115** (1959) 1342.

[15] J. Berges and J. Cox, "Thermalization of quantum fields from time-reversal invariant evolution equations," Phys. Lett. B **517** (2001) 369 [arXiv:hep-ph/0006160].

[16] G. Aarts and J. Berges, "Classical aspects of quantum fields far from equilibrium," Phys. Rev. Lett. **88** (2002) 041603 [arXiv:hep-ph/0107129].

[17] G. Aarts, D. Ahrensmeier, R. Baier, J. Berges and J. Serreau, "Far-from-equilibrium dynamics with broken symmetries from the 2PI-1/N expansion," Phys. Rev. D **66** (2002) 045008 [arXiv:hep-ph/0201308].

[18] J. Berges, S. Borsanyi and J. Serreau, "Thermalization of fermionic quantum fields," Nucl. Phys. B **660** (2003) 51 [arXiv:hep-ph/0212404].

[19] S. Borsanyi and U. Reinosa, "The pressure of QED from the two-loop 2PI effective action," Phys. Lett. B **661** (2008) 88 [arXiv:0709.2316 [hep-ph]].

[20] U. Reinosa and J. Serreau, "Ward Identities for the 2PI effective action in QED," JHEP **0711** (2007) 097 [arXiv:0708.0971 [hep-th]].

[21] U. Reinosa and J. Serreau, "2PI effective action for gauge theories: Renormalization," JHEP **0607** (2006) 028 [arXiv:hep-th/0605023].

[22] A. Arrizabalaga, J. Smit and A. Tranberg, "Equilibration in phi**4 theory in 3+1 dimensions," Phys. Rev. D **72** (2005) 025014 [arXiv:hep-ph/0503287].

[23] A. Rajantie and A. Tranberg, "Looking for defects in the 2PI correlator," JHEP **0611** (2006) 020 [arXiv:hep-ph/0607292].

[24] H. van Hees and J. Knoll, "Renormalization in self-consistent approximations schemes at finite temperature. I: Theory," Phys. Rev. D **65** (2002) 025010 [arXiv:hep-ph/0107200].

[25] J. P. Blaizot, E. Iancu and U. Reinosa, "Renormalizability of Phi-derivable approximations in scalar phi**4 theory," Phys. Lett. B **568** (2003) 160 [arXiv:hep-ph/0301201].

[26] J. Berges, S. Borsanyi, U. Reinosa and J. Serreau, "Renormalized thermodynamics from the 2PI effective action," Phys. Rev. D **71** (2005) 105004 [arXiv:hep-ph/0409123].

[27] J. Berges, S. Borsanyi and C. Wetterich, "Prethermalization," Phys. Rev. Lett. **93** (2004) 142002 [arXiv:hep-ph/0403234].

[28] M. Lindner and M. M. Muller, "Comparison of Boltzmann equations with quantum dynamics for scalar fields," Phys. Rev. D **73** (2006) 125002 [arXiv:hep-ph/0512147].

[29] M. Lindner and M. M. Muller, "Comparison of Boltzmann Kinetics with Quantum Dynamics for a Chiral Yukawa Model Far From Equilibrium," Phys. Rev. D **77** (2008) 025027 [arXiv:0710.2917 [hep-ph]].

[30] G. Aarts and A. Tranberg, "Nonequilibrium dynamics in the O(N) model to next-to-next-to-leading order in the 1/N expansion," Phys. Rev. D **74** (2006) 025004 [arXiv:hep-th/0604156].

[31] G. Aarts and A. Tranberg, "Thermal effects on inflaton dynamics," Phys. Rev. D **77** (2008) 123521 [arXiv:0712.1120 [hep-ph]].

[32] G. Aarts and A. Tranberg, "Particle creation and warm inflation," Phys. Lett. B **650** (2007) 65 [arXiv:hep-ph/0701205].

[33] J. Berges and J. Serreau, "Parametric resonance in quantum field theory," Phys. Rev. Lett. **91** (2003) 111601 [arXiv:hep-ph/0208070].

[34] A. Arrizabalaga, J. Smit and A. Tranberg, "Tachyonic preheating using 2PI - 1/N dynamics and the classical approximation," JHEP **0410** (2004) 017 [arXiv:hep-ph/0409177].

[35] G. Aarts, G. F. Bonini and C. Wetterich, "Exact and truncated dynamics in nonequilibrium field theory," Phys. Rev. D **63** (2001) 025012 [arXiv:hep-ph/0007357].

[36] G. Aarts, N. Laurie and A. Tranberg, "Effective convergence of the 2PI-1/N expansion for nonequilibrium quantum fields," arXiv:0809.3390 [hep-ph].

[37] F. Cooper and G. Frye, "Comment On The Single Particle Distribution In The Hydrodynamic And Statistical Thermodynamic Models Of Multiparticle Production," Phys. Rev. D **10** (1974) 186.

[38] J. D. Bjorken, "Highly Relativistic Nucleus-Nucleus Collisions: The Central Rapidity Region," Phys. Rev. D **27** (1983) 140.

[39] M. Gyulassy and L. McLerran, "New forms of QCD matter discovered at RHIC," Nucl. Phys. A **750**, 30 (2005) [arXiv:nucl-th/0405013].

[40] E. V. Shuryak, "What RHIC experiments and theory tell us about properties of quark-gluon plasma?," Nucl. Phys. A **750** (2005) 64 [arXiv:hep-ph/0405066].

[41] E. Iancu, A. Leonidov and L. McLerran, "The colour glass condensate: An introduction," arXiv:hep-ph/0202270.

[42] P. F. Kolb and U. W. Heinz, "Hydrodynamic description of ultrarelativistic heavy-ion collisions," Invited review for 'Quark Gluon Plasma 3'. Editors: R.C. Hwa and X.N. Wang, World Scientific, Singapore. In *Hwa, R.C. (ed.) et al.: Quark gluon plasma* 634-714. arXiv:nucl-th/0305084.

[43] D. Teaney, J. Lauret and E. V. Shuryak, "A hydrodynamic description of heavy ion collisions at the SPS and RHIC," arXiv:nucl-th/0110037.

[44] P. Romatschke and U. Romatschke, "Viscosity Information from Relativistic Nuclear Collisions: How Perfect is the Fluid Observed at RHIC?," Phys. Rev. Lett. **99** (2007) 172301 [arXiv:0706.1522 [nucl-th]].

[45] P. F. Kolb, U. W. Heinz, P. Huovinen, K. J. Eskola and K. Tuominen, "Centrality dependence of multiplicity, transverse energy, and elliptic flow from hydrodynamics," Nucl. Phys. A **696** (2001) 197 [arXiv:hep-ph/0103234].

[46] P. Huovinen, P. F. Kolb, U. W. Heinz, P. V. Ruuskanen and S. A. Voloshin, "Radial and elliptic flow at RHIC: Further predictions," Phys. Lett. B **503** (2001) 58 [arXiv:hep-ph/0101136].

[47] P. F. Kolb, P. Huovinen, U. W. Heinz and H. Heiselberg, "Elliptic flow at SPS and RHIC: From kinetic transport to hydrodynamics," Phys. Lett. B **500** (2001) 232 [arXiv:hep-ph/0012137].

[48] D. Teaney, J. Lauret and E. V. Shuryak, "Flow at the SPS and RHIC as a quark gluon plasma signature," Phys. Rev. Lett. **86**, 4783 (2001) [arXiv:nucl-th/0011058].

[49] D. Molnar and M. Gyulassy, "Saturation of elliptic flow at RHIC: Results from the covariant elastic parton cascade model MPC," Nucl. Phys. A **697** (2002) 495 [Erratum-ibid. A **703** (2002) 893] [arXiv:nucl-th/0104073].

[50] S. A. Fulling, L. Parker and B. L. Hu, "Conformal energy-momentum tensor in curved spacetime: Adiabatic regularization and renormalization," Phys. Rev. D **10** (1974) 3905.

[51] P. Arnold, J. Lenaghan, G. D. Moore and L. G. Yaffe, "Apparent thermalization due to plasma instabilities in quark gluon plasma," Phys. Rev. Lett. **94** (2005) 072302 [arXiv:nucl-th/0409068].

[52] P. Arnold, J. Lenaghan and G. D. Moore, "QCD plasma instabilities and bottom-up thermalization," JHEP **0308** (2003) 002 [arXiv:hep-ph/0307325].

[53] P. Romatschke and M. Strickland, "Collective modes of an anisotropic quark gluon plasma," Phys. Rev. D **68**, 036004 (2003) [arXiv:hep-ph/0304092].

[54] P. Romatschke and M. Strickland, "Collective modes of an anisotropic quark-gluon plasma. II," Phys. Rev. D **70**, 116006 (2004) [arXiv:hep-ph/0406188].

[55] S. Mrowczynski, "Plasma instability at the initial stage of ultrarelativistic heavy ion Phys. Lett. B **314** (1993) 118.

[56] S. Mrowczynski, "Color filamentation in ultrarelativistic heavy-ion collisions," Phys. Lett. B **393** (1997) 26 [arXiv:hep-ph/9606442].

[57] P. Arnold, G. D. Moore and L. G. Yaffe, "The fate of non-abelian plasma instabilities in 3+1 dimensions," Phys. Rev. D **72**, 054003 (2005) [arXiv:hep-ph/0505212].